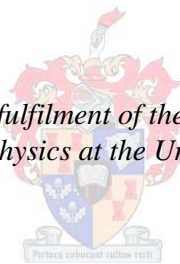


Short-Pulse Generation in a Diode-End-Pumped Solid-State Laser

by
Sandile Ngcobo

*Thesis presented in partial fulfilment of the requirements for the degree
Master of Science in Physics at the University of Stellenbosch*



Supervisor: Prof. Hubertus M. von Bergmann and Dr. Christoph Bollig
Department of Physics

March 2010

Declaration

By submitting this dissertation electronically, I declare that the entirety of the work contained therein is my own, original work, that I am the owner of the copyright thereof (unless to the extent explicitly otherwise stated) and that I have not previously in its entirety or in part submitted it for obtaining any qualification.

March 2010

Copyright © 2010 Stellenbosch University

All rights reserved

Abstract

This thesis consists of two parts; the first part is a discussion on the detailed history of the development of different types of modelocked lasers, especially the neodymium-doped lasers. The second part describes the design and development of a modelocked diode-end-pumped solid state Nd:YVO₄ laser using Semiconductor Saturable Absorbers.

The first part of this work will cover the history of modelocking where different types of lasers were used to generate ultrashort pulses. The discussion will mainly focus on neodymium-doped lasers such as Nd:YVO₄, where we will look at the spectral properties such as energy levels, absorption and emission wavelengths of such a laser.

The discussion will also look at different types of optical pump sources; such as diode lasers and flashlamps, where we will see the advantages of using diode lasers as pump sources due to their better operating conditions and efficiency. We will also look at two different types of diode pumping setup schemes, which are end-pumping and side pumping; where we will discover that diode-end-pumping is a better scheme for laser mode matching resulting in high efficiency and very good beam quality when compared to side pumping.

The gain bandwidth of the laser material will also be discussed showing that a laser material with a very large gain bandwidth and broad emission bandwidth is suitable for generating ultrashort pulses, such as Ti:Sapphire crystal. The discussion will also cover ultrafast lasers that have a small amplification bandwidth suitable for diode-end-pumping and that produce high average output power. Ultrafast lasers with low amplification bandwidth such as Nd:YAG and Nd:YVO₄ will be discussed showing that they can generate very short pulses with durations of down to 19 ps and 20 ps respectively and average output powers of 27 W and 20 W.

The technique of creating ultrashort pulses which is called modelocking will be discussed, where passive modelocking will be shown to be more suitable for creating ultra short pulses in the femtosecond region and active modelocking in the picosecond

region. The discussion will also cover saturable absorbers for passive modelocking where we will discuss the use of semiconductor saturable absorber mirrors to generate reliable self starting modelocked pulses. We will also cover the instabilities associated with using saturable absorbers where we will discuss different methods for reducing the instabilities by using gain media with the smallest saturation fluence.

The second part of the work will deal with the design and development of SESAM modelocked diode-end-pumped Nd:YVO₄ lasers. This part will include a discussion on the resonator design criteria's for achieving a stable modelocked diode-end-pumped solid-state laser. The choice of using Nd:YVO₄ as a gain medium will be shown to be influenced by its large cross sectional area, which is useful in increasing the gain bandwidth for possible ultrashort pulse generation. The resonator for high power continuous wave (cw) output has been designed using simulation software developed at St Andrews University. We will also discuss stability criteria such as the laser spot size inside the crystal and on the end mirror and how they can be incorporated into the resonator design software. The discussion will also include the pump setup design and the efficient cooling method of the crystal using a copper heat sink.

The methodology of obtaining stable, thermal lens invariant, single transverse mode operation during power scaling of Nd:YVO₄ lasers will be discussed. A lens relay approach is used to extend the cavity length so as to introduce spot size control in the designed diode-end-pumped Nd:YVO₄ laser that will be shown to produce a maximum average output power of 10.5 W with an average beam quality factor M^2 of 1.5. We will also discuss the incorporation of a single quantum well SESAM within the extended diode-end-pumped Nd:YVO₄ laser resulting in cw-modelocked pulses at an average output power of 2.8 W with pulse repetition frequency of 179 MHz, equivalent to the cavity round trip time of 5.6 ns. The incorporation of the double quantum well SESAM will also be shown to produce stable Q -switched modelocked pulses at an average output power of 2.7 W with pulse repetition frequency of 208 KHz.

Opsomming

Hierdie tesis bestaan uit twee dele. Deel 1 is 'n indiepte bespreking rondom die ontwikkelingsgeskiedenis van Modusgebonde lasers, veral van Neodemiumdoteerde lasers. Deel 2 beskryf die ontwerp en ontwikkeling van 'n Modusgebonde diode-entgepompde vastetoestand Nd:YVO₄ laser deur van 'n Halfgeleier Versadigbare Absorbeerder (SESAM) gebruik te maak.

Die eerste afdeling fokus op Modusbinding om ultrakort pulse te ontwikkel in verskillende tipes lasers. Die bespreking sentreer rondom Neodemiumdoteerde lasers soos Nd:YVO₄. In hierdie geval beskou ons ook die spektraaleienskappe van die laser vir beide die absorpsie en emissie golflengtes. Verder word verskillende tipes pompbronne ondersoek (soos diodelasers en flitslampe). Die voordele van diodelasers kom sterk na vore a.g.v. beter werking en effektiwiteit. Verskillende pomppostellings word ook ondersoek naamlik ent-en kantpompings. Entpompings kom hier na vore as die beter opsie i.t.v. laser-moduspassing. Dit lei tot 'n hoër effektiwiteit wat 'n beter straalkwaliteit tot gevolg het, in vergelyking met kantgepompde opstellings. Die versterkingsbandwydte word ook bespreek: 'n groot versterkingsbandwydte en breë emissiebandwydte is geskik om ultrakort pulse te ontwikkel. Ti:Saffier is 'n goeie voorbeeld. Ultravinnige lasers met 'n klein versterkingsbandwydte word ook bespreek aangesien dit geskik is vir diode-entpompings wat dan 'n hoër gemiddelde uitsetdrywing lewer. Nd:YAG en Nd:YVO₄ word ondersoek en daar word getoon dat hul pulse van so kort as 19 ps en 20 ps onderskeidelik teen 'n gemiddelde uitsetdrywing van 27 W en 20 W kan lewer. Die tegniek waarmee ultrakort pulse geskep word is Modusbinding: passiewe modusbinding is meer geskik vir femtosekonde pulse en aktiewe modusbinding is meer geskik vir pikosekonde pulse. Verder word versadigbare absorbeerdere bespreek, vir hul gebruik in die betroubare selfinisiërende modusgebonde pulse. Die onstabiele geassosieer met versadigbare absorbeerdere word ook bespreek asook verskillende metodes om dit te minimaliseer.

Die tweede afdeling behandel die ontwerp en ontwikkeling van 'n SESAM modusgebonde diode-entgepompde Nd:YVO₄ laser. Die resonator ontwerp spesifikasies vir stabiele werking word ook bespreek. Die keuse van Nd:YVO₄ as versterkingsmedium

is a.g.v. die groot deursnitarea wat die versterkingsbandwydte verhoog, om ultrakort pulse te genereer. Die resonator vir hoë drywing kontinuestraal werking is ontwerp deur van St Andrews sagteware gebruik te maak. 'n Bespreking van stabiliteitsspesifikasies soos die laser kolgrootte, binne die kristal asook op die entspieël volg, asook die pompmetodiek en effektiewe verkoeling van die kristal. Die totale metodiek rondom die verkryging van 'n stabiele, termieselens invariante, enkele transversale modus laser word bespreek met die oog op drywingsverhoging. Die geval onder bespreking is waar die laser se kolgrootte beheer kan word op die entspieël deur die resonatorlengte aan te pas. Dit word getoon dat dit 'n kontinuestraal laser van 10.5 W drywing kan lewer teen die maksimum gemiddelde straalkwaliteit van $M^2 = 1.5$. Die byvoeging van 'n enkele kwantumput SESAM in die laser het modusgebonde pulse tot gevolg. Die gemete waardes was 2.8 W gemiddelde drywing met 'n pulsherhalingstempo van 179 MHz wat in lyn is met die pulsbevegingstyd in die resonator van 5.6 ns. Deur van 'n dubbele kwantumput SESAM gebruik te maak word Q-geskakelde modusgebonde pulse verkry, teen 'n gemiddelde uitsetdrywing van 2.7 W en 'n pulsherhalingstempo van 208 KHz.

Acknowledgements

I am indebted to the many colleagues who all can not be named, who have over the course of this work supported and provided me with their expertise. But in particular, I would like to thank Dr. Christoph Bollig for providing guidance and technical leadership in making this work a success. I would also like to thank Professor Hubertus von Bergmann at the Laser Research Institute, University of Stellenbosch, for the support and patience he has shown for this work to be feasible and completed and all other people at the LRI who have made my studies a success.

I would also like to give a special thanks to Dr. Ludwig Combrick of HartRAO who introduced and gave me the opportunity to study lasers. I would also like to thank the National Laser Center for the financial support and the support they have shown towards the work which I have done.

Contents

Abstract	iii
Acknowledgements	vii
Contents	viii
List of figures	x
List of tables	xv

Part 1- Ultrashort pulse lasers

1. Introduction	1
1.1 History of modelocking	1
2. Nd: Lasers	5
3. Optical pump sources	10
3.1 Flashlamp source	10
3.2 Diode laser source	11
3.2.1 Side-pumping of gain medium using laser diode	13
3.2.2 End-pumping of gain medium using laser diode	14
4. Gain Media for ultrashort pulse generation	15
5. Modelocking	21
5.1 Active modelocking	28
5.2 Passive modelocking	32
5.3 Saturable absorbers for passive modelocking	42
5.3.1 Semiconductor absorbers	42
5.3.2 Q-Switching instabilities	46
5.4 Summary	50

Part 2 - Design and evaluation of a SESAM modelocked diode-end-pumped Nd:YVO₄ laser

6.	Experimental design	51
6.1	Resonator stability criteria	51
6.2	Resonator design and pump setup	54
6.3	Pump beam characterization	56
6.4	Laser medium	60
6.5	Cooling method for Nd:YVO ₄ crystal	62
6.6	Summary of the design	63
7.	Diagnostic instruments	64
8.	Results	66
8.1	Power scaling of Nd:YVO ₄ laser	66
8.2	Requirements for modelocking a Nd:YVO ₄ laser using SESAM	70
8.3	Calculation of Nd:YVO ₄ resonator parameters for cw-modelocking	74
8.4	Results of the 1:1 relay system on the Nd:YVO ₄ laser.	77
8.5	Results of modelocking a Nd:YVO ₄ laser using a SESAM.	83
9.	Conclusion	88
	References	91
	Appendix	104

List of figures

- Figure 2-1:** Energy level diagram of Nd^{3+} ion in YAG crystal, Stark levels [2.3] 6
- Figure 2-2:** Four level energy diagram of Nd^{3+} in YVO_4 , with inter-Stark transition between the $^4\text{F}_{3/2}$ and $^4\text{I}_{11/2}$ manifolds [2.4]. 7
- Figure 2-3:** Polarization absorption spectrum of $\text{Nd}:\text{YVO}_4$ [2.5]. 8
- Figure 2-4:** $\text{Nd}:\text{YVO}_4$ fluorescence spectrum [2.4] 9
- Figure 3-1:** Flashlamp filled with xenon or krypton gas [3.1] 10
- Figure 3-2:** Schematic representation of a diode laser. 11
- Figure 3-3:** Radiation from a vertical laser diode stack, where the red pipe supplies water to cool the stack during operation [3.2]. 12
- Figure 3-4:** Schematic of a side pumped solid state laser. 13
- Figure 3-5:** Schematic of an end-pumped solid state laser. 14
- Figure 4-1:** Schematic diagram of spectral output of a laser without mode selection [2.2] 17
- Figure 5-1:** Time signal $E(t)$ and its intensity power spectrum for the same signal repeated once and two times in succession. The carrier frequency ω_c of the sine wave signal is shown not to coincide with any of the axial modes ω_q [5.1].23
- Figure 5-2:** Spectral intensity of the same signal repeated 10 times [5.1]. 24

Figure 5-3: Intensity patterns in time that can be synthesized using $N = 8$ equally spaced frequency components with different relative amplitudes and phase angles.	26
Figure 5-4: Instantaneous and average laser power versus time for a modelocked laser exhibiting large Q-switching instabilities [5.1].	26
Figure 5-5: Instantaneous laser power versus time for a stable cw- modelocked laser [5.1].	27
Figure 5-6: Longitudinal modes amplitude-modulated at the frequency $\Delta = \omega_q$ equal to their spacing. For clarity the AM side bands are indicated as dashed lines slightly displaced from the mode frequencies ω_m [5.4].	28
Figure 5-7: Schematic diagram of an active modelocked laser with a cavity round trip time T_R [5.2].	29
Figure 5-8: Schematic setup of an actively modelocked laser.	30
Figure 5-9: Temporal evolution of optical power and losses in an actively modelocked Laser [5.4].	31
Figure 5-10: Schematic diagram of a passively modelocked laser with a cavity round trip time T_R [5.2].	32
Figure 5-11: Schematic setup of a laser which is passively modelocked with a saturable absorber mirror, e.g. a SESAM [5.4].	33
Figure 5-12: Computer simulation of the evaluation of a modelocked pulse from noise. (a-c) regime of linear amplification and linear dye absorption, (d-e)	

nonlinear absorption in the dye cell, (f) regime on nonlinear amplification, dye completely bleached [5.6]. 34

Figure 5-13: Graph of the ratio of peak intensity (I_p) to the saturation intensity versus the effective loss (q) for a fast saturable absorber, where the bottom curve represents $q(I_p)$, the middle curve the Gaussian pulse and top curve the soliton pulse. 36

Figure 5-14: Graph of the normalized loss (q) versus the saturation parameter (S) for a slow saturable absorber, where the solid line represents the loss for a pulse and the dotted curve the loss of the absorber after the pulse. 37

Figure 5-15: Temporal evolution of optical power and losses in a passively modelocked laser with a fast saturable absorber [5.4]. 39

Figure 5-16: Temporal evolution of optical power and losses in a passively modelocked laser with a slow saturable absorber [5.4]. 39

Figure 5-17: A SESAM can absorb photons, whereby electrons are transferred from the valence band to the conduction band [5.2]. 43

Figure 5-18: Structure of a typical SESAM for operation around 1064 nm [5.4]. 44

Figure 5-19: Schematic of the topmost layers of the double quantum well SESAM [5.14]. 45

Figure 5-20: Schematic diagram of the Q-switched modelock transition between zone 2 and zone 3 [5.2]. 47

Figure 5-21: Output power of a SESAM modelocked laser verses input power; showing three different regimes which are cw-regime, Q-switched modelocked

regime and the cw-modelocked [5.2].	48
Figure 6-1: User interface of St. Andrew's design software PSST! representing a resonator cavity length of 225 mm where $L_1 = 150$ mm and $L_2 = 75$ mm.	55
Figure 6-2: Schematic representation of the laser with a cavity length of 225 mm, where M1 is the output coupler, M2 the pump mirror and M3 the end mirror.	56
Figure 6-3: Pump beam profile of the laser diode at the focus.	57
Figure 6-4: Slope efficiency of the laser diode at 30°C.	58
Figure 6-5: Pump beam profile for a focal length of 46.9 mm.	59
Figure 6-6: Absorption spectrum of 1 atomic % Nd:YVO ₄ , where the π -polarization is 42 cm ⁻¹ and σ -polarization is 11cm ⁻¹ .	61
Figure 6-7: Nd:YVO ₄ crystal sandwiched between two copper heat sinks. The glue was used only to secure the crystal.	62
Figure 6-8: Top view (a) and side view (b) of the crystal mount.	63
Figure 7-1: Coherent LM-45 power meter and Coherent Field Master readout.	64
Figure 7-2: Coherent CCD camera and the Spiricon M ² -200 instrument.	65
Figure 7-3: Tektronix 500 MHz oscilloscope and the Hamamatsu photo diode detector.	65
Figure 8-1: Resonator with cavity length of 225 mm showing resonator mirrors and other components.	66

Figure 8-2: Slope efficiency for the lasers with cavity lengths of 225 mm, 200 mm and 170 mm.	67
Figure 8-3: Beam profiles of lasers with cavity length of 170 mm, 200 mm and 225 mm at an average output power of 8 W.	68
Figure 8-4: Beam quality factor M2 versus pump power for the laser with a cavity length of 225 mm.	69
Figure 8-5: Q-switched modelocked transitions ($P_{QSM,th}$) average output power at different temperatures for a single quantum well SESAM [8.1].	72
Figure 8-6: Temperature tuning of a single quantum well SESAM [8.1].	73
Figure 8-7: Schematic diagram of the 1:1 relay system laser resonator with a cavity length of 825 mm.	77
Figure 8-8: Arrangement for measuring the laser spot size using a ccd camera behind the flat high reflector end mirror.	78
Figure 8-9: Derived spot sizes measured at distances of 2.5 mm up to 25 mm behind the end mirror of the laser with a cavity length of 825 mm at an average output power of 7 W. The + and – sign show the far field and near field solutions for each measured spot size diameter.	80
Figure 8-10: Slope efficiency of the laser with cavity length of 825 mm.	81
Figure 8-11: Beam quality factor at different input powers of the lasers with cavity lengths of 225 mm and 825 mm.	82

- Figure 8-12:** Beam profile at different output power for the lasers with cavity lengths of 225 mm and 825 mm. 83
- Figure 8-13:** Long 825 mm laser resonator with a SESAM mounted on to a thermoelectric device. 84
- Figure 8-14:** Continuous wave modelocking at an average output power of 2.8 W using a SQW SESAM which was not temperature controlled. 85
- Figure 8-15:** Continuous wave modelocking at average output power of 2.8 W using a SQW SESAM temperature controlled at 30°C. 86
- Figure 8-16:** Stable Q-switched modelocking at average output power of 2.7 W using a DQW SESAM temperature controlled at 30°C. 87

List of tables

Table 4.1: CW modelocked solid-state lasers using different modelocking techniques. ML: modelocking. SESAM: saturable absorber modelocking using SESAMs. CCM: coupled cavity modelocking. APM: additive pulse modelocking. Soliton-SESAM: Soliton modelocking with a SESAM. KLM: Kerr lens modelocking.	16
Table 8.1: Designed laser resonator cavity lengths.	67
Table 8.2: Designed and calculated parameters of the modelocked laser. Non bold numerical figures are design parameters and bold numerical figures are calculated parameters.	75
Table 8.3 (a): Measured spot sizes at different distances.	79
Table 8.3 (b): Calculated spot sizes at different distances.	79

Part 1 – Ultrashort pulse lasers

1. Introduction

The laser is without doubt one of the greatest inventions of the last 50 years. The discovery of the laser nearly half a century ago has stimulated the use of light in an extremely wide range of applications spanning to medical, industrial, military and consumer applications and has also extended to environmental monitoring. The usefulness of the laser lies in its ability to produce electromagnetic radiation with a wide range of useful properties, including coherence, monochromaticity, high intensity, focusability, pulse shape and generation of ultrashort pulses. The latter, that is ultrashort pulse generation, is the focus of this research study.

The field of ultrashort pulse generation started in the mid-1960s, rather soon after the invention of the laser. Since then it has been developing rapidly, and indeed this process is still continuing, with new regimes of operation being penetrated by ultrafast lasers and with new types of ultrafast lasers being developed, for applications such as micromachining.

1.1 History of modelocking

The generation of ultrashort pulses in the order of picoseconds and femtoseconds is made possible by the technique of modelocking [1.1], which was first demonstrated in the mid-1960s by the use of gas lasers such as a HeNe laser [1.2] in 1964, then solid state lasers as the ruby laser [1.3] in 1965 and also a Nd:glass laser [1.4] in 1966. These lasers, however, had a problem that they were unable to produce cw-modelocked output i.e. an infinite train of pulses with constant energy. They only produced bursts of short pulses lasting for microseconds which were repeated with frequencies of around one kilohertz. This is because the saturable absorber used for generating modelocked pulses caused the laser to operate in a much-less-stable Q -switched modelocking regime. The Q -switched modelocked regime is unsuitable for many applications when compared to cw-modelocking, because it results in unpredictable pulses of high energy and peak

power. The tendency of a passively modelocked solid-state laser to operate in the unstable Q -switched modelocked regime was overcome in 1992, when for the first time; an intracavity saturable absorber was designed and manufactured, which then allowed for the prevention of the Q -switching instability [1.5]. The details of this theory will be discussed in detail in the next chapters.

The popularity of dye lasers [1.6] and colour center lasers [1.7] diverted attention away from solid state lasers during the late 1960's till the 1980's. In the mid 1970's the first femtosecond passively modelocked laser pulses (~ 300 fs) were generated from dye lasers [1.8, 1.9, 1.10], because Q -switching instabilities are not a problem for dye lasers due to their large emission cross section, which also allows for the generation of much shorter pulses. During the early 1980's there were two important discoveries in the generation of stable femtosecond pulses. In 1981 the first novel passive modelocking technique called colliding pulse modelocking (CPM) [1.11] was demonstrated using a dye laser yielding sub ~ 100 femtosecond pulses. For example the CPM dispersion compensated Rhodamine 6G-dye laser [1.13], generated pulses with durations of 27 fs with average output powers of 20 mW, which proved useful for many years in ultrafast laser spectroscopy. However, its lack of tuneability, poisonous and short lived dyes and limited output powers were a serious drawback. The second advancement occurred in 1983 when it was shown that the group velocity dispersion (GVD) in the laser oscillator could be continuously adjusted and optimized by introducing a prism sequence into the cavity [1.12]. In 1989 shorter pulses were produced by combining additional amplification and external pulse compression and pulses as short as 6fs at very low repetition rates [1.14] were demonstrated.

During 1989 and 1990 the advances in diode lasers to high average power impacted positively on diode pumped solid state lasers such as Nd:YAG and Nd:YLF producing much shorter pulses of 7 ps to 12 ps durations, respectively, when actively modelocked; a great improvement when compared to the flashlamp-pumped solid state lasers which generated pulses around 100 ps to 30 ps duration, respectively. However, passive modelocking of diode pumped solid state lasers proved difficult since it resulted in

Q-switching instabilities.

In 1991 the first passively modelocked solid state laser was a Kerr lens modelocked (KLM) [1.15] Ti:sapphire laser that produced pulses with durations of less than 6 fs [1.16, 1.17, 1.18] directly from the laser cavity without any additional external pulse compression. The Ti:sapphire medium renewed interest in ultrashort pulse generation since its broad fluorescence emission showed potential to support light pulses of only a few femtoseconds in duration. Much shorter pulses, less than 5 femtoseconds, have also been demonstrated using additional external pulse compression [1.19, 1.20] and continuum generation combined with parametric amplification [1.21], but these techniques all rely on KLM, high dispersion control and ultra-broadband amplification [1.22]. The limitation of the KLM laser lies in it not being self-starting and requiring a critical cavity alignment when optimizing the laser for short pulses. This in turn resulted in the reduction of the stability and efficiency of the laser output power. Based on these limitations of KLM and the development of semiconductor materials, the use of intracavity modelocking using semiconductor saturable absorber mirrors (SESAMs) became an attractive option.

The *Q*-switching instabilities and the passive non self-starting KLM of diode-pumped solid state lasers was overcome in 1992 by the use of SESAMs [1.4, 1.23] and the technique was also demonstrated for different types of solid state lasers with different gain medium. The main attraction of SESAMs is that they can be custom designed for both the linear and nonlinear optical properties over a wide range, thus allowing for more freedom in choosing a cavity design that suits a particular criteria. A diode pumped Nd:glass laser with pulses as short as 60 fs [1.24] duration has been demonstrated by modelocking with a low finesse, anti-resonant Fabry-Perot saturable absorber.

One advantage of the SESAM is that it can be manufactured for different types of operation regimes such as *Q*-switching or continuous modelocking since the absorbers saturation fluence, operation wavelength, absorber lifetime and modulation depth can be custom designed so as to fit the operation regime of the laser. The other advantage of the

SESAM is its simplicity as demonstrated in 1995 when it was integrated into a flat cavity mirror thus affording for both, negative dispersion control and saturable absorption [1.30; 1.31; 1.32].

Also in 1995 it was demonstrated, using soliton modelocking [1.25, 1.26, 1.27], that pulses with duration less than the absorbers recovery time can be formed using a SESAM. Here the pulse was formed by the soliton effect and the SESAM was used to start and stabilize the modelocking, though it was believed that if the net gain appears after the pulse, the pulse will not form. The way of how the saturable absorber can form pulses well below its recovery time was demonstrated in 2001 without the use of soliton effect [1.26], where the saturable absorber was shown to constantly delay the pulse, thereby attenuating the leading part which then shifted the center of the pulse. Soliton modelocking with Ti:sapphire lasers has also been demonstrated to produce pulses with durations as short as 13 fs [1.27].

The low SESAM damage threshold did limit the increase of average output power, but this was overcome, when a Nd:YAG laser produced 27 W of average power with 19 ps pulses [1.28]. In this work researchers demonstrated that it is the design of the laser gain material with small mode area that will allow suppressing Q -switching instabilities and avoid the SESAM being damaged by high peak powers. The problem of getting multi-watt output powers in the subpicosecond regime was also solved by the same idea of using thin disk laser gain material [1.29], where a thin disk Yb:YAG laser generated 16 W of average power with pulse durations of 730 fs [1.30]. This was achieved with the understanding that using low saturation fluence SESAMs with not too high modulation depth [1.31] will suppress Q -switching instabilities and also with the understanding of the effect of spatial hole burning in the laser gain material at high powers [1.32].

2. Nd: Lasers

The discovery of Neodymium yttrium vanadate (Nd:YVO₄) crystal as an important laser material occurred in the early 1966 [2.1]. Nd:YVO₄ fulfils most of the conditions for a high power gain medium. For example, the crystal can be doped with active Nd³⁺ ions, which occupy less than 1% of the lattice sites by substituting it with Y³⁺ of similar size. Initially the presence of absorbing colour center defects and scattering centers prevented the growth of high optical quality Nd:YVO₄ crystals in the early 1966. Today the crystal growth process has been improved so much that high quality crystals which are chemical inert are now readily available with very good optical quality [2.2].

The first stimulated emission using the rare earth ions was observed with the Nd³⁺ ion. The Nd³⁺ ion is a trivalent rare earth ion which has three electrons in the unfilled 4*f* subshell. This makes Nd³⁺ the obvious choice since it exhibits sharp laser transitions even in the presence of the strong local crystal fields as a result of the shielding effect of the outer complete 5*s*² and 5*p*⁶ subshells. The ground state of Nd³⁺ is Xe: 4*f*² 5*s*² 5*p*⁶ and this makes the angular momentum at the ground state for Nd³⁺ to total up to 6 which is expressed by letter *I*, since the orbital angular momentum is symbolised by letters where *s, p, d, f* stand for *l* = 0, 1, 2, 3, ... and the orbital angular momentum numbers *L* = 1, 2, 3, 4, ... are expressed by capital letters *S, P, D, F, G, ...*. The spins of three electrons which are aligned parallel or antiparallel to each other give a spin angular momentum of $\frac{3}{2}$ and $-\frac{3}{2}$ respectively, and when two electrons are aligned parallel and one electron antiparallel give an angular momentum $\frac{1}{2}$ and $-\frac{1}{2}$ vice versa [2.2].

These four combinations of spins result in a total angular momentum *J* of $\frac{9}{2}, \frac{11}{2}, \frac{13}{2}$ and $\frac{15}{2}$, since the angular momentum of *J* is the vector sum of *L* and *S*, where *S* is the combination of the resultant spin of valance electrons. The multiplicity of each of the angular momenta is 4, which is given by the quantum rule of 2*S*+1. Therefore according to the quantum rule of ^{2*S*+1}*L* *J* and the total angular momentum *J*, four energy levels corresponding to four different combinations which are ⁴*I*_{9/2} the ground state, and the first

few excited states ${}^4I_{11/2}$, ${}^4I_{13/2}$, and ${}^4I_{15/2}$ are presented. Higher excited states such as ${}^4F_{3/2}$ and ${}^4F_{5/2}$ can be obtained by other combination of L and S [2.2].

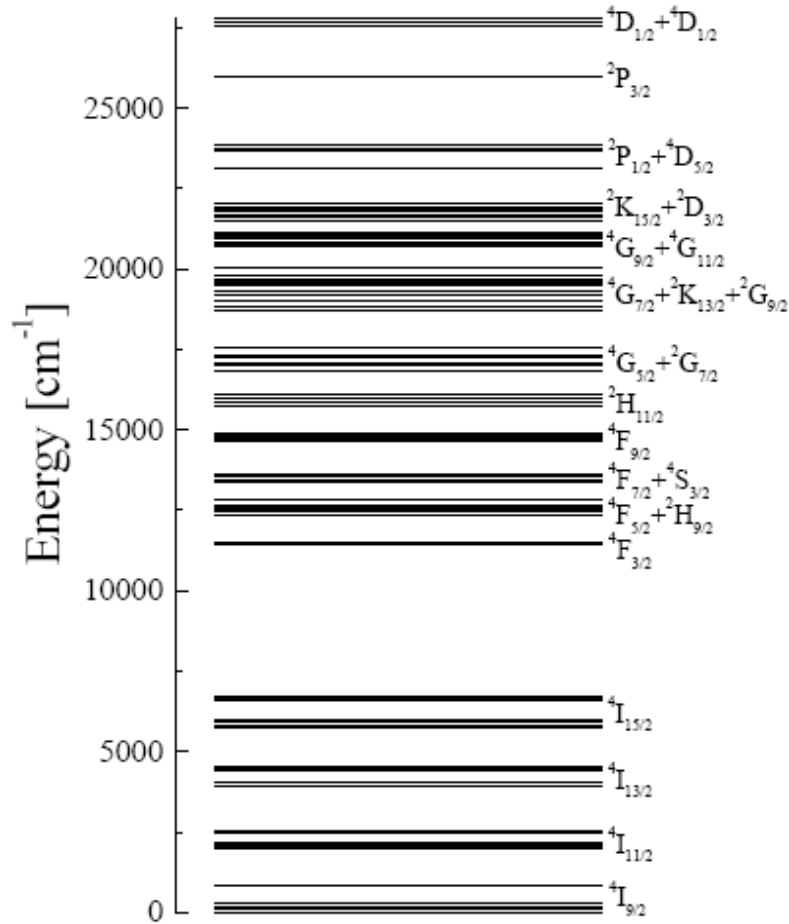


Figure 2-1: Energy level diagram of Nd^{3+} ion in YAG crystal, Stark levels [2.3]

The splitting of the Nd^{3+} free-ion energy levels or manifolds into sublevels of closely spaced levels is a result of the Stark effect due to the YAG crystal field. The magnitude of the Stark effect of Nd^{3+} varies depending on the host material. The energy levels of Nd^{3+} in a host material such as YAG can be illustrated by Figure 2-1 showing the Stark effects.

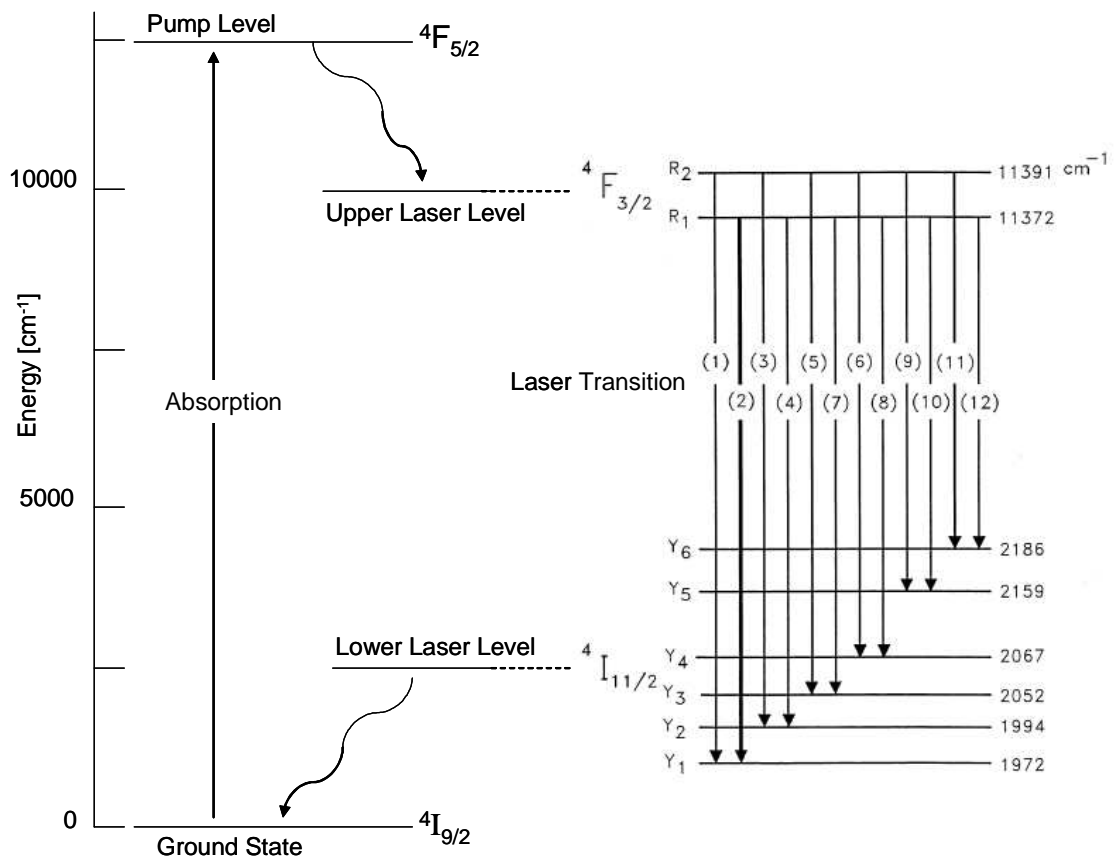


Figure 2-2: Four level energy diagram of Nd³⁺ in YVO₄, with inter Stark transitions between the ⁴F_{3/2} and ⁴I_{11/2} manifolds [2.4].

The Nd:YVO₄ laser is a four level system as shown in Figure 2-2. The Nd³⁺ ions in YVO₄ are excited from the ground state ⁴I_{9/2} to the pump level ⁴F_{5/2} by absorbing radiation energy at 808 nm which has the highest absorption cross section as depicted by the absorption spectrum of Nd:YVO₄ in Figure 2-3.

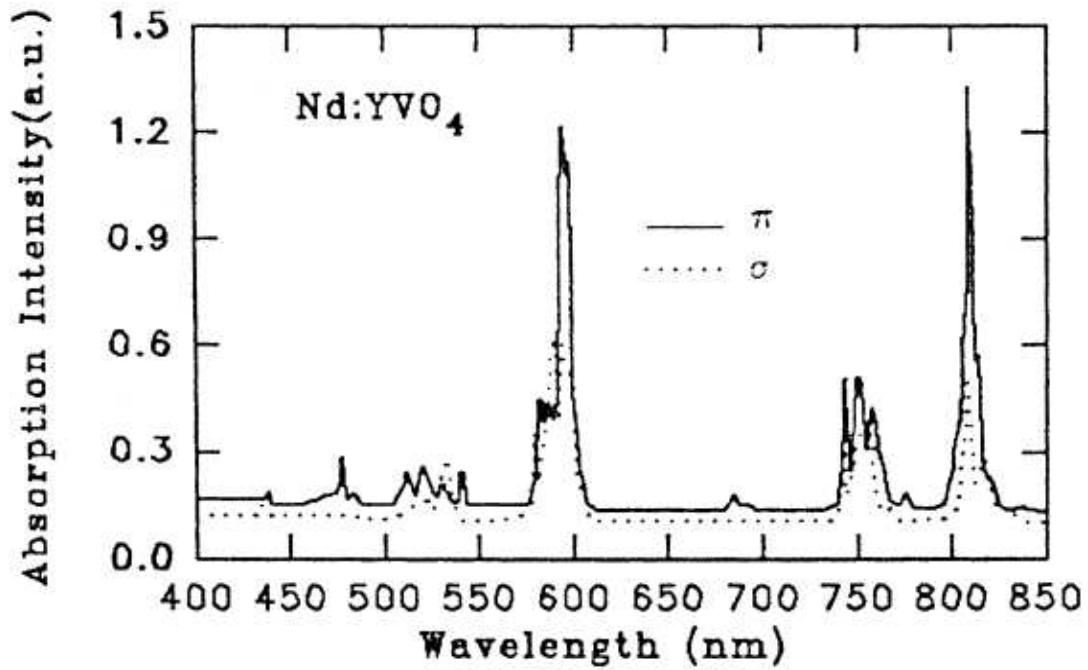


Figure 2-3: Polarization absorption spectrum of Nd:YVO₄ [2.5].

The excited ions at the pump level ${}^4F_{5/2}$ decay very fast to the next lower energy level ${}^4F_{3/2}$, the upper laser level. The 1064 nm line is the strongest stimulated laser transition, which occurs when the Nd³⁺ ion in the excited upper laser level ${}^4F_{3/2}$ decays by form of stimulated emission to the lower laser level ${}^4I_{11/2}$. This corresponds to the R₁ → Y₁ transition on Figure 2-2 and is designated as 2 on the fluorescence spectrum of Nd:YVO₄ in Figure 2-4.

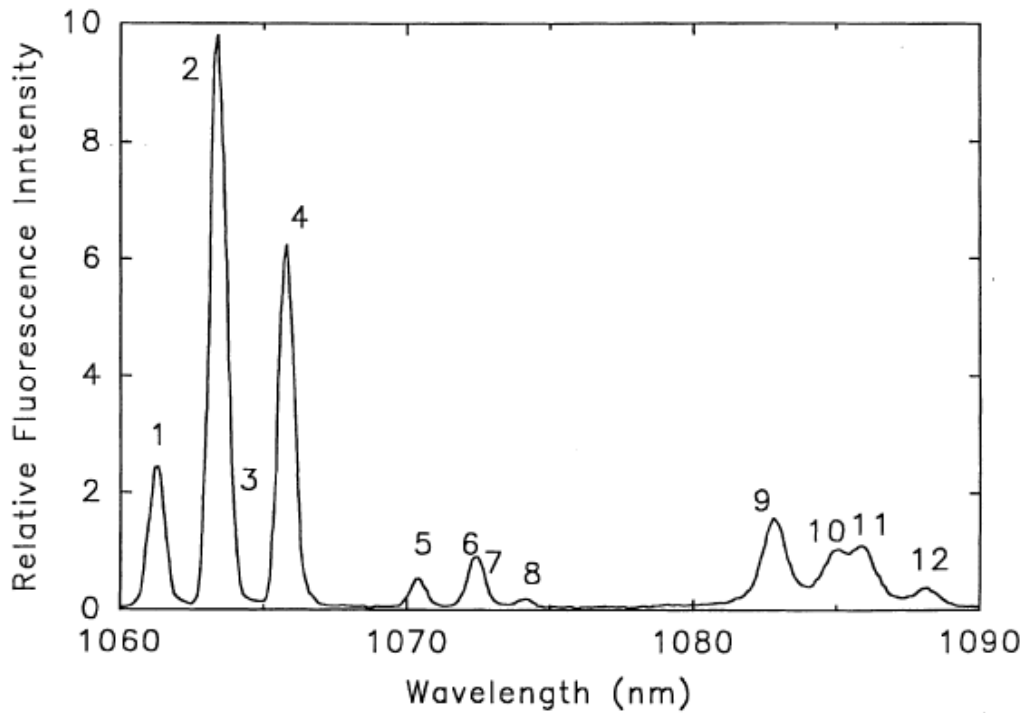


Figure 2-4: Nd:YVO₄ fluorescence spectrum [2.4]

The upper laser level of the Nd³⁺ ions $^4F_{3/2}$ is metastable with lifetimes ranging from 100 μ s in YVO₄ to 230 μ s in YAG, 330-340 μ s in Glass to 480 μ s in YLF. This makes all the ions which are transferred from the ground level to the pump level accumulate in the upper laser level creating a population inversion between the upper and lower laser level. The meta-stable upper laser level with its long fluorescence life time also means greater energy storage. The Nd³⁺ ion in the lower laser level decays very fast to the ground state and the life time of the lower laser level $^4I_{11/2}$ and the pump level $^4F_{5/2}$ are very short almost by a factor 100 to 1000 respectively for different crystals when compared to the upper laser level $^4F_{3/2}$ life time.

3. Optical pump sources.

There are several ways of pumping solid state lasers which have been employed extensively for quite some time, such as flashlamps, arc lamps and lately diode lasers. The choice of pump source influences the quality of the output laser beam as well as the laser operating conditions. As a general rule, the pump source which produces the maximum emission at wavelengths that excite fluorescence in the laser material, while producing minimal emission in all spectral regions outside of the useful absorption band, will be the most efficient pump sources to convert electrical input power into optical output power.

3.1 Flashlamp source

Flashlamps used for optical pumping are essentially arc discharge devices consisting of a quartz tube filled with xenon or krypton gas and enclosed by two electrodes at the end of the tube. Applying a high voltage between the electrodes causes an arc discharge to occur inside the tube. The spectral distribution of the emitted light from the gas discharge is very broad. However, the overlap efficiency of the absorption band of the laser crystal and the emission of the arc lamp is very low and only a small fraction of the radiation is absorbed by Nd^{3+} ions in the ground state.



Figure 3-1: Flashlamp filled with xenon or krypton gas [3.1]

The electrical to optical efficiency for solid state lasers such as Nd:YAG is in the order of a few percents when using flashlamp pumping. The main disadvantages of lamp pumped solid state lasers are the short life time of the lamps and the high voltages needed to discharge the arc lamps. The unreliability of the laser output due to the instabilities of the discharge of the flashlamps and their bulkiness also limits their usage.

3.2 Diode laser source

Diode lasers used for optical pumping of solid state lasers are essentially semiconductor based, where a pn-junction is formed by doping the one part with electron donors to form n-type material and the other part with electron acceptors to produce a p-type material. In order to produce stimulated emission in the pn-junction, the junction is forward biased by applying voltage to the pn-junction and thereby creating a population inversion and optical gain. Optical feedback is created by a Fabry-Perot resonator by cleaving and chipping the end face of the material along the parallel crystal plane (see Figure 3-2).

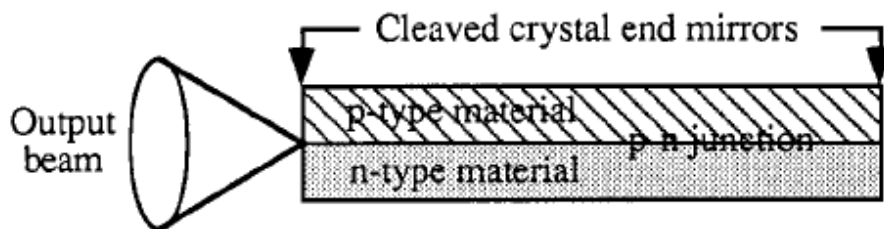


Figure 3-2: Schematic representation of a diode laser.

The advantages of using diode lasers as pump sources for solid state lasers stem from the fact that they are monochromatic, have narrow spectral bandwidth, high brightness and are directional (see Figure 3-3). The diode laser emission wavelength falls within the absorption band of Nd^{3+} ions at 808 nm. This yields a higher efficiency when compared to flashlamp pumping systems. This is despite the fact that flashlamps have a higher efficiency in respect of total radiation output to electrical input of up to 70% when compared to laser diodes of 25 to 50%.



Figure 3-3: Radiation from a vertical laser diode stack, where the red pipe supplies water to cool the stack during operation [3.2].

The long lifetime of laser diodes is another positive factor. Diode lasers have a lifetime in the order of 10 thousand hours in cw operation and 10^9 shots in the pulsed mode, compared to flashlamps with an operation lifetime of 500 hours cw and 10^8 shots pulsed.

The beam quality of the solid state laser also improves greatly when pumped with diode lasers and particularly in an end-on configuration. This can be attributed to the very good overlap between the diode laser emission and the wavelength absorption band of Nd^{3+} ions, which reduces the amount of heat deposited in the crystal, when compared to flashlamp side-pumped systems where the whole crystal is illuminated by the discharge increasing the heat deposited into the crystal. The output brightness of the solid state laser can also be improved by creating a good spatial overlap between the resonator mode and the diode pump beam.

A further feature which has caused wide range usage of diode lasers is the ability and the flexibility of shaping and transferring the output beam from the diode pump source to the solid state laser material by optical fibres. This has greatly reduced the bulkiness of diode-pumped solid state lasers when compared to flashlamp-pumped lasers. The flexibility of coupling the diode radiation into the solid state laser material has created

various types of solid states lasers, such as microchip lasers, end-pumped systems and side-pumped systems which will be discussed in the next section.

3.2.1 Side-pumping of gain medium using laser diode

A basic configuration for side pumping is illustrated in Figure 3-4. In this instance the laser crystal is illuminated along the whole length by the pump diode laser radiation. However, while desirable, direct coupling of the diode laser radiation proves inefficient due to the non flexibility of shaping the pump radiation which then makes this method unsuitable. The use of imaging optics such as lenses, elliptical and parabolic mirrors to couple the diode radiation into the crystal is the favoured method since the pump distribution from the diode laser can be designed to peak at the centre of the crystal, allowing for better match with resonator mode TEM_{00} .

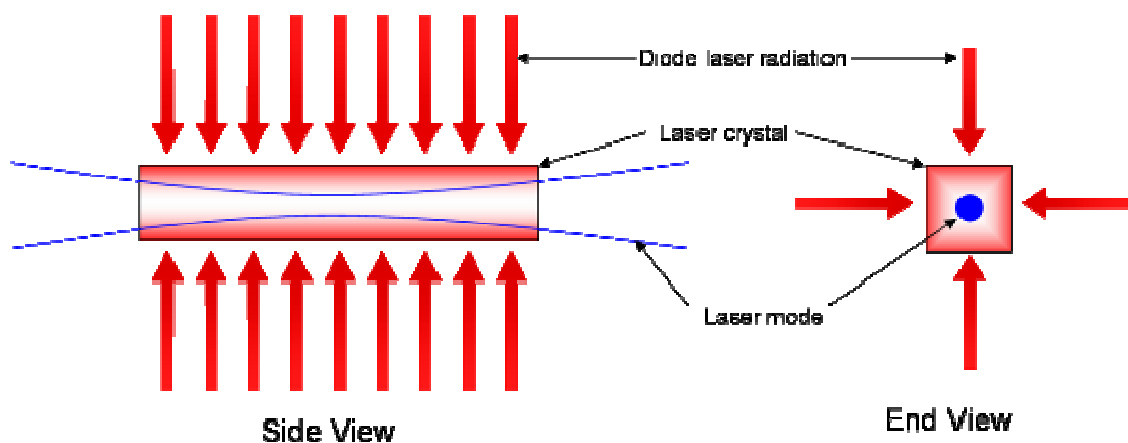


Figure 3-4: Schematic of a side pumped solid state laser.

The side pumping configuration in Figure 3-4 shows that the whole crystal can be excited and the whole crystal acts as the gain medium for the laser. One disadvantage of side-pumped lasers is that the spatial overlap of pump radiation and laser mode only occurs at the centre of the gain medium and not at the edges of the crystal where there is a high gain. This makes the side pumped laser less efficient since the intensity of the stimulated emission is determined by how good the spatial overlap is between pump beam and laser mode. Poor spatial overlap of the laser mode and pump radiation means

that the unutilized pump radiation is deposited inside the crystal as heat, which might lead to reduced efficiency since this energy can not be extracted. This also leads to poor beam quality since high order modes can occur.

3.2.2 End-pumping of gain medium using laser diode

End-pumping of the gain medium is achieved by introducing the diode laser radiation longitudinally to the axis of the gain medium, which is collinear with the laser mode in the resonator as illustrated in Figure 3-5.

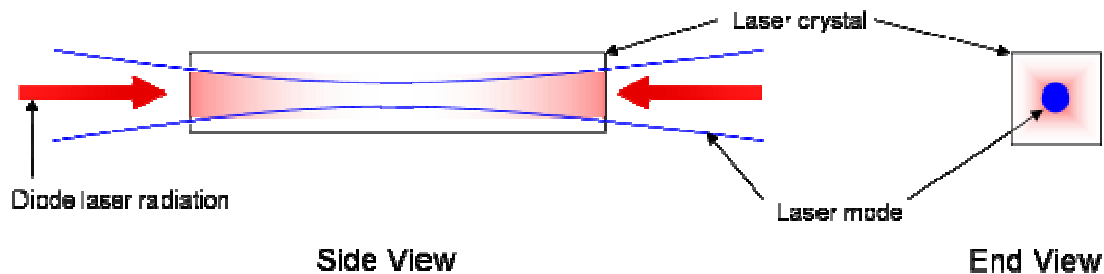


Figure 3-5: Schematic of an end-pumped solid state laser.

The excellent spectral overlap of the radiation emitted by the pump diode lasers and the absorption band of the solid state laser material in conjunction with the good spatial overlap with the laser mode volume in the resonator makes the end-pumped system the most efficient geometry for diode pumped lasers.

If the end-pumping configuration is properly designed so that the pump beam is collinear with the resonator mode, the solid state laser usually emits a very good beam quality, and high order modes are eliminated by the limited gain for higher order transverse modes.

4. Gain Media for ultrashort pulse generation

For a gain medium to be suitable for ultrafast pulse generation it has to meet a number of conditions. The first condition for cw laser operation is that the gain medium should have a laser transition in the desired wavelength range. The pump transition should be at a wavelength for which pump sources are readily available. For the laser to have a high efficiency the gain medium should have a high quantum efficiency at the transition of interest. The gain medium should be suitable for use with a relatively high transmission output coupler, so that the laser will be less sensitive to intracavity losses. The gain medium should have good optical, mechanical and thermal properties for high power laser application; including hardness, chemical inertness, absence of internal strain and refractive index variation, resistance to radiation-induced colour centres. They should also have a lattice which is able to accept suitable dopant ions and large scale fabrication of the gain medium should be relatively easy.

The second main condition for generating ultrashort Gaussian pulses comes from the time-bandwidth product given as:

$$\tau_p \Delta\nu_p = \left(\frac{2 \ln 2}{\pi} \right) \left[1 + \left(\frac{\beta}{\alpha} \right)^2 \right]^{\frac{1}{2}}, \quad (4.1)$$

where τ_p is the pulse length, $\Delta\nu_p$ the pulse bandwidth limit at full width half maximum, β the pulse chirp and α determines the Gaussian envelope of the pulse [4.1].

The exact value of the time-bandwidth product $\tau_p \Delta\nu_p$ depends on the exact shape of the pulse (Gaussian, square, exponential, ect.) and especially on the amount of chirp or other amplitude or phase substructure within the pulse. For a Gaussian pulse where $\beta = 0$, signifying that there is no frequency chirp, one obtains:

$$\tau_p \Delta\nu_p \approx 0.44, \quad (4.2)$$

and the time-bandwidth product for a chirped Gaussian pulse is more than in Equation 4.2.

Therefore, a laser material with a very large gain bandwidth will support a very short pulse length as shown by Equation 4.2 for a pulse with a Gaussian shape. Gain bandwidth is a property of a laser material. The following Table 4.1 shows some of the ultrashort pulses which have been achieved using different gain materials. The table shows that the laser material Ti:Al₂O₃ with the largest bandwidth of 73.33 THz is able to generate shortest pulses of 6 fs while the laser material Nd:YVO₄ which has the smallest bandwidth of 0.163 THz has the longest pulse duration of 2.7 ps. A laser material with a very large gain bandwidth and a broad emission bandwidth is most suitable for ultra short pulse lasers.

Table 4.1: CW modelocked solid-state lasers using different modelocking techniques. ML: modelocking. SESAM: saturable absorber modelocking using SESAMs. CCM: coupled cavity modelocking. APM: additive pulse modelocking. Soliton-SESAM: Soliton modelocking with a SESAM. KLM: Kerr lens modelocking.

Laser material	ML technique	Laser wavelength	Pulse duration	Bandwidth	Reference
Nd:YVO ₄	SESAM	1.064 μm	2.7 ps	0.163 THz	[4.2]
Nd:YAG	CCM-APM	1.064 μm	1.7 ps	0.259 THz	[4.3]
Yb ³⁺ :KGW	Soliton-SESAM	1.037 μm	112 fs	3.93 THz	[4.4]
Yb ³⁺ :YAG	Soliton-SESAM	1.03 μm	340 fs	1.29 THz	[4.5]
Nd ³⁺ :glass	Soliton-SESAM	1.065 μm	60 fs	7.33 THz	[4.6]
Cr ²⁺ :LiSGaF	KLM	895 nm	14 fs	31.4 THz	[4.7]
Ti:Al ₂ O ₃	KLM	~800 nm	6 fs	73.3 THz	[4.8]

For the laser material to have a broad emission bandwidth, the gain material should have a large range of wavelengths where a smooth shaped gain spectrum is obtained at a fixed inversion level, as shown in Figure 4-1. The difficult requirements of a gain medium to

have a large range of wavelengths where there is a fixed inversion explains why the achievable modelocked bandwidth is in some cases considerably smaller than the tuning range achievable with tuneable cw lasers, particularly for quasi-three-level gain media such as Yb^{3+} -doped media [4.9] where the emission bandwidth is small and the gain large.

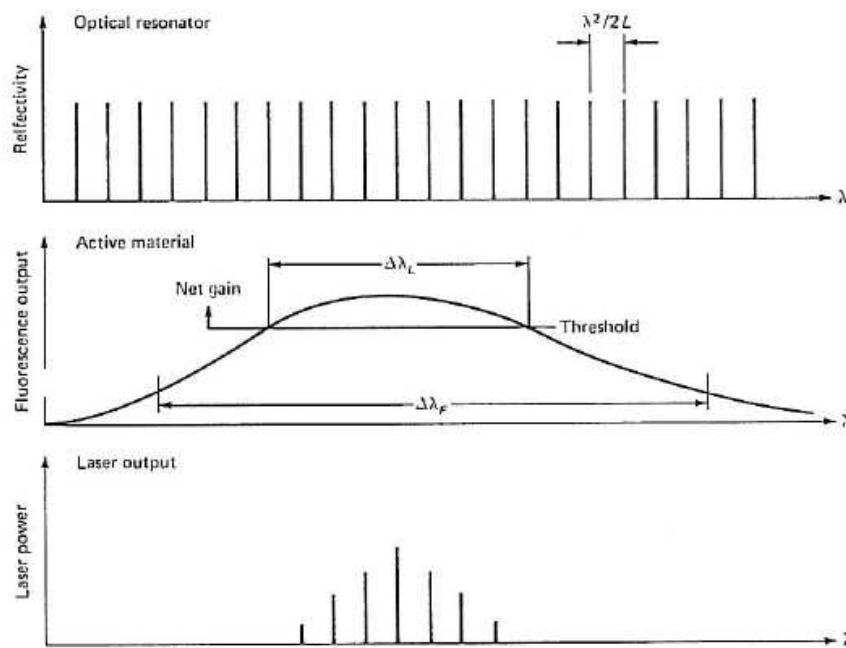


Figure 4-1: Schematic diagram of spectral output of a laser without mode selection [2.2]

The stimulated gain emission cross section, σ needs to be also large to obtain a large gain bandwidth, even though a reasonably small pump threshold can be obtained using a low emission cross section if the fluorescence lifetime is large enough. But it can be difficult to overcome Q -switching instabilities in a passively modelocked laser because of the gain medium having a low laser emission cross section. There are limited numbers of broad-band gain laser materials which are used in passive modelocking because they are hindered by the fact that they have a low gain emission cross section, especially at high pulse repetition rates and in other situations where a poor pump beam quality or poor thermal properties create large mode areas in the gain medium.

There are two different types of ultrafast lasers. The first type is based on a gain medium with small amplification bandwidth which makes this type of laser very suitable for diode pumped high power cw operation. The fact that these ultrafast lasers such as Nd:YVO₄ and Nd:YAG have a small amplification bandwidth means that they can not be used in femtosecond pulse generation.

Using high power laser diodes in an end-pumping or side-pumping configuration and using a SESAM for modelocking, these lasers have produced laser pulses as short as 19 ps with an average output power of 27 W using Nd:YAG [4.10] as the gain medium; and 20 ps with average output power of 20 W with Nd:YVO₄ [4.11]. Much shorter pulses of 1.5 ps with 20 mW output power have been achieved by the method of additive pulse modelocking [4.12]. The stimulated emission cross section of these laser materials, Nd:YAG and Nd:YVO₄ is relatively large, which means they can achieve stable modelocking by avoiding the *Q*-switching instabilities of the SESAM.

The second type of ultrafast lasers is determined by a larger and broader amplification bandwidth which can be used to create pulses which are less than 0.5 ps in duration, with the decrease in the pulse duration mostly limited by lower emission cross section and thermal stress of the material, which is attributed to poor thermal properties of the gain medium.

Titanium sapphire (Ti:Al₂O₃) is a suitable laser material for ultrafast lasers because of the combination of desired gain medium properties for ultrafast lasers [4.13]. These properties include very high thermal conductivity, good chemical inertness, mechanical rigidity and the relatively large gain cross section, which is half of that of Nd:YAG, and a long fluorescence lifetime. Ti:sapphire crystals have a broad absorption band located in the blue-green region of the visible spectrum with the maximum absorption peak at 490 nm. The location of the absorption band requires pumping sources for Ti:sapphire lasers to be argon ion lasers or frequency doubled diode-pumped, solid-state lasers since there are no commercially available diode lasers at 490 nm wavelength. Ti:sapphire lasers using Kerr lens modelocking (KLM) and SESAM for self starting modelocking

[4.15] have been shown to produce average powers of close to 1 W with pulse durations below 6 fs [4.14]. The usage of only SESAMs to modelock Ti:sapphire lasers has been shown to produce average powers of 80 mW at pulse durations of 13 fs [4.16]. Another gain medium very similar to Ti:sapphire with a very broad bandwidth is $\text{Cr}^{2+}:\text{ZnSe}$. It emits radiation in the mid-infrared around 2.2 to 2.8 μm and has been demonstrated to produce pulses with duration of around 4 ps [4.17]. $\text{Cr}^{2+}:\text{ZnSe}$ has the potential of producing pulses well below 20 fs because of its broad bandwidth.

The use of phosphate and silicate glasses doped with rare-earth ions like Nd^{3+} and Yb^{3+} also produces materials with broad bandwidth, suitable for generating pulses with durations well below 60 fs and output powers in a region of a few hundred mW [4.18, 4.19], which is limited by the poor thermal properties of the lasing material. The $\text{Nd}^{3+}:\text{glass}$ laser has been able to produce pulses with an average output power of 1.4 W with a pulse duration of 275 fs [4.20] and another $\text{Nd}^{3+}:\text{glass}$ laser with slightly less average output power of 1 W with a shorter pulse duration of 175 fs [4.21] was demonstrated. High average powers above 2 W have not been obtained with these lasers due to poor thermal properties of the lasing material even when using a thin gain medium which can be efficiently cooled from both flat sides when using a strongly elliptical pump beam and laser mode geometry [4.22]. The elliptical pump geometry makes the heat flow to resemble a one dimensional type of heat flow, which reduces the thermal lensing greatly when comparing to cylindrical rod geometry with sufficiently large aspect ratio.

There is also $\text{Yb}^{3+}:\text{YAG}$ with a much large amplification bandwidth when compared to $\text{Nd}^{3+}:\text{YAG}$, but with similar properties such as thermal conductivity, favourable small quantum defects and a small laser cross section favouring Q -switching. End-pumping of $\text{Yb}^{3+}:\text{YAG}$ rod lasers has been demonstrated to generate short pulses with durations of 340 fs and output powers of 170 mW [4.23], while other $\text{Yb}^{3+}:\text{YAG}$ lasers with an elliptical laser mode have been demonstrated to generate high average output power of 8.1 W but with somewhat longer pulse durations of 2.2 ps [4.24]. There are also passively modelocked thin disk $\text{Yb}^{3+}:\text{YAG}$ lasers [4.25], which can generate pulses with a duration of 700 fs and average output power of 16.2 W [4.26]. The quasi-three-level nature and

the small cross section area of Yb^{3+} :YAG makes it difficult for power scaling, but strong pumping of a passively modelocked Yb^{3+} :YAG thin disk laser has shown that power scaling is possible and this has been demonstrated by an average output power of 60 W with a pulse duration of 5 ps [4.27] with power levels expected to grow.

There are many other Yb^{3+} -doped gain materials such as Yb^{3+} :SFAP [4.28], Yb^{3+} :KGW [4.29], Yb^{3+} :YCOB [4.30] and Yb^{3+} :YGdCOB [4.31], which have a relatively broad amplification bandwidth. These are sufficient for generating pulses in the range of hundreds of femtoseconds but their thermal properties are not as good as those of the other broad-band materials such as YAG and sapphire. The end-pumping of Yb^{3+} :KGW rods has been demonstrated to produce pulses with average output power of 1.1 W with pulse duration of 176 fs. The power scaling of Yb^{3+} :KYW and Yb^{3+} :KGW thin disk lasers has been shown to generate pulses with an average output power of 23 W and a duration of 420 fs and there are also possibilities that pulsed output with average powers greater than 60 W and durations of less than 200 fs can be generated. There are also the Yb^{3+} -doped sesquioxides [4.31] with the laser materials Y_2O_3 , Sc_2O_3 and Lu_2O_3 which appear to be suitable for high power operation.

All of the above materials have a reasonably large gain bandwidth, which explains why most of them are used to generate ultrashort pulses by the technique of modelocking which will be discussed in the next section.

5. Modelocking

Modelocking is a technique used to generate periodically modulated laser pulses and ultrashort laser pulses. The technique involves setting up a single short pulse within the laser resonator which circulates between the resonator mirrors creating a periodic train of short output pulses. The generated output pulses can be classified as short compared to the cavity round-trip time of the pulse in the laser resonator.

The oscillating laser signal inside a laser resonator can be described in two ways, either in the time domain or in the frequency domain. The time domain uses the recirculating pulse concepts, while the frequency domain uses the multiple axial mode concept. When the field pattern inside the resonator circulates without experiencing any change during each pass, the output signal from the laser resonator will have a periodic repetition of the same pattern, where the period of each pulse is given as $T = 2L/c$ or $T = p/c$ for a standing-wave cavity of length L or a ring cavity of perimeter p . The periodic repetition frequency which is also known as the axial mode spacing frequency of the laser resonator can then be represented as [5.1]:

$$\omega_{ax} \equiv \omega_{q+1} - \omega_q = \frac{2\pi c}{p} = \frac{2\pi}{T}. \quad (5.1)$$

The requirement for keeping the circulating field pattern constant inside the laser cavity can be fulfilled by a single transverse mode laser (i.e. TEM₀₀) or a single-frequency laser, in which only one axial mode will be oscillating in the cavity; making the circulating pattern within the laser cavity to have a constant amplitude and frequency everywhere within the cavity, and the number of repeated round trips to be indefinitely large.

The mathematical understanding of the modelocking concept can be developed by looking at the time limited real optical signal or pulse $\varepsilon(t)$, which comes out of a laser resonator cavity during the first single round trip time, given as $0 \leq t \leq T$. The optical pulse signal $\varepsilon(t)$ will than become zero (i.e. $\varepsilon(t) = 0$) when $t < 0$ or $t > T$. The time

duration of the optical pulse signal $\varepsilon(t)$, will normally be very small when compared to the laser resonator round trip time interval, that is $\tau_p \ll T$.

The Fourier transform of the optical signal $\varepsilon(t)$ is shown to be $\tilde{E}(\omega)$ by Figure 5-1. The optical carrier frequency signal given as ω_c does not coincide with any axial cavity modes ω_q of the laser cavity. When the optical signal $\varepsilon(t)$ is assumed to be similar to a sine wave with definite carrier frequency ω_c then the axial mode spacing frequency ω_{ax} is greater when compared to the frequency of the optical signal.

If we were to assume that the second optical signal $\varepsilon^{(2)}(t)$ contains some of the same first optical signal $\varepsilon(t)$ after two cavity round trips, then $\varepsilon^{(2)}(t) \equiv \varepsilon(t) + \varepsilon(t - T)$. The Fourier transform of the added signal $\varepsilon(t - T)$, which is delayed by time T will be given as $\exp(-jT\omega) \times \tilde{E}(\omega)$ in the frequency domain. This means the Fourier transform of the second optical signal $\varepsilon^{(2)}(t)$, normalized to unity peak value will be represented [5.1 Chap 27]:

$$\tilde{E}^{(2)}(\omega) = \frac{1}{2}[1 + e^{-jT\omega}] \times \tilde{E}(\omega) = \tilde{E}(\omega) \cos(T\omega/2) \exp(-jT\omega/2). \quad (5.2)$$

Equation 5.2 gives rise to an intensity power spectrum which can be represented as:

$$I^{(2)}(\omega) \equiv |\tilde{E}^{(2)}(\omega)|^2 = \frac{1}{2}[1 + \cos T\omega] \times I(\omega) = I(\omega) \cos^2 \frac{T\omega}{2}. \quad (5.3)$$

The graph in Figure 5-1 shows that the second intensity power spectrum is similar to the first intensity power spectrum. The only difference is that the second intensity power spectrum's amplitude is twice at frequencies where $\omega = \omega_q = q2\pi/T$, and added to this the amplitude decreases to zero halfway between each signal on the second intensity power spectrum as shown by Figure 5-1.

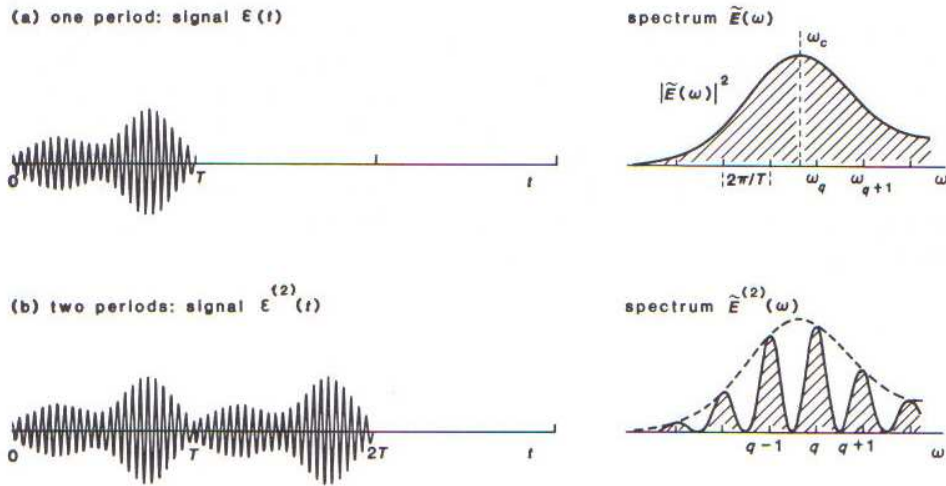


Figure 5-1: Time signal $E(t)$ and its intensity power spectrum for the same signal repeated once and two times in succession. The carrier frequency ω_c of the sine wave signal is shown not to coincide with any of the axial modes ω_q [5.1].

Combining N round trips of identically delayed copies of the time function $\varepsilon(t)$ results in an optical signal $\varepsilon^{(N)}(t)$ to be represented as:

$$\varepsilon^{(N)}(t) = \sum_{n=0}^{N-1} \varepsilon(t - nT). \quad (5.5)$$

The Fourier transformation of the function $\varepsilon^{(N)}(t)$ in Equation 5.5 can be expressed as:

$$\tilde{E}^{(N)}(\omega) = \sum_{n=0}^{N-1} e^{-jnT\omega} \times \tilde{E}(\omega) = \frac{1 - e^{-jNT\omega}}{1 - e^{-jT\omega}} \tilde{E}(\omega), \quad (5.6)$$

Which leads to an intensity power spectrum represented as:

$$I^{(N)}(\omega) \equiv |\tilde{E}^{(N)}(\omega)|^2 = \frac{1 - \cos NT\omega}{1 - \cos T\omega} I(\omega). \quad (5.7)$$

When there are 10 identically delayed copies of the time function $\varepsilon(t)$, that is $N = 10$, the above Equation 5.7 gives out a graph as shown in Figure 5-2 when plotting the power spectral intensity over the axial mode frequencies [5.1].

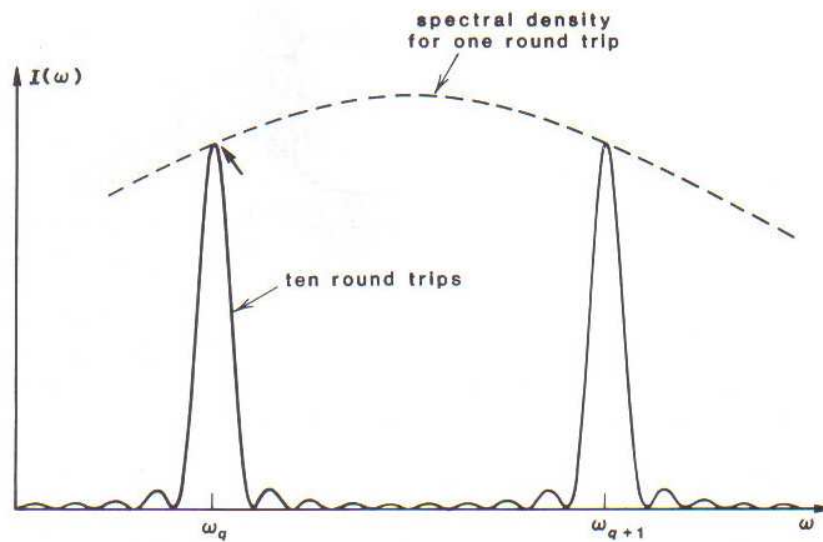


Figure 5-2: Spectral intensity of the same signal repeated 10 times [5.1].

The graph in Figure 5-2 shows the fixed time delay T , between each cavity round trip that gives rise to the axial mode character of the laser output pulse signal. The output signal is also independent of the waveform $\varepsilon(t)$ or the carrier frequency ω_c , which characterizes the optical sine wave signal under the output signal envelope.

When a short pulse laser has an optical signal within the resonator cavity that lasts for a number of cavity round trips N , then the intensity power spectrum of the output pulse signal will be made out of sharp peaks at the steady axial mode frequency ω_q of the laser resonator cavity, where the frequency width of the pulse signal will be expressed as

$\delta\omega_q \approx \omega_{ax} / N$. The total number of axial modes within the spectrum will basically be the spectral width of the single pass pulse signal $\varepsilon(t)$ divided by the axial mode spacing ω_{ax} , and the spectral width of the single pass pulse signal $\varepsilon(t)$ will not depend on the total number of round trips N . The number of axial modes for a short circulating pulse signal of any large amplitude with a pulse width will be $N_{\text{modes}} \approx T / \tau_p$ [5.1].

When there is a large number of sidebands N of equally spaced axial mode frequencies, where these sidebands all have the same amplitude and are in phase, the total wave amplitude associated with this signal will be:

$$\varepsilon(t) = \sum_{n=0}^{N-1} e^{j(\omega_0 + n\omega_{ax})t} = \frac{e^{jN\omega_{ax}t} - 1}{e^{j\omega_{ax}t} - 1} e^{j\omega_0 t}, \quad (5.8)$$

and the intensity derived from Equation 5.8 can be shown to be:

$$I(t) = |\varepsilon(t)|^2 = \frac{1 - \cos N\omega_{ax}t}{1 - \cos \omega_{ax}t} = \frac{\sin^2 N\omega_{ax}t/2}{\sin^2 \omega_{ax}t/2}. \quad (5.9)$$

The periodic time envelopes solution given by Equation 5.9 for $N = 8$ is shown by Figure 5-3, where the short pulse signal from the graph results from adding together N equal amplitude sine waves or complex phases, which are all in phase at $t = 0$, and also again at $t = \pm T, \pm 2T$, and so forth. At these peaks, the intensity of the ε field amplitude is N times the amplitude of any one component. Between the peaks which are separated by $\Delta t = \pm T / N$, the total intensity field amplitude is zero. This behaviour gives rise to short intense modelocked pulses, which will have a full pulse width duration of $2T / N$ or a FWHM pulse width of $\tau_p \approx T / N$. In between the modelocked pulse peaks there are $N - 2$ weaker peaks which have a pulse width at the baseline of T / N when compared to the $2T / N$ for the modelocked pulse peaks [5.1].

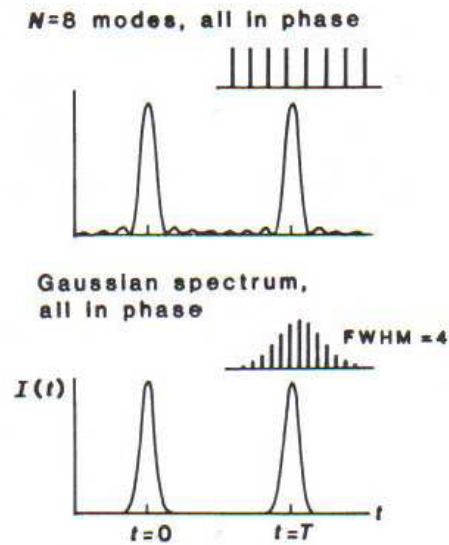


Figure 5-3: Intensity patterns in time that can be generated using $N = 8$ equally spaced frequency components with different relative amplitudes and phase angles [5.1].

There are two types of modelocking regimes. There is a Q -switched modelocked regime illustrated by Figure 5-4 where the modelocked pulses are contained under the envelope of a Q -switched pulse. There is also cw-modelocking which is equivalent to the normal cw laser but has a constant output power in each axial cavity mode over time of operation, as shown by Figure 5-5.

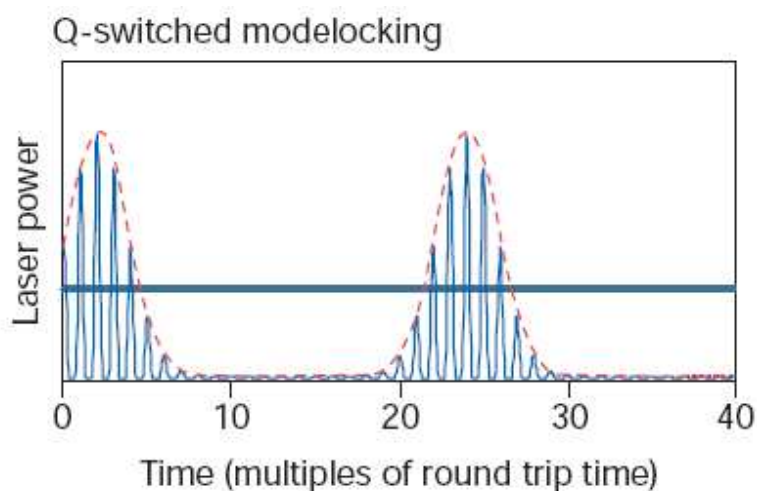


Figure 5-4: Instantaneous and average laser power versus time for a modelocked laser exhibiting large Q -switching instabilities [5.2].

The cw-modelocked laser pulses are usually favoured over the unpredictable and unstable *Q*-switched modelocked pulses. The factor which causes modelocked pulses to be unstable is that short pulses have a very broad bandwidth, competing with the cw signal, thereby reducing the gain for the modelocked pulses. Increasing the gain for the modelocked pulses so as to make them stable requires a mechanism which will favour short pulses over any other modes in the laser cavity. The mechanism would introduce a low loss for modelocked pulses and a high loss for the competing cw signal.

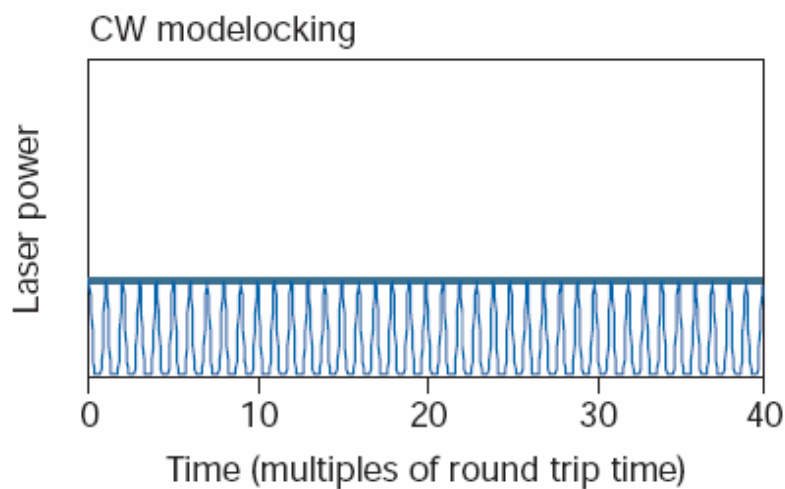


Figure 5-5: Instantaneous laser power versus time for a stable cw-modelocked laser [5.2].

There are two types of mechanisms to make modelocked pulses stable, and these are active modelocking and passive modelocking. These two types of modelocking will be discussed in the following section.

5.1 Active modelocking

The first type of mechanism to make modelocked pulses stable is active modelocking, which uses an amplitude modulator (AM) element in the laser resonator like an acousto-optic modulator (AOM) which generates a loss modulation of frequency ω_m that is sinusoidal and synchronized with the cavity round-trip time, T_R [5.3].

From a frequency domain viewpoint, each of the oscillating axial modes present in the laser cavity at frequency ω_q will acquire modulation sidebands at frequencies $\omega_q \pm n \times \omega_m$ as a result of the active modulation. The modulator will normally be driven at a modulation frequency ω_m equal or very close to the axial mode spacing, or one of its integer multiples. Hence the modulation sidebands from each axial mode will fall on top of, or very close to, one of the other axial modes in the cavity, as shown by Figure 5-6.

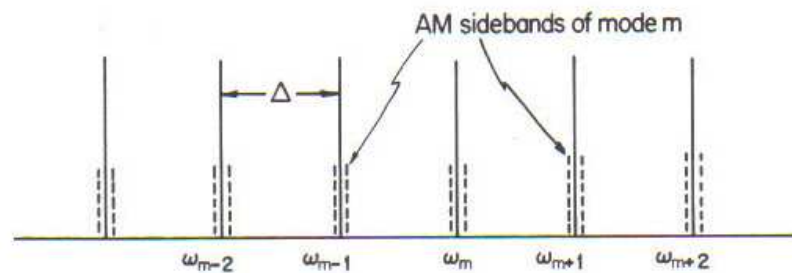


Figure 5-6: Longitudinal modes amplitude-modulated at the frequency $\Delta = \omega_q$ equal to their spacing. For clarity the AM side bands are indicated as dashed lines slightly displaced from the mode frequencies ω_m [5.3].

Each of these sidebands will then tend to injection lock the axial mode with which it is in resonance; and so the intracavity modulator will tend to couple together, or modelock, each axial mode to one or more of its neighbouring modes. This kind of intracavity modulation, whether viewed in the time or the frequency domain, thus represents the most common form of active modelocking, in which the pulse formation process is controlled and synchronized by the applied modulation frequency which must be tuned very close to the natural round trip frequency ω_{ax} in the laser cavity.

The shorter the circulating pulse becomes in such an actively modelocked laser, the less loss it experiences in passing through the modulator; at least until the pulse becomes quite short compared to the modulator period. At the same time, however, the pulse spectrum necessarily becomes wider, and encompasses more axial modes. Since laser media often have very wide atomic linewidths, the laser medium can still continue to provide gain as the pulse becomes narrower, but this gain will decrease as the spectral width of the pulse begins to approach the amplification bandwidth of the laser medium. In another way, the saturated gain at a steady state only supports net gain around the minimum of the loss modulation and therefore only supports pulses that are significantly shorter than the cavity round trip time, as illustrated in Figure 5-7.

The limiting pulsewidth for an actively modelocked laser therefore usually results from a compromise between the pulsewidth narrowing effects of the intracavity modulator and the spectral narrowing or pulsewidth broadening effects of the laser gain medium. This makes active modulation to be limited by external electronic circuits that drive the acousto-optic modulator, which result in relatively slow modulation generating pulses. The only advantage of using active modelocking is the ability of synchronizing a number of lasers in time.

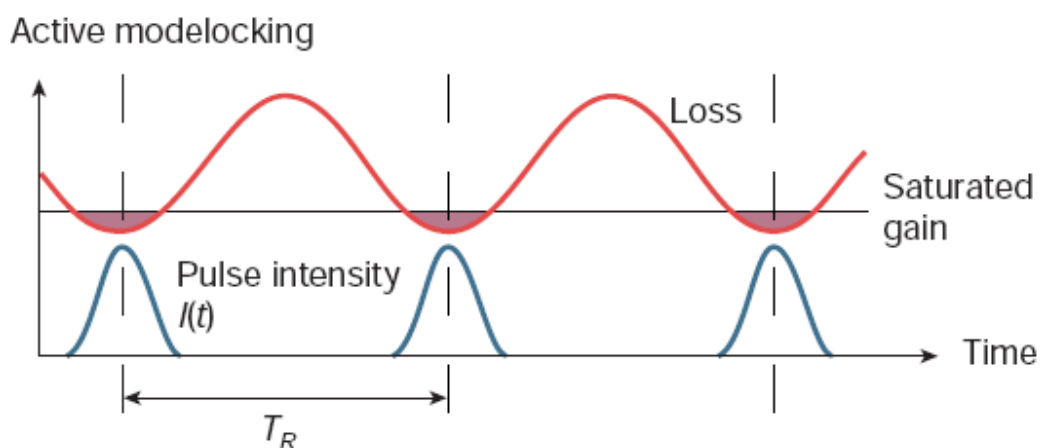


Figure 5-7: Schematic diagram of an active modelocked laser with has a cavity round trip time T_R [5.2].

In active modelocking the intracavity light field is modulated by the introduction of an optical modulator into the laser cavity. In the most commonly employed technique an acousto-optic modulator (AOM) is placed inside the laser cavity as illustrated by Figure 5-8. The active modelocking is achieved by externally driving and controlling the piezo-electric transducer with an electrical signal, which generates acoustic standing waves with a frequency which ranges from hertz to megahertz in the acousto-optic medium. The refractive index of the AOM becomes periodically modulated forming a Bragg grating which causes the beam to be refracted out of the laser cavity. This refraction loss caused by the AOM oscillates with twice the frequency of the acoustic wave because the refractive index modulation only depends on the modulus of the pressure change.

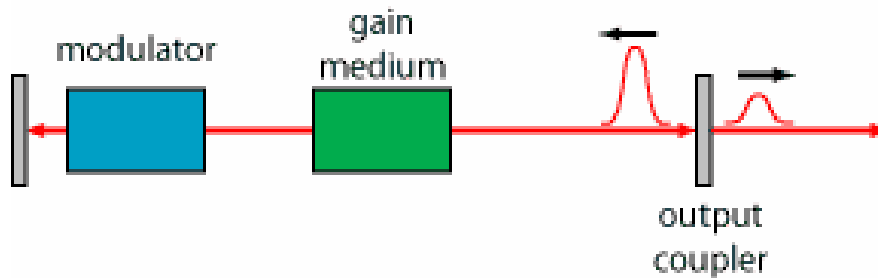


Figure 5-8: Schematic setup of an actively modelocked laser [5.4].

When the modulator is at a minimum loss, the head of the pulse circulating inside the cavity is hardly affected, while the tail of the pulse is cut by the modulator. The modulator therefore causes increased losses for the pulse wings as shown in Figure 5-9, effectively shortening the pulses. As the pulse duration relative to the pulse period is typically much smaller than that shown.

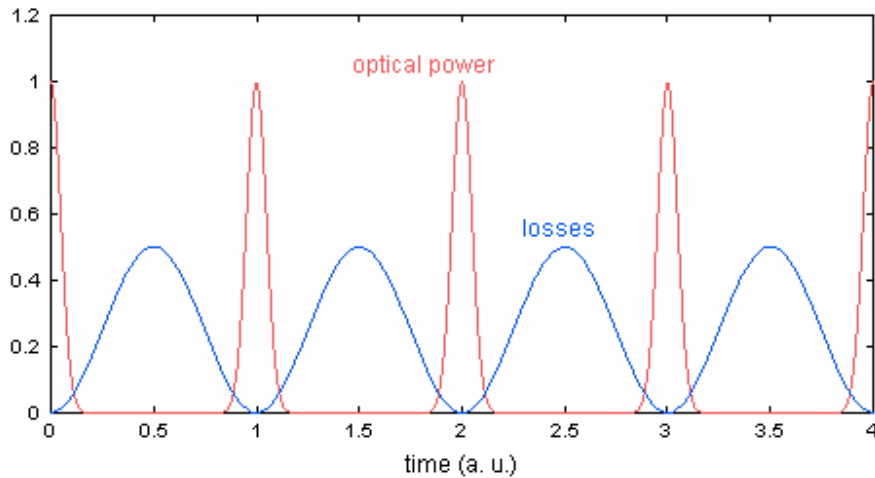


Figure 5-9: Temporal evolution of optical power and losses in an actively modelocked laser [5.4].

The effects of limited gain bandwidth in a laser material can cause the pulse bandwidth to decrease which then increases the pulse duration. The effects of dispersion or self-phase modulation (SPM) which will be discussed later can cause the pulse duration to increase or decrease depending on the original phase profile of the pulse.

The use of a gain medium which is homogeneously broadened leads to a distorted gain spectrum which causes the pulse duration to increase. This is explained by the theory of Kuizenga and Siegman [5.5, 5.6] which will not be discussed here in detail. They assume a modulator which is in exact synchronism with the cavity and the gain filter, but with no dispersion or SPM; their theory is valid for a gain medium which is homogeneously broadened with a Lorentzian line shape.

Active modelocking of solid state lasers has demonstrated that the time window for the low loss modulator would be much longer than the pulse duration of a few tens of picoseconds which are currently produced by laser materials such as $\text{Nd}^{3+}:\text{YVO}_4$ and $\text{Nd}^{3+}:\text{YAG}$, which is around 6.2 ps [5.7]. This means pulses with durations of less than picoseconds will not be possible with active modelocking.

5.2 Passive modelocking

The second mechanism for making modelocked pulses stable is passive modelocking, which utilizes a passive type of loss modulation that relies on saturable absorbers. Some saturable absorbers have a very fast loss modulation, capable of generating very short pulses, as illustrated in Figure 5-10. The saturable absorber is placed inside the laser cavity and it can be any material, a solid, a liquid or a gas, which has an optical absorption that is constant at low intensities, but saturates and decreases to lower values as the laser intensity rises. When the laser pumping process is first turned on, this absorption may even be larger than the laser gain, so that no signal can build up in the laser cavity. As the laser gain continues to increase because of continued laser pumping, however, the round trip gain eventually begins to exceed the total saturable and non saturable losses in the laser cavity, and an initial laser oscillation will begin to form.

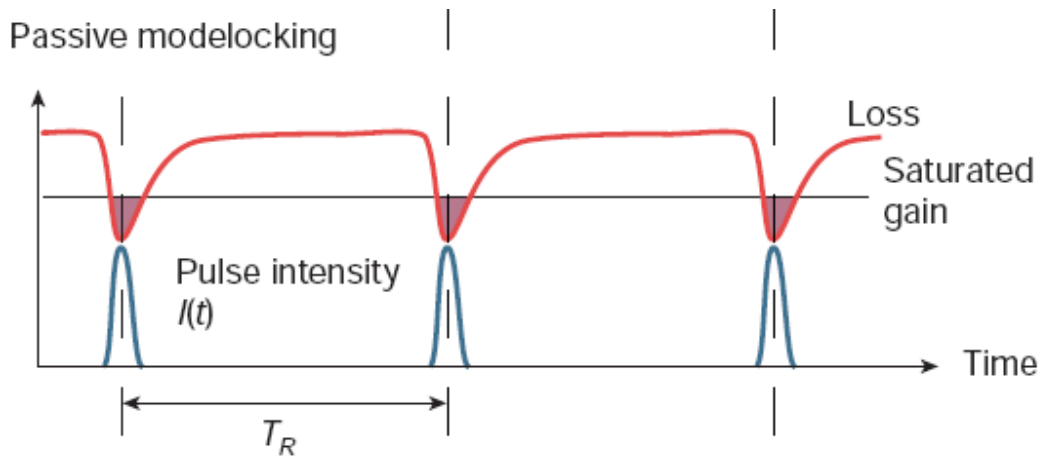


Figure 5-10: Schematic diagram of a passively modelocked laser with a cavity round trip time T_R [5.2].

The advantages of using passive saturable absorbers are that they are simple to use and do not require external driving schemes and that they can create very short pulses. Their disadvantage is that it is difficult to synchronise other lasers with a passively modelocked laser. This is because for modelocking to occur the gain medium should be able to store the excited energy over a time which is more than one cavity round trip, which in most

cases is in the range of a few nanoseconds. Solid state laser gain materials are well within this range even at very low cavity round trip times. This is because the excited upper laser level lifetime in solid state laser material ranges from microseconds to milliseconds in some cases, which means normal diode laser sources, can be used for pumping modelocked lasers.

Passive modelocking is achieved by inserting saturable absorber elements into the resonator as shown by Figure 5-11 which favour the development of short pulses over any other mode of operation like cw operation. For instance when a laser is operating in the cw-mode any small noise spikes which develop are favoured by the saturable absorber up to the extent that they contain a significant amount of the circulating energy enabling them to saturate the gain and thereby suppressing the cw background.

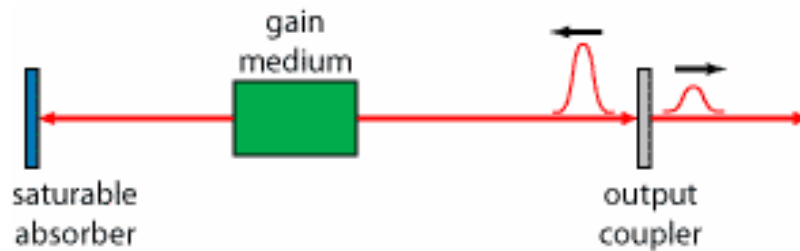


Figure 5-11: Schematic setup of a laser which is passively modelocked with a saturable absorber mirror, e.g. a SESAM [5.4].

During the decay of the cw background there will be an energetic noise spike which will grow faster than all the other noise spikes since it will experience less absorption by the saturable absorber. At some point the energetic noise spike will have sufficient energy to saturate the gain to a level which other smaller noise spike can not reach which then effectively experience a net loss during each roundtrip until they are eliminated and only a single short pulse propagates in the laser cavity. The duration of the single circulating pulse will further be reduced by the saturable absorber which favours growing the peak of the pulse instead of its wings, up to a point where pulse broadening occurs because of dispersion limiting it from being reduced any further (see Figure 5-12).

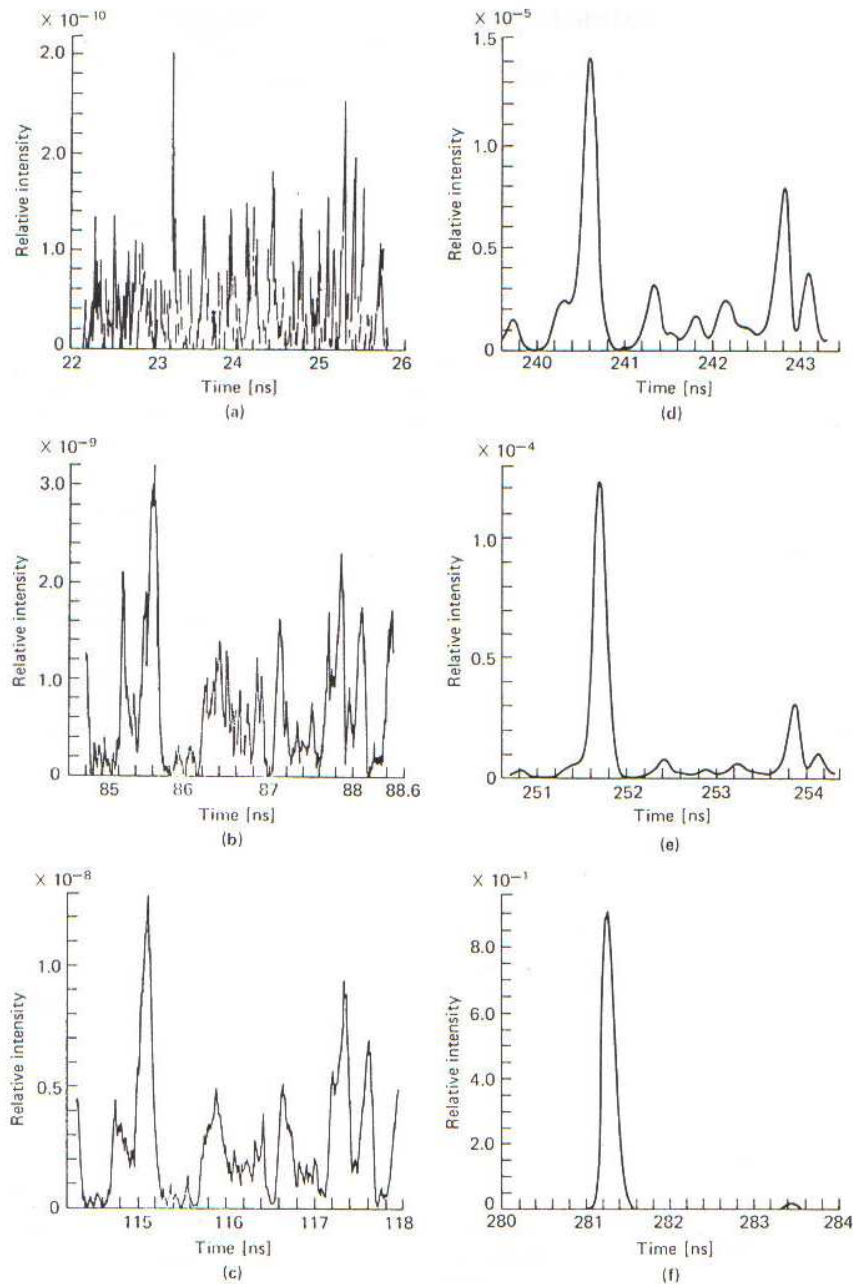


Figure 5-12: Computer simulation of the evaluation of a modelocked pulse from noise. (a-c) regime of linear amplification and linear dye absorption, (d-e) nonlinear absorption in the dye cell, (f) regime on nonlinear amplification, dye completely bleached [5.3].

The chaotic formation of the pulse can be prevented by introducing strong pulse broadening, in the form of a strong saturable absorber which will then start the

modelocking process. A strong saturable absorber usually has a longer recovery time; that is low saturation intensity, which makes it useful for fast self-starting modelocking. Weak saturable absorbers have the shortest recovery time which means high saturation intensity, making them useful for generating shorter pulses.

A fast saturable absorber is termed to be fast in a sense that it will recover on a time scale less than the pulse duration. This makes the state of the absorber to largely depend on the instantaneous pulse intensity and the shape of the leading edge of the pulse as well as the tail. The slow saturable absorber is also termed to be slow because its recovery time is more than the pulse duration and the state of the absorber is completely different from the fast saturable absorber. Slow saturable absorbers are frequently used for generating pulses with durations less than the recovery time of the saturable absorber which will be discussed later.

In other words, to understand the behaviour of a saturable absorber a quantitative analysis has to be done for the fast and the slow saturable absorber. For the fast saturable absorber the intensity loss q which is generated by the absorber depends on the instantaneous intensity I , the incident power divided by the mode area. This leads to a reasonable approximation of the saturable absorber model by [5.9]:

$$q(I) = \frac{q_0}{1 + I/I_{sat}} \quad (5.10)$$

The response of the fast saturable absorber is characterized by the saturation intensity given as I_{sat} and the unsaturated loss q_0 . The effective loss for the pulse can then be calculated if the peak intensity I_p and the average value of q are given. Figure 5-13 below is a plot of the function $q(I_p)$, soliton (sech^2) pulse and the normalized peak intensity for a Gaussian pulse, showing that the pulse form has little influence on the average loss.

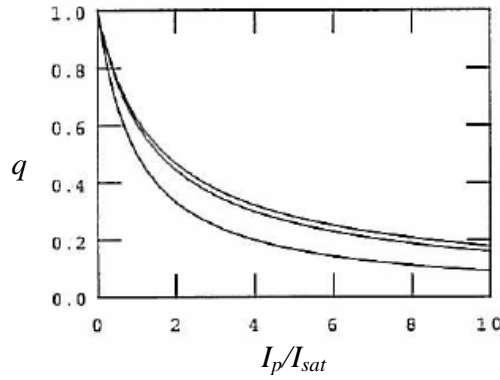


Figure 5-13: Graph of the ratio of effective loss (q) for a fast saturable absorber versus the peak intensity (I_p) to the saturation intensity, where the bottom curve represents $q(I_p)$, the middle curve the Gaussian pulse and top curve the soliton pulse [5.9].

The quantitative behaviour of the slow saturable absorber is described by a differential equation:

$$\frac{dq}{dt} = \frac{q - q_0}{\tau} - \frac{1}{F_{sat}} q. \quad (5.11)$$

With the loss factor q assumed to be less than 1, the recovery time being τ , the unsaturated loss q_0 , and the saturation fluence F_{sat} . Assuming a very slow recovery time the above equation reduces to:

$$\frac{dq}{dt} = -\frac{1}{F_{sat}} q. \quad (5.12)$$

The value of q after transmission of a pulse with fluence F_{sat} is $q_0 \exp(-F_p/F_{sat})$ if the absorber is initially unsaturated. The effective loss of the pulse, since it is independent of the pulse form, is derived to be:

$$q_p(F_p) = q_0 [1 - \exp(-F_p/F_{sat})] \times F_{sat}/F_p = q_0 [1 - \exp(-S)]/S, \quad (5.13)$$

Where the saturation parameter S , is given by:

$$S = F_p / F_{sat} . \quad (5.14)$$

For strong saturation, S is greater than 3 as normally employed for modelocking, the absorbed pulse fluence (F_p) is approximately equal to the saturation fluence times the modulation depth, which results in:

$$q_p(S) \approx q_0 / S . \quad (5.15)$$

The following Figure 5-14 shows a plot of the Equation 5.15 and the loss of the saturable absorber after the pulse. The graph shows that the loss of the pulse gets very small for S greater than 3, while the average loss q_p for the pulse is still significant.

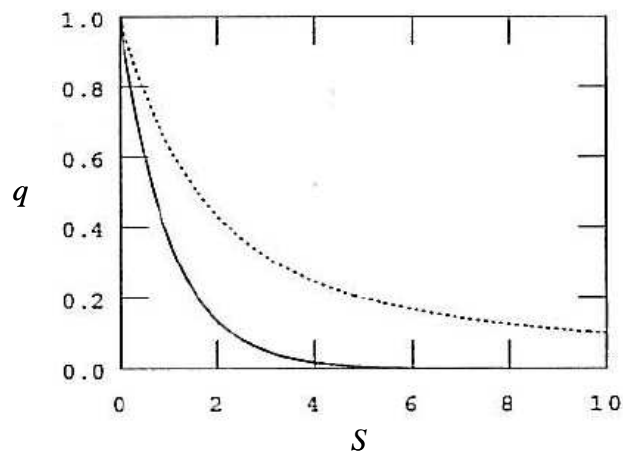


Figure 5-14: Graph of the normalized loss (q) versus the saturation parameter (S) for a slow saturable absorber, where the solid line represents the loss for a pulse and the dotted curve the loss of the absorber after the pulse [5.9].

Passive modelocking does produce the shortest possible ultrashort pulses in high power diode-pumped solid-state lasers. This type of modelocking is very effective in that it uses

the light in the cavity to cause a change in the intracavity saturable absorber element, which will then itself produce a change in the intracavity light. The other more practical importance for this type of modelocking is that it requires no external controlling of the laser to produce pulses when compared to active modelocking, even though this is a complex process and difficult to control because passive modelocking relies on the nonlinearity process of the saturable absorber to produce modelocked pulses. The nonlinearity process is very complex to describe and less amenable to simple analytical treatment when compared to active modelocking and this provides a challenge in that one needs to understand these nonlinear processes when one is interested in producing passive modelocked pulses that are stable and reliable. Therefore in this chapter we will not go through the complete detailed analyses of passive modelocking but we will look at an overview of the most important forms of passive modelocking when using either a fast or slow saturable absorber, so that there could be a good understanding of what passive modelocking is.

Therefore the basic outcome in all passively modelocked lasers is that short laser pulses are generated when the laser light is transmitted through a saturable absorber element and the most important thing in passive modelocking is the different time variation of the modelocked pulses. This time variation of the modelocked pulses is slow when compared to the dephasing time in the saturable absorber medium and the saturation behaviour of the absorption which is essentially that of simple homogeneous atomic transition.

When the pulse passes through the absorber it will experience a change in its shape and this depends strongly on whether the saturable absorber is a fast or slow saturable absorber. Fast saturable absorbers are characterised by having an absorption recovery time that is much shorter than the pulse-width τ_p , where the absorber saturates with the instantaneous intensity $I(t)$ of the optical pulses as shown by Figure 5-15. For fast saturable absorber the shorter the pulse becomes, the faster will be the loss modulation. In reality, the ratio of the pulse duration to the pulse period is usually much smaller than shown in this Figure 5-15.

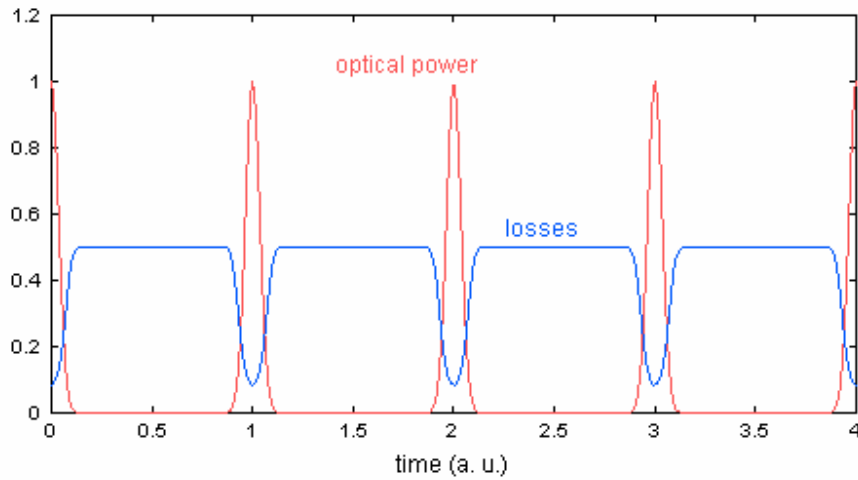


Figure 5-15: Temporal evolution of optical power and losses in a passively modelocked laser with a fast saturable absorber [5.4].

This is in contrast to the slow saturable absorber, where the absorption recovery time is much longer than the pulse-width τ_p , and the absorption saturates primarily on the integrated intensity of the optical pulse as shown by Figure 5-16. The slow saturable absorber causes a loss modulation which is fast for the leading wing of the pulse and the recovery of the absorber takes some longer time. Passive modelocking can often be achieved even when the recovery time is more than an order of magnitude longer than the pulse duration.

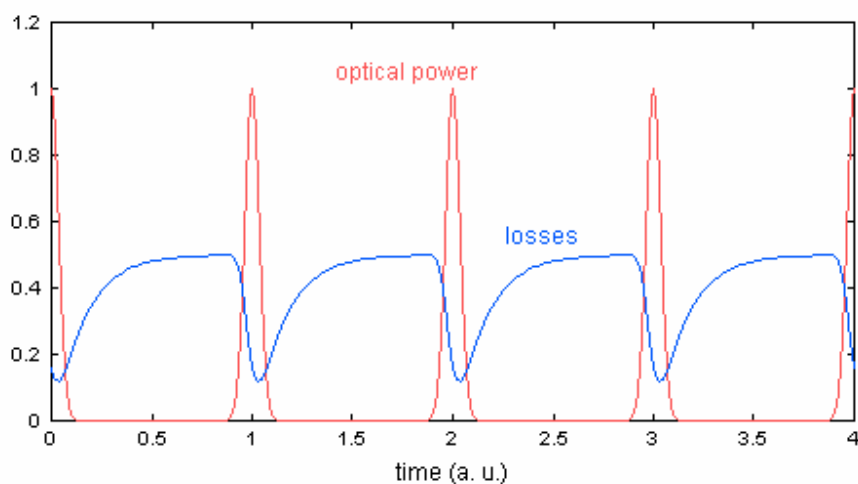


Figure 5-16: Temporal evolution of optical power and losses in a passively modelocked laser with a slow saturable absorber [5.4].

The estimation of the pulse duration resulting from using a fast saturable absorber has to take into account that there should be very little effect of dispersion or self-phase modulation which causes the phase velocity of the laser light to depend on its frequency and also that of gain saturation during the pulse shorting process. This is because the effect of dispersion and gain saturation has been shown analytically by Haus [5.10] to often affect picosecond solid-state lasers modelocked by semiconductor saturable absorber mirrors (SESAM's), where his model was only valid for weak absorber saturation and the analytical simulation estimated that the pulse duration using a saturable absorber can be estimated to be:

$$\tau_p \approx \frac{0.9}{\Delta f_g} \sqrt{\frac{g}{\Delta R}} . \quad (5.16)$$

Where g is the gain coefficient, ΔR the modulation depth of the absorber and Δf_g the FWHM gain bandwidth. A factor which causes significantly longer pulses is weaker or stronger absorber saturation. The introduction of self-phase modulation can reduce the pulse duration because it increases the pulse bandwidth; however, the pulse becomes unstable if too much self-phase modulation takes place. The increase in modulation depth also requires that an increase in gain should occur, so that the value of the modulation depth larger than the linear cavity losses does not significantly reduce the pulse duration, since the limit for the pulse duration is in the order of $1/\Delta f_g$.

The slow absorber produces longer pulse durations and the estimated pulse duration without significant influence of dispersion and self-phase modulation is shown to be [5.10]:

$$\tau_p \approx \frac{1.07}{\Delta f_g} \sqrt{\frac{g}{\Delta R}} . \quad (5.17)$$

Equation 5.17 is similar to the one which uses a fast saturable absorber and it uses an empirical fit to the numerical simulations. The equation is only valid when the absorber is used at between 3 to 5 times the saturation fluence. The pulse duration increases if there is significant weak or strong absorber saturation. The influence of self-phase modulation increases the pulse duration in contrast to the fast saturable absorber, apart from the instability occurring when the effect of self-phase modulation is too strong, especially in femtosecond lasers.

Making self-phase modulation weak enough in femtosecond lasers is difficult to achieve which then requires soliton modelocking as a solution. This is because in soliton modelocking, a balance between self-phase modulation and dispersion is maintained when the pulse propagates through the absorber. The soliton pulse will then propagate with constant temporal and spectral shape; and will only acquire an overall nonlinear phase shift.

The pulse duration obtained using a slow saturable absorber can be more than an order of magnitude shorter than the absorber recovery time. This is attributed to the ability of the slow absorber to clean up only the leading part of the pulse, but not the trailing part. This is also enforced by the pulse maximum (not the tail of the pulse) being constantly delayed since the absorber only attenuates the leading edge. This causes the pulse to 'eat up' the trailing part, and the noise left will have only a limited time to grow before it could merge with the pulse.

Apart from achieving the shortest pulse duration, self-starting modelocking is usually a good and desirable property that a laser should have. This makes the slow saturable absorber superior over the fast saturable absorber because it has a lower saturation intensity which facilitates the modelocking process in an early phase. Reliable self-starting modelocking has been demonstrated to be achievable with (slow) semiconductor saturable absorbers, while Kerr lens modelocked lasers are usually not self starting, when particularly designed to produce short pulses.

5.3 Saturable absorbers for passive modelocking

Passive modelocking behavior depends critically, however, on the saturation properties of the gain medium and the saturable absorber, and these can deteriorate with time or with repeated laser shots. The most common examples of saturable absorber modelocking are solid-state lasers modelocked by organic saturable absorber dye solutions, such as Nd:YAG or Nd:glass lasers modelocked with various commercially available dyes such as Eastman Kodak 9860 or 9840. There are also semiconductor saturable absorber mirrors (SESAMs) for passive modelocking illustrated by Figure 5-17, which we will mainly concentrate on, since they are used in this work.

5.3.1 Semiconductor absorbers

The energy levels of the semiconductor band gap structure which represents a gap between the valence band and the conduction band can be shown using Figure 5-17. The figure illustrates that the SESAM will absorb the laser light when the photon has enough energy to excite the electrons from the valence band to the conduction band; and when the laser light contains very high number of photons the absorption of light by the electron leads to saturation because all the possible initial states of the valence band are depleted while the final states of the conduction band are partially occupied. After the excitation of the electrons from the valence band to the conduction band, the electrons in the conduction band start thermalising between 60-300 fs which leads to a partial recovery of the absorption. On a longer time scale between a few ps and a few ns the electrons will be removed from the conduction band by recombination and trapping. The absorption saturation will recover partially by intraband thermalisation shown by an orange arrow, and then followed by interband transitions via spontaneous emission and/or via traps and defects.

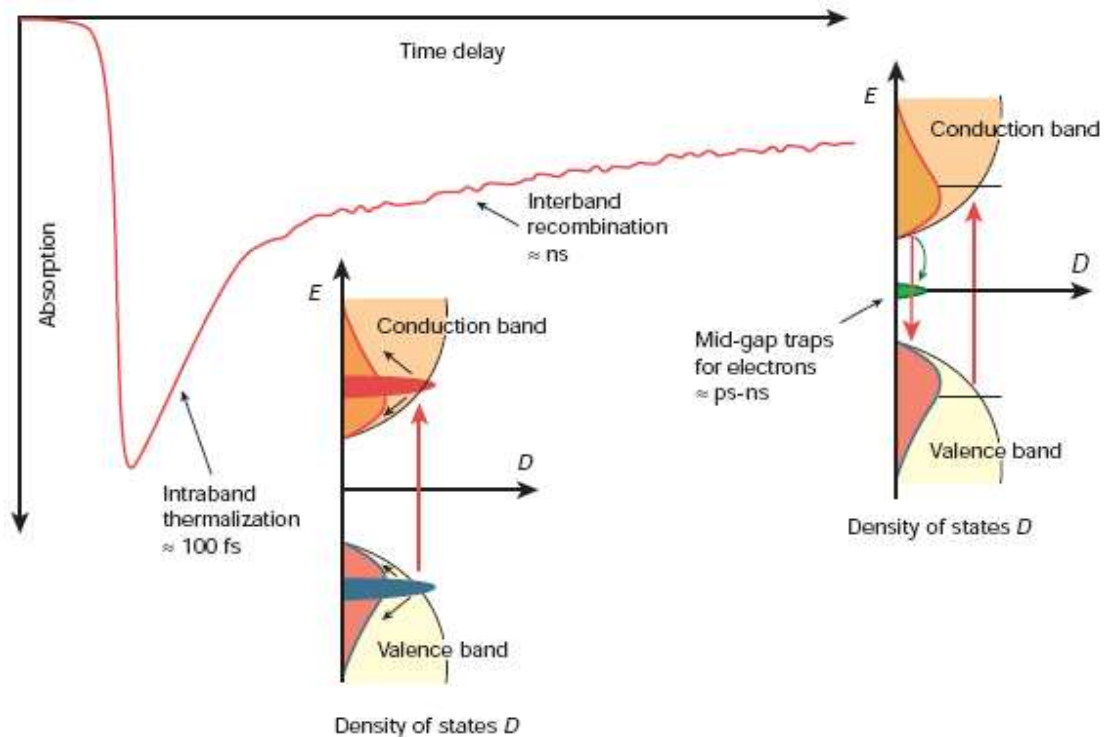


Figure 5-17: A SESAM can absorb photons, whereby electrons are transferred from the valence band to the conduction band [5.2].

Already a small amount of the radiation incident on the semiconductor layer of a few nanometers thickness would be absorbed. This type of structure is called a quantum well because with structures of small dimensions such as this, the density of states is usually modified by quantum effects. The quantum well (QW) absorbers are combined into a microstructure which is surrounded by different semiconductor materials which are not absorbing due to their larger band gap. Usually this type of structures are grown on a ~ 0.5 mm thick semiconductor wafer of GaAs and contain a GaAs/AlGaAs Bragg mirror structure so that they can be operated in reflection [5.2]. Within the top layers of the structure, there is an InGaAs quantum well absorber layer, which may be 10 nm thick, as shown by Figure 5-18. In some cases, a Bragg mirror is replaced by a metallic mirror resulting in broader bandwidth [5.11]. Such a structure is called SESAM (semiconductor saturable absorber mirror) and was first used for modelocking in 1992 [5.12]. This acronym includes all types of semiconductor saturable absorbers which are operated in reflection. Most SESAMs contain a Bragg mirror, and if the absorber is incorporated into

the top part of this Bragg mirror, the term saturable Bragg mirror (SBR) was introduced in 1995 [5.13].

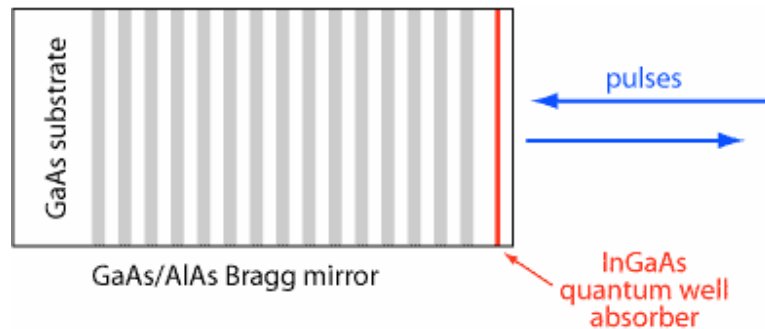


Figure 5-18: Structure of a typical SESAM for operation around 1064 nm [5.4].

A double quantum well (DQW) SESAM can be achieved by reducing the indium content of the QW, which reduces the saturable absorption at the laser wavelength and at the same time eliminates any possible strain relaxation and defects generation. This means that two QW structures have to be incorporated to make a DQW SESAM. Combining two QW is better than developing one single DQW when making a DQW SESAM. This is because single QW SESAM can be developed with low indium content. This is because large indium content in the SESAM causes the exciton resonance to shift to shorter wavelength and at the same time causes the saturable absorption (i.e. the modulation depth) at the laser wavelength to be reduced. The DQW SESAM structure developed by Dr. Bente for high-average power output consists of strain compensating GaAsP intermediate layers which reduce the total devices strain to almost zero. The DQW structure consists of the following layers as shown in Figure 5-19. A GaAs substrate, onto which 29 $\lambda/4n_{hi,lo}$ -thick layer pairs of $Al_{0.8}Ga_{0.2}As/GaAs$ are deposited (where $n_{hi,lo}$ is the refractive index of the respective layers at the design wavelength); a $\lambda/4n_{lo}$ thick layer of $Al_{0.8}Ga_{0.2}As$ followed by the sequence $GaAs/GaAs_{0.7}P_{0.3}/In_{0.22}Ga_{0.78}As$, $QW/GaAs_{0.7}P_{0.3}/In_{0.22}Ga_{0.78}As$, $QW/GaAs_{0.7}P_{0.3}/GaAs$; the total thickness of this sequence is equivalent to $\lambda/4$ at the designed wavelength of 1064 nm.

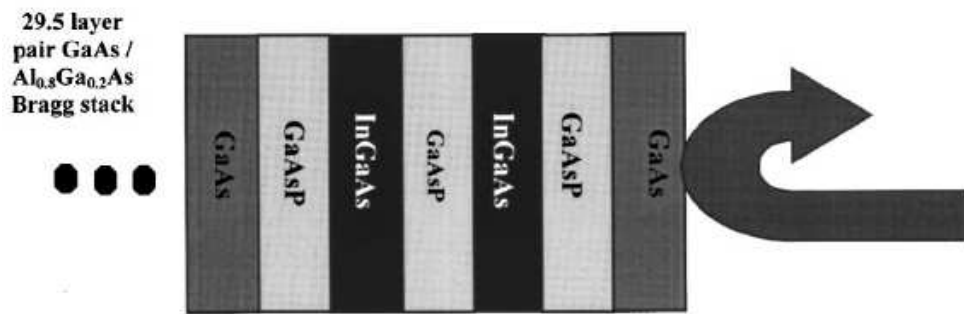


Figure 5-19: Schematic of the topmost layers of the double quantum well SESAM [5.14].

There are two methods of producing SESAMs. The first method is metal-organic chemical vapour deposition (MOCVD) which is a fast method for mass production of SESAMs and is done at a high temperature of about 600 °C. The second method is the slow type called molecular beam epitaxy (MBE) and is done at low temperatures of about 200 °C. The most favoured method for producing SESAMs suitable for high-power operation is the MOCVD since it produces SESAMs which have relatively small non-saturable losses. The MBE method also does produce SESAMs with relatively small losses but this method is more suitable for ultrafast lasers. This is because SESAM that are grown at low temperature have microscopic structural defects. These defects will then act as traps for excited carriers reducing the recovery time of the SESAM, making them more suitable for ultrafast modelocked lasers.

The presences of non-saturable losses in the SESAM when using either one of the above growing techniques increases when the growth temperature of the process decreases. This affects the speed of recovery and the surface quality of the SESAM. A compromise has to be done to improve both the speed of recovery and the surface quality of the SESAM by optimising the annealing procedures or by beryllium doping [5.15, 5.16].

The usefulness of SESAMs for modelocking is because of them having two different time scales of recovery which results in carrier trapping, intra-band thermalisation and recombination. The first longer time scale constant of the SESAM causes the saturation

intensity to decrease for part of the absorption resulting in self-start modelocking of the laser and the second fast time scale constant does cause shaping of subpicosecond pulses.

5.3.2 *Q*-Switching instabilities

The graph in Figure 5-20 represents different regimes of modelocking when using a saturable absorber, where zone 1 shows no modelocking, zone 2 *Q*-switched modelocking (*QML*) and zone 3 cw-modelocking. The desired and most favoured type of operation is cw-modelocking because it produces a train of predictable pulses which have constant duration, constant energy and constant pulse shape as shown by the inserted small graph in zone 3. The *Q*-switched modelocked operation in zone 2 is not as much favoured because this type of operation emits a bunch of pulses which are unpredictable in terms of shape, duration and energy and also might not have a stable *Q*-switched envelope shape.

The reason for the laser to operate in the *QSML* regime is because from the steady state of cw-modelocking there is a small increase of pulse energy that leads to stronger saturation of the saturable absorber. This causes a positive net gain in the laser and thus causes an exponential growth in the pulse energy, where the growth in the energy of the pulse will be stopped by gain saturation. The high energy *Q*-switched pulses will eventually be suppressed and be dropped to a steady-state value. This is because solid-state lasers usually exhibit large gain saturation fluence and this often occurs after many cavity round trips. The steady-state which leads to stable cw-modelocking is usually obtained when the gain saturation sets in fast enough to reduce the positive gain of the laser as shown by the transition from zone 2 to 3 in the Figure 5-20 below.

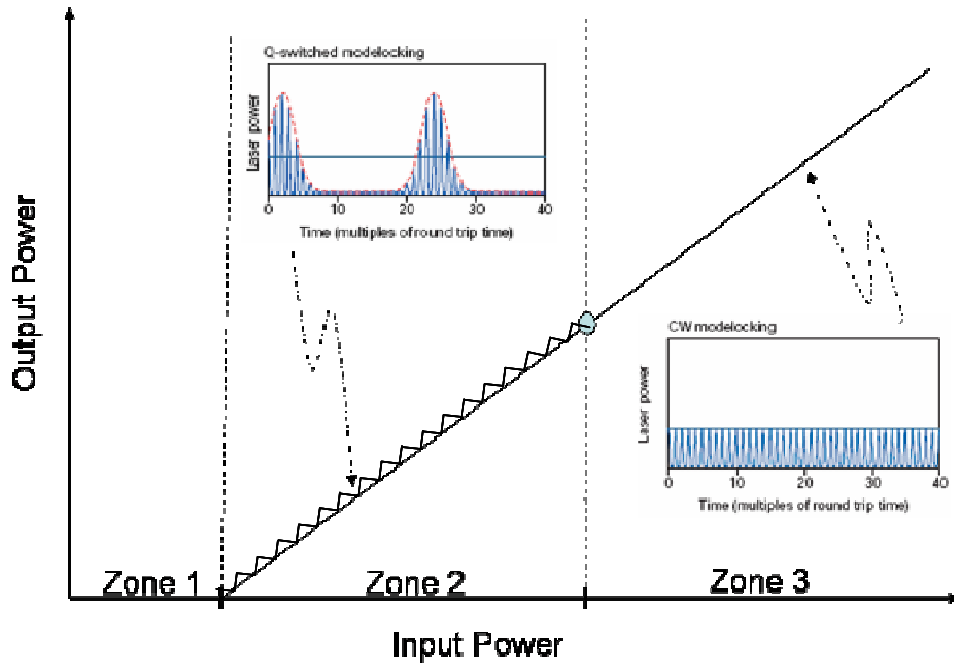


Figure 5-20: Schematic diagram of the Q -switched modelock transition between zone 2 and zone 3 [5.2].

Incorporating a SESAM in a solid-state laser usually will lead to three different types of operational regimes [5.17] if the gain saturation does not set in fast enough as shown by Figure 5-21. The first regime is cw-operation, which usually occurs at low output powers. The Q -switched modelocked operation is the second regime, where the laser output consists of modelocked pulses underneath a Q -switched envelope. The Q -switching modulation is usually in the kilohertz region and is attractive for applications such as nonlinear frequency conversion and precise fabrication of microstructures, because of the high energy that is still concentrated in the ultrashort modelocked pulses. The third regime of operation is called cw-modelocking, where the laser output consists of a train of modelocked pulses with constant energy. The cw-modelocked pulses have a repetition rate which is typically in the order of 100 MHz determined by the cavity length. The transition from the Q -switched modelocked state to the cw-modelocked state is well defined since there is a change in terms of the average output power of the laser. The transition is then referred to as the Q -switched modelocked transition ($QSML$) and the

average output power threshold of the *QSML* transition is termed as $P_{QSML,th}$ as indicated in Figure 5-21.

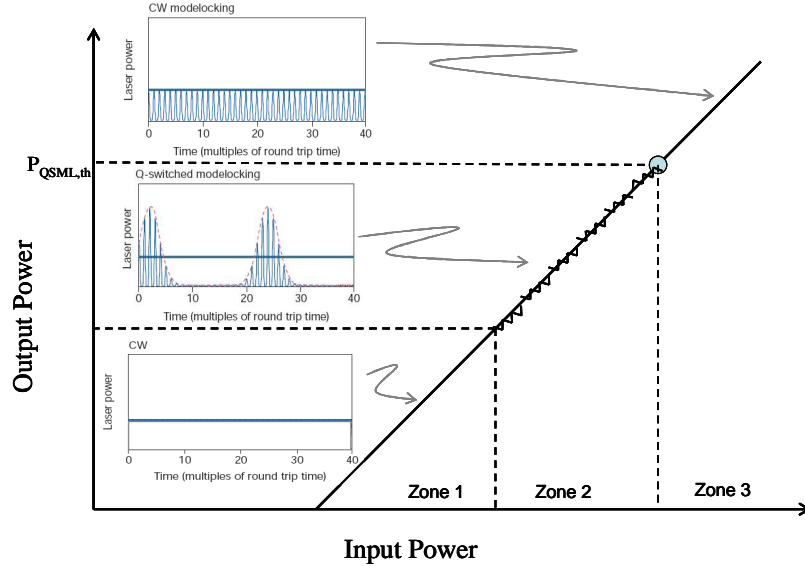


Figure 5-21: Output power of a SESAM modelocked laser verses input power; showing three different modelocking regimes of cw, *Q*-switched modelocked and the cw-modelocked [5.2].

The work done by C Honninger [5.17] and separately by F.X. Kartner [5.18] on identifying the transition between the cw-modelocking and *Q*-switched modelocking of slow saturable absorbers have shown that an absorber that is fully saturated will always fully recover after two cavity round trips without the soliton shaping effect taking place. This has lead to a condition that stable cw-modelocking will occur if:

$$E_{p,int}^2 > E_{L,sat} E_{A,sat} \Delta R, \quad (5.18)$$

Where $E_{p,int}$ is the intracavity pulse energy, $E_{L,sat}$ the gain saturation energy which is given as $E_{L,sat} = F_{sat,L} A_{eff,L}$, $F_{sat,L}$ is the gain fluence and $A_{eff,L}$ the laser beam effective area on the gain crystal, while $E_{A,sat}$ is the absorber saturation energy given as

$E_{A,sat} = F_{sat,A} A_{eff,A}$ with $F_{sat,A}$ the saturable absorber fluence and $A_{eff,A}$ the laser beam effective area on the saturable absorber.

Substitution of the saturation parameter S from Equation 5.15 into Equation 5.18 gives:

$$E_{p,int} > E_{L,sat} \frac{\Delta R}{S}, \quad (5.19)$$

which can easily illustrate why passively modelocked lasers regularly operate at the *QSML* regime when weakly pumped and in the stable cw-modelocked regime when pumped at high powers. When the gain saturation energy, $E_{L,sat}$ is large, meaning that the laser beam area on the laser medium is large or that the laser medium has a small laser emission cross-section, Equation 5.19 shows that the *QSML* threshold will be high. The increase in the amount of intracavity energy of the pulse $E_{p,int}$ is limited by the amount of pump power available from the pump source. The amount of intracavity energy of the pulse $E_{p,int}$ would be reduced if large amounts of intracavity losses are present in the resonator and a high modulation depth value would also cause the $E_{p,int}$ to be low.

The inequality of Equation 5.18 has always to be kept true in order to avoid the *QSML* regime and therefore gives us guidelines on how to avoid the *QSML* regime. One has to make sure that the gain saturation energy is reduced by choosing a gain medium with a small saturation fluence and also using a laser beam which would have a small area on the gain medium. The use of a small laser beam also applies to the saturable absorber because this would lead to a small absorber saturation energy, even though this could lead to damaging the absorber. When using a saturable absorber with a small modulation depth, a long resonator with low repetition rate would attribute to avoiding the *QSML* regime.

5.4 Summary

To obtain stable passive modelocking a number of requirements will have to be taken into consideration and they are summarised as follow:

- The laser must operate on the fundamental transverse mode TEM_{00} , with good spatial beam quality.
- The conditions for avoiding Q -switch modelocking to occur which are discussed in section 5.3.5 will have to be fulfilled in order to get stable cw-modelocking.
- The use of a strong saturable absorber with a long recovery time is usually suitable to get stable self starting cw-modelocking.
- The saturable absorber should also be strong and fast enough to compensate for the smaller effective gain of the short pulses by having a sufficient loss difference between the pulses and cw background.
- The use of SPM should not be too strong to get stable cw-modelocking, especially in a situation where there is zero or positive dispersion. But a strong SPM is desirable for soliton modelocking.

Part 2 – Design and evaluation of a SESAM modelocked diode-end- pumped Nd:YVO₄ laser

6. Experimental Design

6.1 Resonator stability criteria

The aim of the project was to develop a cw-modelocked diode-end-pumped solid-state Nd:YVO₄ laser, using semiconductor saturable absorber mirrors (SESAM) as a modelocking mechanism. The physics behind developing a stable cw-modelocked laser is given by the fundamental Equation 5.18, where the square of the intracavity pulse energy ($E_{p,int}^2$) should be greater than the product of saturation energy of the laser medium ($E_{sat,L}$), the saturation energy of the absorber ($E_{sat,A}$) and the modulation depth of the saturable absorber (ΔR) [6.1]:

$$E_{p,int}^2 > E_{sat,L} E_{sat,A} \Delta R . \quad (5.18)$$

The modelocking of ion-doped solid state lasers is hindered by three obstacles. The first problem is related to the self- Q -switching instabilities, where the laser produces a bunch of modelocked pulses which may or may not have a stable Q -switching envelope. The second problem are Q -switching instabilities which are influenced by the fact that ion-doped solid-state lasers have an emission cross-section that is typically more than 1000 times smaller than gas lasers, which results in high saturation fluence leading to Q -switching instabilities. The third problem is that the upper state lifetime of the laser transition for ion-doped solid state lasers is more than 1000 times longer than gas lasers, which allows enough time for Q -switching problems to occur when trying to passively modelock the laser.

The saturation energy of the gain $E_{sat,L}$ is defined as the product of saturation fluence

$F_{sat,L} = \frac{h\nu}{m\sigma_L}$ and the effective laser mode area $A_{eff,L}$ inside the gain medium. The factor

m in the definition of $F_{sat,L}$ is the number of passes through the gain element per cavity round trip. Due to the factor m the gain saturation depends on the geometry of the laser cavity; where $m = 1$ will be a ring cavity and $m = 2$ will be a for a simple standing wave cavity. The effective mode area is defined as $A_{eff,L} = \pi w_L^2$, where w_L is the $1/e^2$ Gaussian beam radius with respect to intensity. Therefore the saturation energy can be expressed in the following Equation 6.2 as:

$$E_{sat,L} = F_{sat,L} A_{eff,L} = \frac{h\nu}{m\sigma_L} \pi w_L^2 . \quad (6.2)$$

The underlying physics that promotes self- Q -switching instabilities are related to the emission cross section of the laser medium (σ_L):

$$E_{sat,L} \propto \frac{A_{eff,L}}{m\sigma_L} . \quad (6.3)$$

It has been shown that the smaller the emission cross-section, the stronger the tendency of the laser to operate in a Q -switched regime. Therefore the use of Nd:YVO₄ as a gain medium should alleviate the tendency of the laser to operate in a Q -switched regime since it has a large emission cross-section of about $25.0 \times 10^{-19} \text{ cm}^2$ at 1064 nm compared to other ion-doped solid state lasers such as Nd:YAG with an emission cross-section of $2.8 \times 10^{-19} \text{ cm}^2$. This means a laser material with a large stimulated emission cross section σ_L is therefore desirable for stable modelocking since σ_L is inversely proportional to the saturation energy of the gain medium as shown in Equation 6.3.

The large emission cross section leads to a smaller saturation energy of the laser gain medium thereby satisfying the inequality in Equation 5.18 as to avoid Q -switching instabilities. This can also be achieved by choosing a resonator geometry with multiple

passes through the gain medium to decrease the gain saturation fluence. Selecting an inhomogeneously broadened laser material with the same average stimulated emission cross section σ_L would also reduce the gain saturation because the type of laser ions with the highest cross section dominate the gain saturation.

The average mode area inside the laser medium ($A_{Aff,L}$) should also be kept small because it also influences the saturation energy since both are directly proportional to one another. To obtain high powers from a modelocked laser was initially a problem since high power scaling required one to maintain the fundamental Gaussian beam quality and at the same time also suppressing Q -switching instabilities. Many high-power lasers have a large beam size inside the laser medium resulting from the high-power pump diode bars. Although for CW lasers this is not a problem, for passively modelocked lasers it leads to excessive Q -switching instabilities. That is why power scaling typically comes at the expense of longer pulses, because the modulation depth of the SESAM has to be reduced. Using a smaller mode in the laser medium and on the absorber can reduce the tendency of the laser to Q -switch, but at the same time the mode size on the absorber should not be too small because it will lead to the SESAM being damaged, which is a further problem when trying to modelock solid-state lasers.

Typically SESAMs are operated with an incident pulse fluence of about three to five times that of the saturation fluence. This saturation level of the absorber provides nearly the maximum modulation depth without damaging the device. Higher saturation also reduces the tendency for Q -switching instabilities because of thermal effects. Therefore the average laser mode area ($A_{eff,A}$), inside the saturable absorber should be not too large since it will increase the saturation energy of the absorber (see Equation 6.4):

$$E_{sat,A} \Delta R = A_{eff,A} F_{sat,A} \Delta R, \quad (6.4)$$

and thereby increasing the tendency of the laser to operate in a Q -switching regime as shown in Equation 5.18. This means that the laser spot size w_A on the end mirror or on the SESAM should be small since the average laser mode area is defined as in Equation 6.5:

$$A_{eff,A} = \pi w_A^2. \quad (6.5)$$

In order to develop and design a good modelocked laser all the parameters which have been discussed above, such as laser mode size on the crystal and absorber, the material used for lasing and the resonator length all are independent parameters which will have to be optimum in order to achieve a good modelocked laser.

6.2 Resonator design and pump setup

The laser resonator was designed using the St Andrew's software model PSST! [6.2]. The software uses the standard ABCD matrix formalism and is appropriate for the design of cavity optics for high-power single transverse-mode operation of the Nd:YVO₄ laser. The model calculates the spot sizes within the crystal and on the end mirrors as a function of the focal length of the thermal lens as well as the curvature of the end mirrors and the relative position of the mirrors with respect to the crystal.

A set of cavity optics parameters and their relative position can be entered in the model to achieve the appropriate allowed beam size within the crystal, on the end mirror and the output coupler (OC) and also an appropriate allowed resonator cavity length. There were a number of resonator cavity length designs that were done, but the final resonator that gave the desired small spot sizes on the end mirror and in the crystal for a stable resonator had the total length of 225 mm as seen on the following Figure 6-1 where L_2 is 75 mm and L_1 is 150 mm, with 1 representing the centre of the crystal. The curved mirror represents the output coupler (OC) with a radius of curvature R of 300 mm.

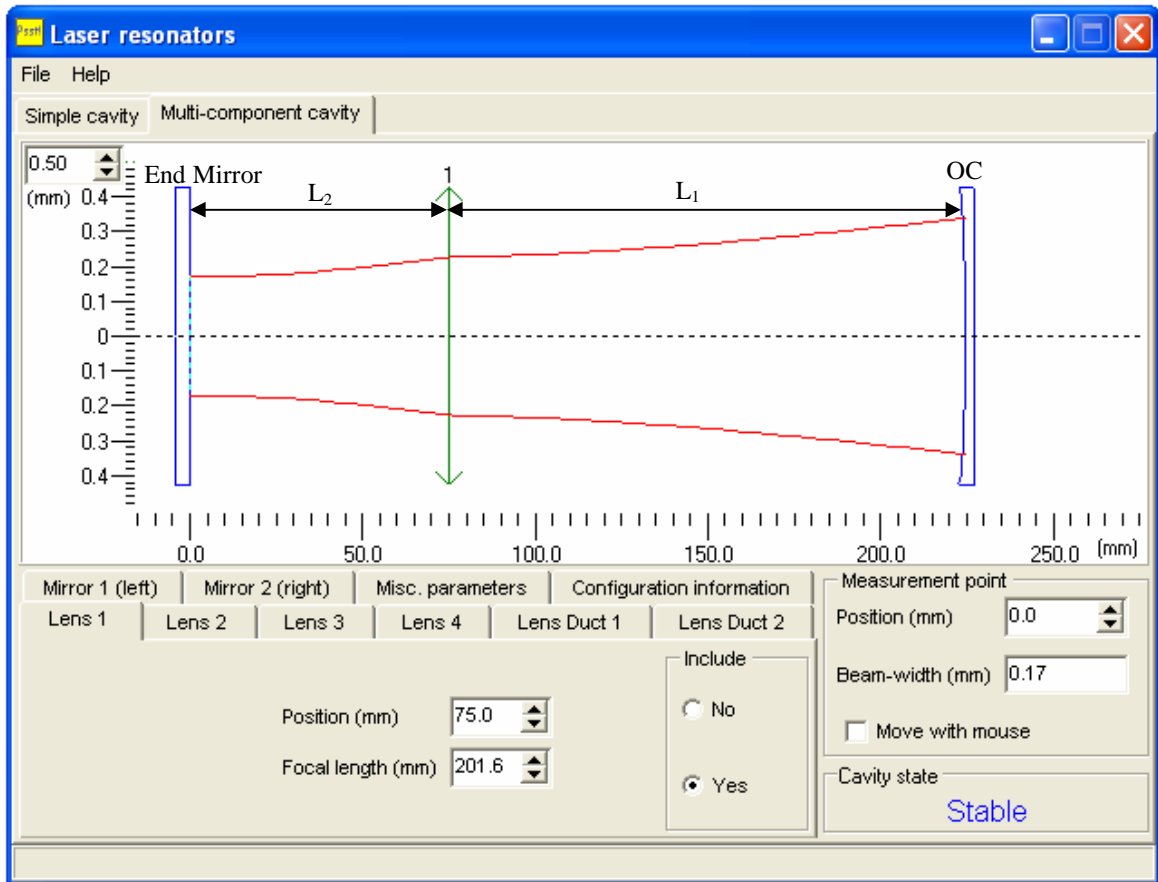


Figure 6-1: User interface of St.Andrew’s design software PSST! representing a resonator cavity length of 225 mm where L_1 is 150 mm and L_2 is 75 mm.

The spot size on the flat end mirror was designed to be $\sim 170 \mu\text{m}$ and on the crystal $\sim 250 \mu\text{m}$. The L_1 distance between the crystal and the output coupler was folded at approximately 20 degrees at a distance of 33 mm from the crystal centre by using a flat pump mirror as shown in the following Figure 6-2. The actual inclusion of the pump folding mirror does not change the resonator parameters such as the spot size on the crystal and on the end mirror.

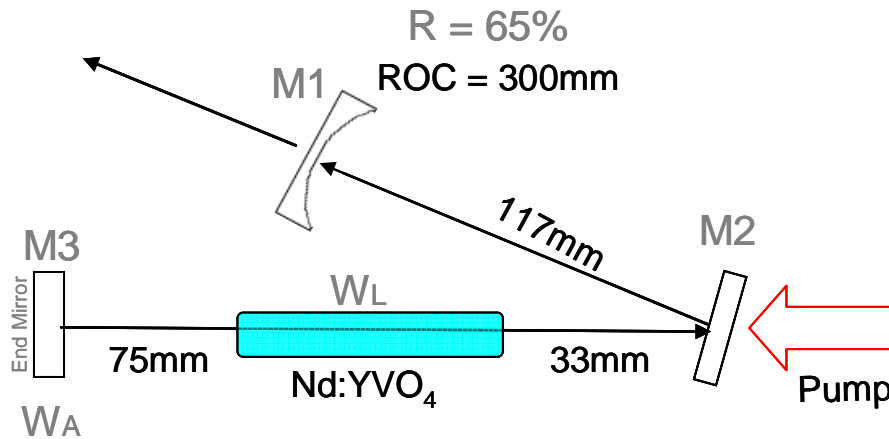


Figure 6-2: Schematic representation of the laser with a cavity length of 225 mm, where M1 is the output coupler, M2 the pump mirror and M3 the end mirror.

The addition of the folding pump mirror (M2) allowed the crystal to be longitudinally pumped through M2. This was also essential since the resonator length had to be extended at a later stage. The pump mirror was designed to have an anti-reflection (AR) coating to transmit the 808 nm pump wavelength and a high reflection (HR) coating for the laser wavelength at 1064 nm.

6.3 Pump beam characterization

For efficient mode matching between the resonator mode and the large pump mode in the Nd:YVO₄ crystal, a fibre-coupled diode laser had to be used. The pump diode laser was obtained from Jenoptik (Model JOLD-24-CPFN-1L) and it had a maximum output power of 24 W. The diode pump radiation was delivered by the use a 0.4 mm diameter 0.22 numerical aperture optical fibre. The fibre end was imaged on to the focusing lens with a focal length of 50 mm and the pump beam profile measured using a Coherent 4812 CCD camera at the foci inside the crystal is shown in Figure 6-3. This related to a pump beam quality M^2 value of approximately 200 in the far field approximation.

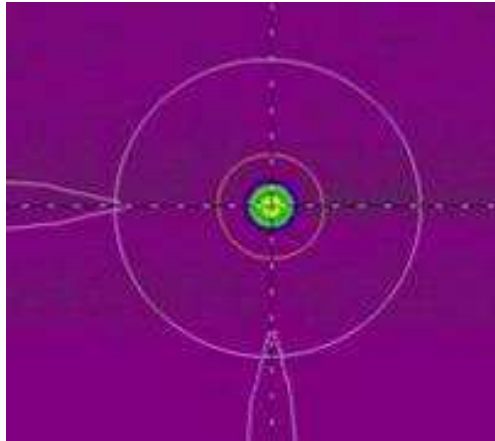


Figure 6-3: Pump beam profile of the laser diode at the focus.

The manufacturer of the laser diode specified the operating wavelength at 25 °C to be 808 nm with 2.5 nm FWHM (Full width half maximum) spectral width and with a 3.0 nm 90 % width. The laser diode was mounted on a water-cooled copper heat sink. The cooling water for the diode laser and the laser crystal was controlled to circulate at a flow rate of 2 litres per minute while at the same time keeping the water temperature constant at 20 °C. In addition to the water-cooling controller an extra Peltier-cooler-controller was used to actively control the temperature of the diodes at 30°C so as to maintain a constant wavelength during operation.

The efficiency of the diode laser is determined by measuring the optical output power versus electrical input current to the diode laser at a constant temperature of 30 °C. The electrical input power was measured using a multimeter and the output power of the laser diode with a Coherent LM-45 power head and the Coherent Field Master power meter. The result shown in Figure 6-4 closely approximates the expected trend that the optical output power of the laser diode should increase linearly with an increase in electrical input power.

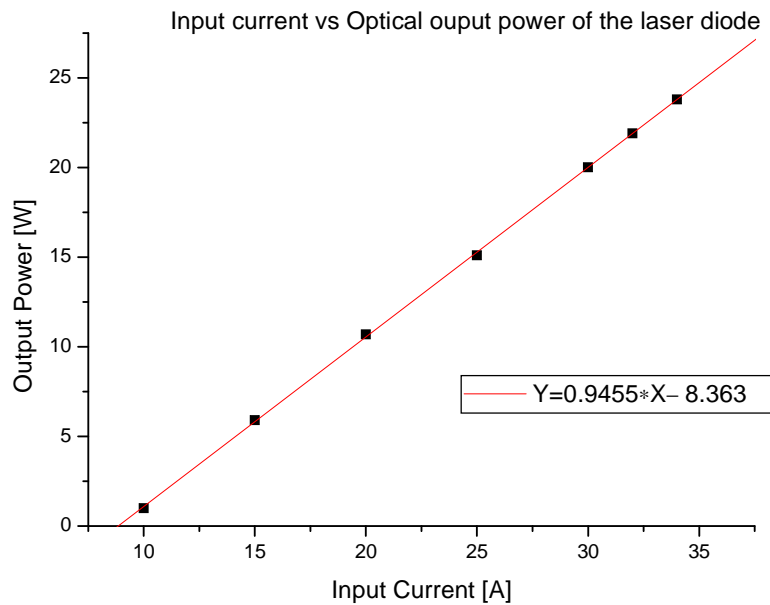


Figure 6-4: Slope efficiency of the laser diode at 30°C.

The maximum output power was 23.8 W which was very close to the value specified by the manufacturer of 24 W.

Two lenses were mounted inside a cylindrical barrel on an xyz-adjustable mount, to allow for accurate positioning of the pump waist inside the crystal. The first lens was used for collimating the pump light and the second lens for focusing the beam into the crystal. The waist of the pump beam created by the second lens was adjusted to overlap with the resonator mode in order to get maximum coupling efficiency, while at the same time determining the optimum pump waist position along the optical axis to be 52 mm away from the centre of the crystal. The beam profile of the diode pump radiation measured using a Coherent 4812 ccd camera was 0.47 mm in diameter at the focus as seen on Figure 6-5. The pump beam waist diameter was measured to be 500 μm , which fitted well within our calculated design parameters of the high power laser or modelocked laser (see Table 8.2 for the calculations).

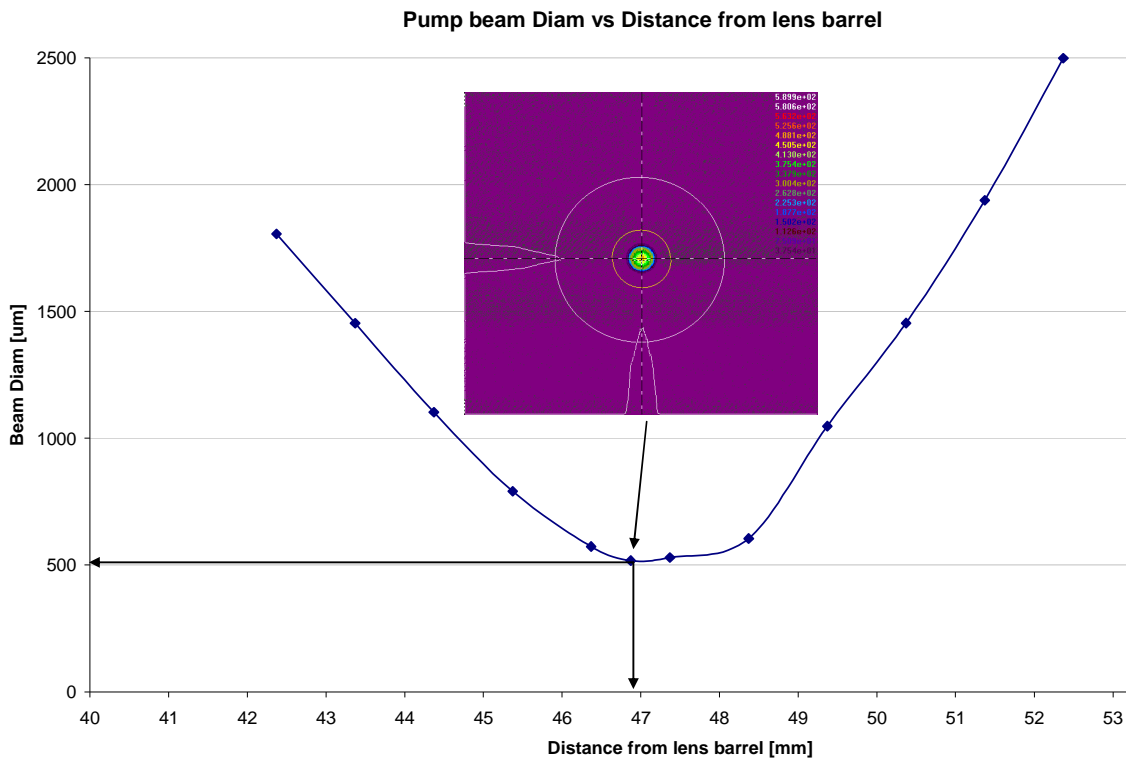


Figure 6-5: Pump beam profile for a focal length of 46.9 mm.

The requirements for a high-power-scalable laser are that the pump beam should be large inside the lasing material, to limit the possibility of thermal damage and fracture of the crystal. The use of a small pump beam mode which deposits large amounts of heat into a small volume inside the lasing material frequently leads to thermal damage. A pump beam diameter of 500 μm is sufficiently large to reduce the possibility of fracturing the crystal and at the same time will allow better coupling efficiency of the laser mode and pump mode so as to achieve an efficient modelocked laser.

6.4 Laser medium

The design of the laser resonator incorporated a Nd:YVO₄ laser crystal with a low Nd³⁺ doping concentration of 0.27 % designed to minimize and reduce the risk of thermally induced fracture. It has been shown by P.J. Hardmann [6.1] that a low doping concentration will minimize the overall heat generated in the crystal without compromising the laser efficiency. Therefore a laser medium with a very low doping concentration was chosen resulting in a low excitation density which will reduce the heat density factor in the gain medium [6.3] thereby making the modelocked laser stable.

The Nd:YVO₄ laser crystal used in the laser design and experimental setup was 12 mm long. The length of the crystal was chosen to be long since crystals with low doping concentration need to absorb a sufficient amount of pump radiation. This makes the low doping advantageous in reducing thermal fracture, since the heat deposited or generated in the crystal is spread along the full length of the crystal which is fairly easy to cool if the crystal is a square or cylindrical rod. In our laser design and experimental setup we used a square rod, since it was the only available Nd:YVO₄ crystal at that time.

The use of a large pump diameter of 500 μm in the crystal was also an additional measure to decrease the excitation density in the crystal [6.3]. The crystal dimensions were 4 \times 4 \times 12 mm, meaning the side distance from the centre of the crystal to the edge was \sim 2 mm, much larger than the pump radius of 250 μm and by more than 3 times as required for limited diffraction losses due to the hard aperture of the crystal edges [6.4 Ch 4].

The pumping of the Nd:YVO₄ crystal using an un-polarized pump source such as the fibre-coupled laser diode, in our case, tuned at a wavelength of 808 nm causes greater absorption of pump energy for the π -polarization than that of the σ -polarization, as shown in Figure 6-6, taken from LASCAD 3.1 – Manual [6.5].

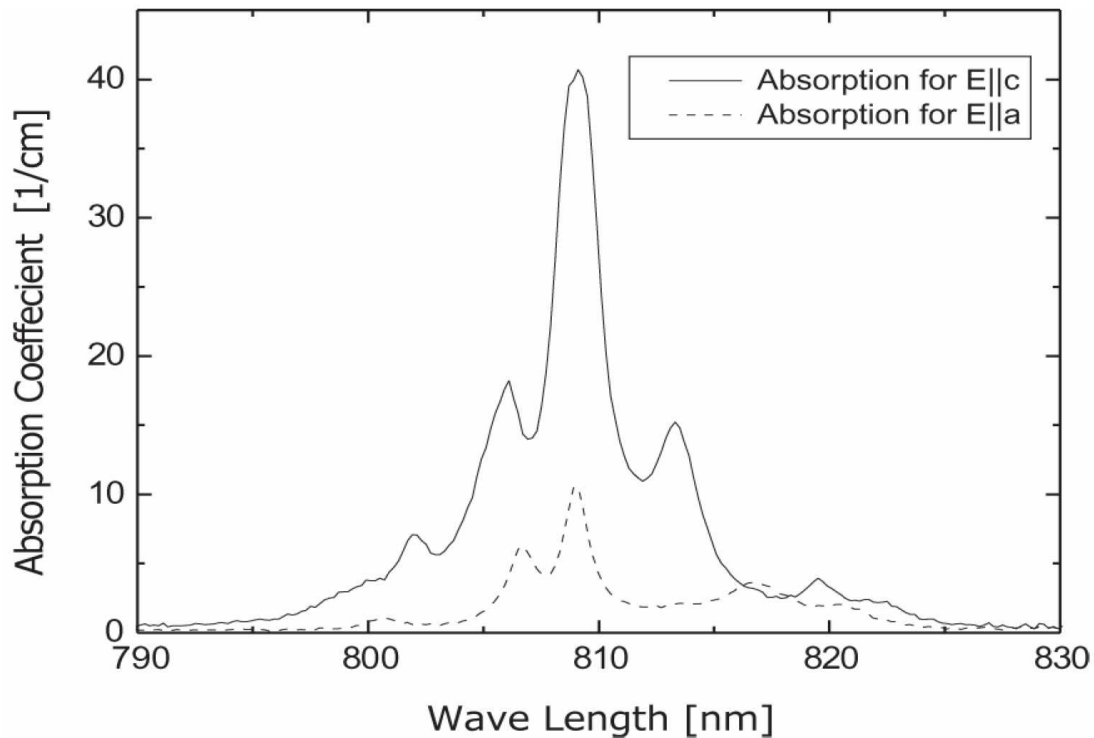


Figure 6-6: Absorption spectrum of 1 atomic % Nd:YVO₄, where the π -polarization is 42 cm⁻¹ and σ -polarization is 11 cm⁻¹ [6.5].

This is because the absorption coefficient on the π -polarization for Nd:YVO₄ is high at this specific wavelength of 808 nm. For an example a 1 % (at.) doped Nd:YVO₄ crystal has been shown by C. Czeranowsky [6.6] to have an absorption coefficient on the π -polarization of 79 cm⁻¹ and 17 cm⁻¹ for the σ -polarization, while on the above Figure 6-6, the absorption coefficient on the π -polarization is 42 cm⁻¹ and 11 cm⁻¹ on the σ -polarization. In the literature several differing values have been stated for the absorption of Nd:YVO₄ for both polarizations but in this project we used the Czeranowsky results.

As shown above the absorption coefficient of the π -polarization is almost 4 times greater than that of the σ -polarization; the laser will therefore emit on the π -polarization. The only possible time the laser emission could be on the σ -polarization is when the resonator is unstable for the π -polarization.

6.5 Cooling method for Nd:YVO₄ crystal

When the Nd:YVO₄ crystal absorbs almost all the pump power, heat is generated in the crystal. The use of a square rod geometry is helpful because it allows end-pumping while at the same time the heat generated in the crystal can be easily removed by conductive cooling of two sides of the crystal which are clamped on a copper heat sink as shown the following Figure 6-7.

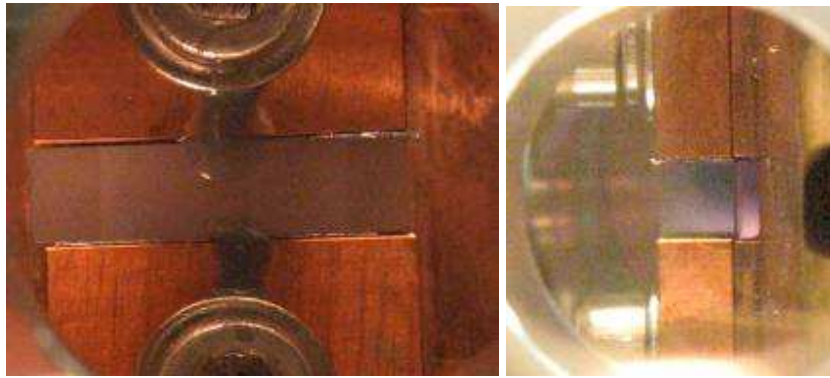


Figure 6-7: Nd:YVO₄ crystal sandwiched between two copper heat sinks. The glue was used only to secure the crystal.

The design of the heat sink where the crystal was mounted allowed a two side heat extraction gradient from the centre, while the other two faces of the crystal were not in contact with the heat sink. The two side heat extraction was sufficient to cool the crystal.

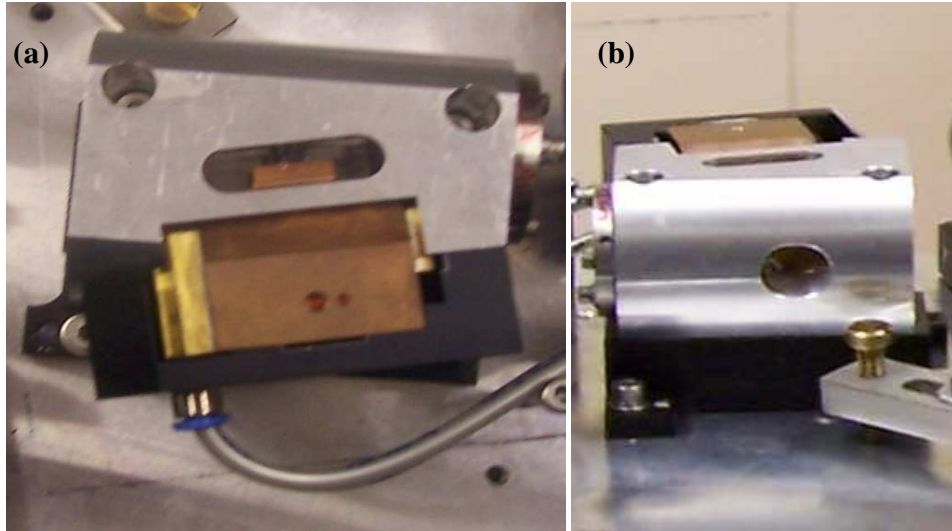


Figure 6-8: Top view (a) and side view (b) of the crystal mount.

The top and side openings of the heat sinks shown in Figure 6-8 allowed for easy observation of the alignment of the pump beam mode and the laser mode. The heat sink configuration was very robust, compact and allowed for easy mounting within the laser cavity.

The heat sink was also designed in such a way that the folding pump mirror M2, (as shown in Figure 6-2) was mounted on the left hand side of the crystal mount as shown in Figure 6-8. This makes the resonator design compact and the pump mirror M2 stable, meaning that the pump mirror M2 will not get misaligned since it is hard-mounted on to the heat sink.

6.6 Summary of the design

The laser mode size at the flat end mirror (w_A) and in the crystal (w_L) as well as the spatial overlapping of the pump mode with the laser mode in the crystal were all designed in order to achieve a stable and efficient laser. This type of laser as shown schematically in Figure 6-2 was designed so that it avoids modal instabilities at high output powers. Therefore power scaling such a laser will result in a laser that will operate with only a single-transverse mode. Since the absorption coefficient of the σ -polarization is 4 times

smaller than for the π -polarization, the possibilities of thermal fracture due to non-uniform heat distribution in the crystal is minimized, but for high power operation there could still be a problem. But the risk of thermal fracture could be avoided by using a low-doped crystal with increased length in order to absorb enough pump power and at the same-time using an efficient cooling method to remove most of the heat from the crystal. This makes the way of how the laser crystal was mounted and cooled during lasing operation very important in avoiding instabilities at high output powers.

7. Diagnostic instruments

The laser performance was determined by using equipment such as the Coherent LM-45 power head which measured continuous wave power in conjunction with the Coherent Field Master power meter for value readings.



Figure 7-1: Coherent LM-45 power meter and Coherent Field Master readout.

The beam shape of the laser was captured using the Coherent 4812 CCD camera. The beam profile, and also the beam quality factor M^2 were measured using an automated Spiricon M^2 -200 machine.

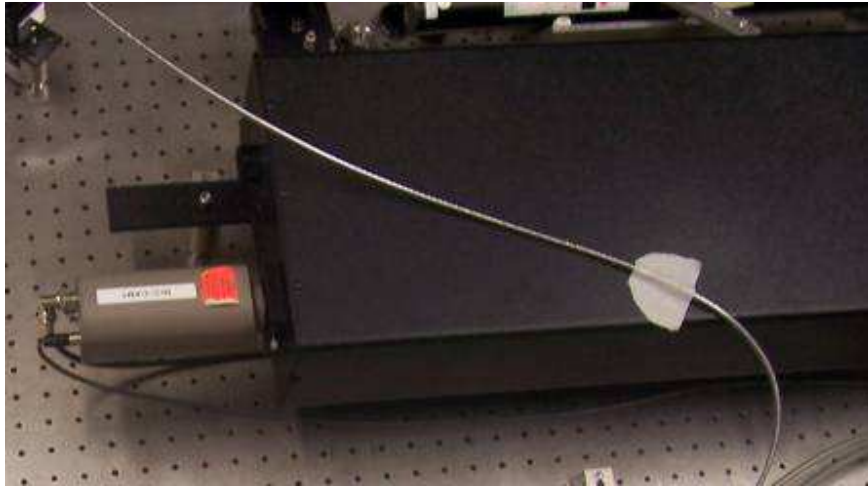


Figure 7-2: Coherent CCD camera and the Spiricon M^2 -200 instrument.

During pulsed operation of the laser, the time resolved pulse length was measured with a Hamamatsu C5658 photo diode detector with a 1GHz wideband detection limit, connected to a Tektronix 500 MHz oscilloscope. The modelocking of the laser pulses was determined by observing the pulse repetition rate on the oscilloscope which should be equivalent to the cavity round trip time of the laser.

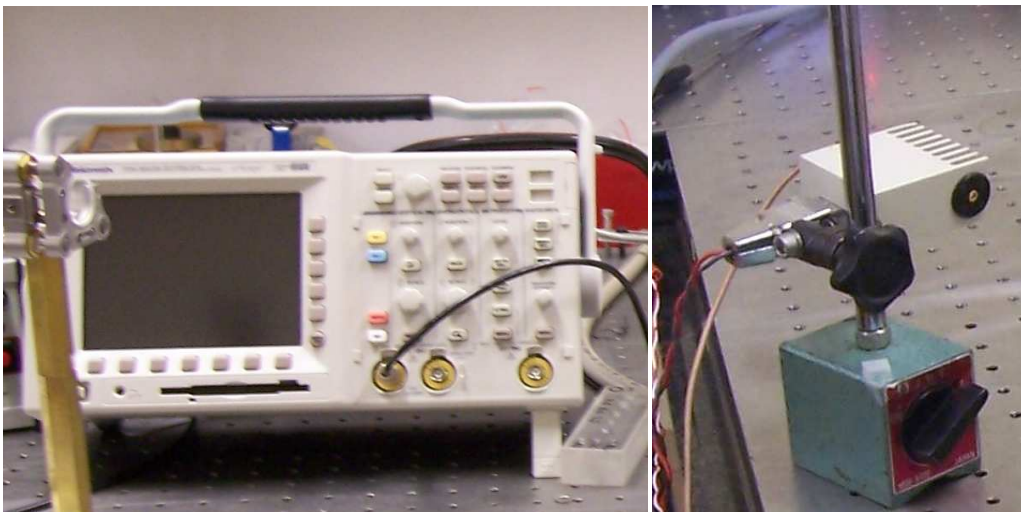


Figure 7-3: Tektronix 500 MHz oscilloscope and Hamamatsu photo diode detector.

8. Results

8.1 Power scaling of Nd:YVO₄ laser

There were a number of laser cavities of different lengths designed for the Nd:YVO₄ laser, that were investigated, varying only the resonator cavity length while keeping all the other optical elements such as the output coupler, pump mirror, end mirror and the crystal size constant. This was done to get an indication of how stable the laser performance would be when the cavity length of the laser is varied during power scaling. The finding was that the stability of the laser during power scaling does get affected by varying the cavity length and this was measured using a power meter that measured the average output power of the laser and a Spiricon M²-200 with a Coherent CCD camera to measure the laser beam quality and profile.

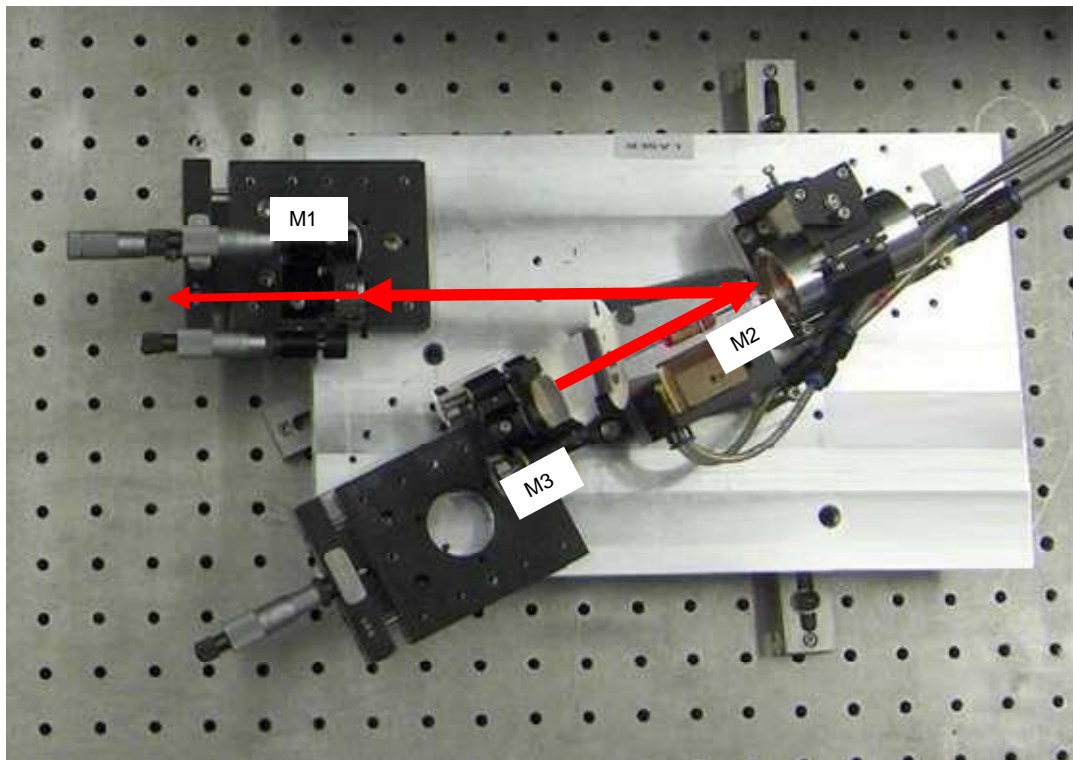


Figure 8-1: Resonator with cavity length of 225 mm showing resonator mirrors and other components.

The three designed laser resonator cavity lengths are shown in Table 8.1.

Table 8.1: Designed laser resonator cavity lengths.

Resonator	L_1 [mm]	L_2 [mm]	L_{tot} [mm]
1	67.5	102.7	170.2
2	73.2	126.8	200
3	75	150	225

All three of the laser resonators had a small laser spot size diameter in the crystal and on the end mirror. For example the laser resonator with a total cavity length of $L_{tot} = 200$ mm, the laser spot size in the crystal W_L was 222.7 mm; while the laser resonator with a total cavity length of $L_{tot} = 225$ mm shown in Figure 8-1, the laser spot size in the crystal W_L was 225.4 mm.

The graph in Figure 8-2 shows the measured efficiency curves of the Nd:YVO₄ lasers of different cavity lengths with identical optical elements of the laser resonator. The reflectivity of the output coupler used was 65 %.

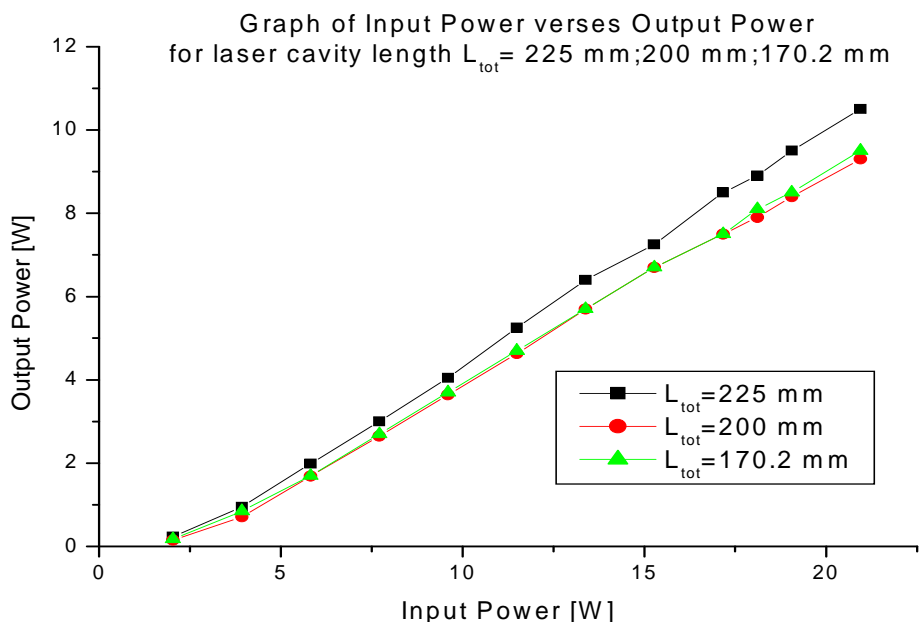


Figure 8-2: Slope efficiency for the lasers with cavity lengths of 225 mm, 200 mm and 170.2 mm.

At the maximum pump power of 22 W, the lasers with the total cavity length of $L_{tot} = 170.2$ mm and $L_{tot} = 200$ mm had the lowest output power of 8.5 W and 9.7 W respectively and also with the lowest optical-to-optical efficiency of 39 % and 44 %, and the lowest slope efficiency of 45.2 % and 48 % respectively. The other laser with the total resonator cavity length of $L_{tot} = 225$ mm had the highest output power of 10.5 W at the maximum output power of 22 W and also the highest input-to-output power efficiency of 55.7 %. The decision was clear that the laser with the highest output power and the highest optical-to-optical efficiency was going to be modelocked by replacing the end mirror with the SESAM, since the laser showed stable operation with almost linear increase of output power during power scaling even at high input powers.

The far field beam profile of the laser outputs is shown in Figure 8-3. For all three lasers the beam profiles were nearly circular at an average output power of 8 W, which indicated that the laser operated on the fundamental transverse laser mode TEM_{00} , which is what was desired during power scaling.

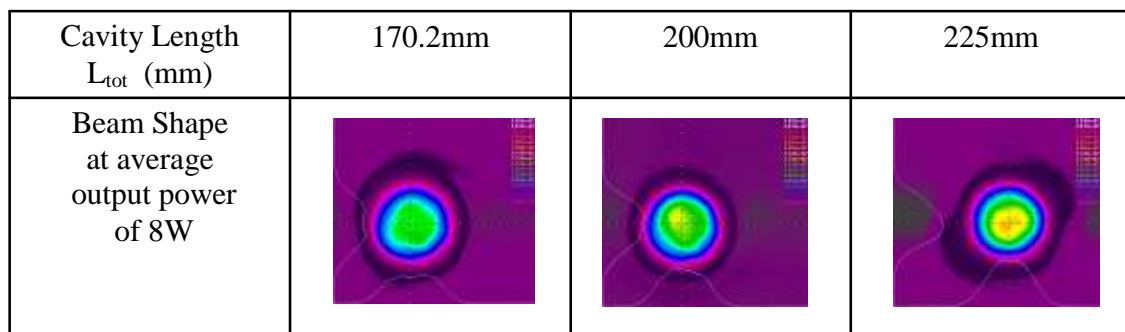


Figure 8-3: Beam profiles of lasers with cavity lengths of 170.2 mm, 200 mm and 225 mm at an average output power of 8 W.

The graph in Figure 8-4, represents the measured beam quality factor M^2 for the laser with the total cavity length $L_{tot} = 225$ mm. The change in the beam shape and the beam quality factor M^2 at input power of around 18 W which corresponded to an output power of 8 W is due to the increase in the thermal lens of the gain medium at high input powers. Even though the beam shape is slightly oval at 8.5 W output power; the beam quality is

still good for the laser with cavity length of 225 mm, with an M^2 value below 2 as shown in the following Figure 8-4.

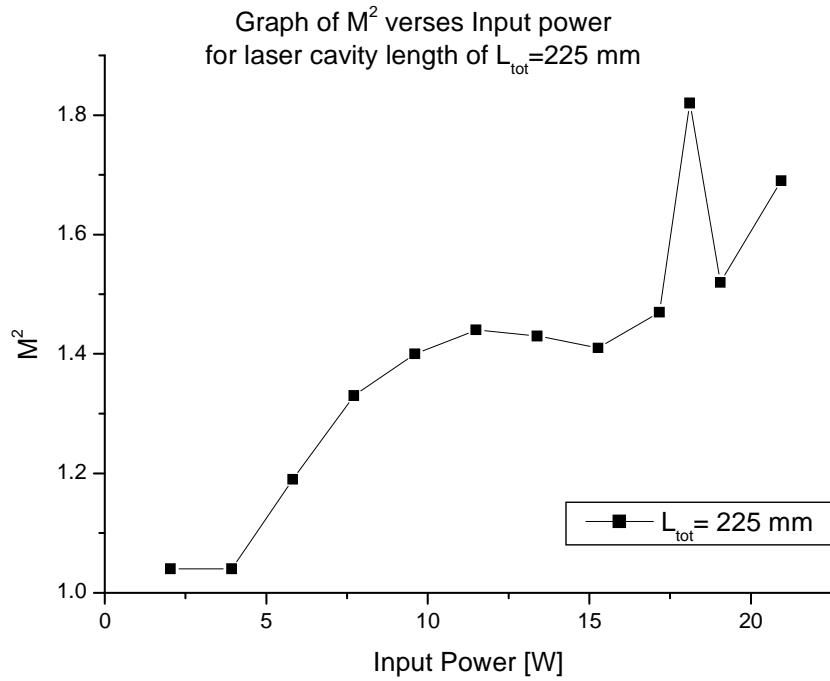


Figure 8-4: Beam quality factor M^2 versus pump power for the laser with a cavity length of 225 mm.

It was unfortunate that we did not have Nd^{3+} crystals of different doping levels as well as output couplers with a range of transmissions and different radius of curvature to experiment with, so as to find the most stable laser for high power operation. Even though there were limitations the more appropriate laser to use for modelocking by SESAM was found to be the laser with the total resonator cavity length of $L_{tot} = 225$ mm , since it exhibited better properties during power scaling such as good beam profile and also optical-to-optical efficiency.

8.2 Requirements for modelocking a Nd:YVO₄ laser using SESAM

The available SESAMs were obtained from Dr. Erwin Bente of the Institute of Photonics at the University of Strathclyde in the United Kingdom. There were two types of SESAMs available, a single quantum well (SQW) and a double quantum well (DQW) SESAM, both were suitable for operation at 1064 nm wavelength. The SESAM quantum well was constructed from In_xGa_{1-x}As material and grown on GaAs, where the indium content x was adjusted to obtain a small band gap. This made the material suitable for use as absorbing layer within semiconductor saturable absorber mirror which would be compatible with 1 μ m-neodymium-doped lasers. The SESAM was constructed using a 10 nm saturable absorber layer composed of In_{0.25}Ga_{0.75}As embedded within the topmost layer of a 30 pair GaAs/Al_{0.8}Ga_{0.2}As stack. The structure was grown by non-rotated metal-organic chemical vapour deposition (MOCVD).

Modelocking the laser with the cavity length of $L_{\text{tot}} = 225$ mm could have been done by replacing the flat end mirror with a semiconductor saturable absorber (SESAM). But using such a short laser cavity would have made cw-modelocking of the laser unstable or could have even damaged the SESAM, since the QSML transition would have occurred at very high output powers where the laser could have been producing unstable high energy peak pulses. This is shown by Equation 8.1, where the internal pulse energy squared ($E_{p,\text{int}}^2$) would increase if the laser resonator length decreases (or the frequency of the laser increases).

By definition the intracavity pulse energy ($E_{p,\text{int}}$) is given by Equation 8.1:

$$E_{p,\text{int}} = \frac{P_{\text{int}}}{f}, \quad (8.1)$$

with the intracavity average power (P_{int}) and the pulse repetition rate (f_{rep}). A cw-modelocked laser with a cavity length of $L_{\text{tot}} = 225$ mm would of have had a pulse

repetition rate of 666 MHz which is extremely high. This would have made the intracavity pulse energy ($E_{p,int}$) very small since it is inversely proportional to the pulse repetition rate. When the intracavity pulse energy (E_p) is very small, the pulse becomes unstable due to noise fluctuations in the laser cavity resulting in Q -switching instabilities.

If the Q -switched modelocked state was achieved at high average output powers, with a focal spot of 170 μm on the SESAM it would cause optical damage to the SESAM. To avoid damaging the SESAM, the Q -switched modelocked output power threshold ($P_{QSM,th}$), has to be achieved at very low input powers. This can be done by solving Equation 5.18, which defines the condition for stable cw-modelocking in terms of $P_{QSM,th}$, (refer to equation in Appendix). The result is given by the following Equation 8.2:

$$P_{QSM,th} = K T_{OC} \frac{w_L w_A}{L} \sqrt{F_{sat,A} \Delta R}, \quad (8.2)$$

where $K = \sqrt{\frac{\pi^2 h c^3}{4 m \sigma_L \lambda}}$.

To achieve a low $P_{QSM,th}$, Equation 8.2 shows that the laser spot size inside the crystal (w_L) and on the SESAM (w_A) should be very small, since they are directly proportional to the $P_{QSM,th}$. Not only do small spot sizes in the crystal and on the SESAM reduce $P_{QSM,th}$ they also avoid Q -switching instabilities, where a balance between stronger saturation of the SESAM and stronger saturation of the gain makes the pulse energy stable thereby achieving stable cw-modelocking. Our designed spot size of 250 μm in the crystal and 170 μm on the SESAM were sufficient to saturate both the crystal and the SESAM.

The output coupler transmission of the laser also plays a role in reducing the Q -switched modelocked transition threshold to lower output powers, since the two are directly

proportional to another, as shown by Equation 8.2. Using a low output coupler transmission, the $P_{Q\text{SML,th}}$ will also be reduced, but in the case of our laser, we were restricted to an output coupler with a 35 % transmission, the only output coupler available with a radius of curvature of 300 mm.

The temperature tuning of the SESAM also affects the $P_{Q\text{SML,th}}$ and this was shown by D. Burns and colleagues [8.1]. The output power which corresponds to the transition between the Q -switched modelocked state and the stable cw-modelocked state increases as the SESAM temperature is increased as shown in Figure 8-5.

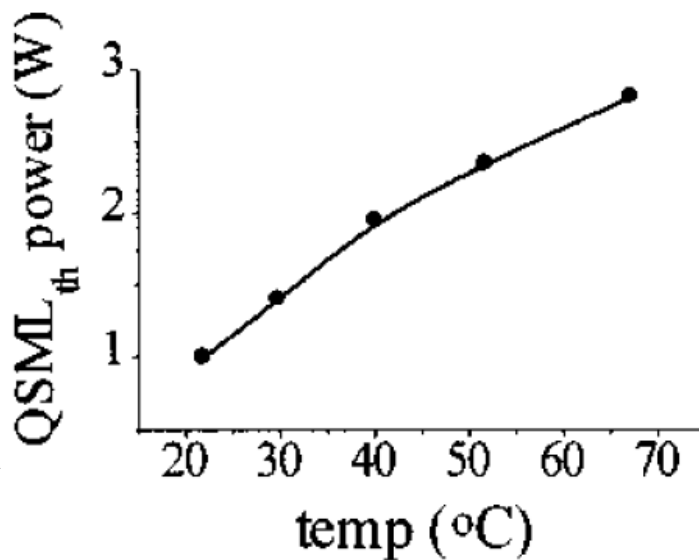


Figure 8-5: Q -switched modelocked transition ($P_{Q\text{SML,th}}$) average output power versus temperatures for a single quantum well SESAM [8.1].

The pulse duration can also get reduced as the temperature of the SESAM is increased. These effects occur when the exciton absorption resonance is at a shorter wavelength than the laser emission. The increase in temperature of the SESAM also makes the absorption peak shift to longer wavelengths, which then causes the laser to experience greater saturable absorption and so increases the modulation depth ΔR , as shown by the graph of $P_{Q\text{SML,th}}$ versus temperature in Figure 8-6 depicting calculated values of $F_{\text{sat},\Delta R}$

(as detailed in Reference [8.2] Honninger *et al*) versus temperature. The data are useful for the comparison of the underlying saturable absorption properties of the different saturable absorber structures and devices.

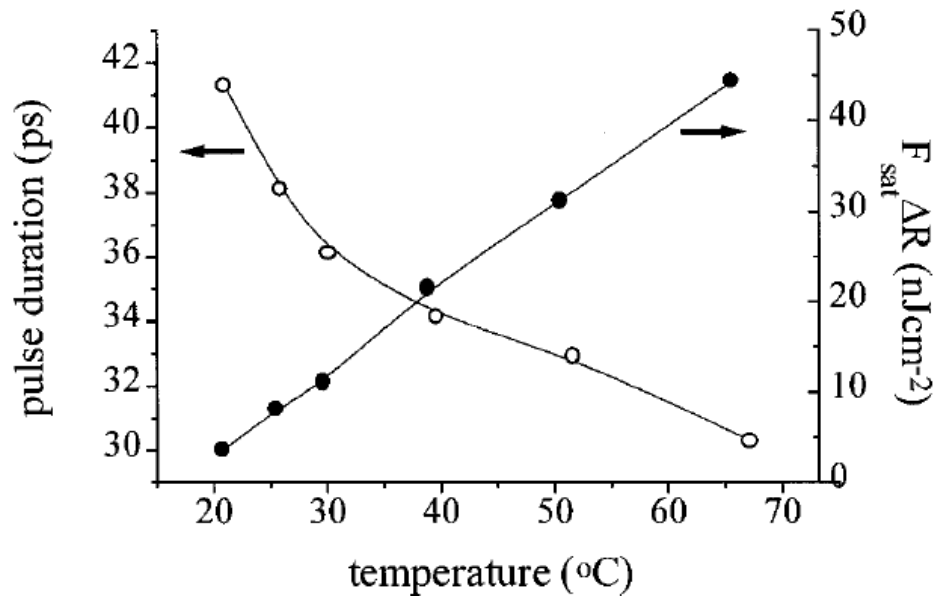


Figure 8-6: Temperature tuning of a single quantum well SESAM [8.1].

The cavity length (L) also affects the Q -switched modelocked transition threshold as shown in Equation 8.2. For a very long cavity length, the $P_{QSM,th}$ output power gets reduced which is ideally suitable for reducing the possibility of damaging the SESAM, since the cavity length is indirectly proportional to the $P_{QSM,th}$.

8.3 Calculation of Nd:YVO₄ resonator parameters for cw-modelocking

The calculation of the resonator parameters to achieve a low Q -switched modelocked output power threshold ($P_{\text{QSML,th}}$) are shown in Table 8.2 and are based on Equation 8.2. The bold numerical figures in Table 8.2 represent calculated parameters and the non bold ones design parameters. The calculation produced a $P_{\text{QSML,th}}$ of 2.1 W based on a single quantum (SQ) SESAM where the product of the saturation fluence of the SESAM ($F_{\text{sat,A}}$) and the modulation depth (ΔR) is 10 nJ/cm²; while for the double quantum (DQ) SESAM the calculation showed a $P_{\text{QSML,th}}$ of 7.8 W, if the product of $F_{\text{sat,A}}$ ΔR is 140 nJ/cm². The calculations also show that if the $F_{\text{sat,A}}$ ΔR of the SQ and DQ SESAMs reaches 4 mJ/cm² and 9.8 mJ/cm² respectively, the SESAMs will be damaged and this is represented by ‘Damage $F_{\text{sat,A}}$ ΔR ’ in the table.

A resonator length of 825 mm will be required to achieve an appropriate repetition frequency that will result in a low internal pulse energy ($E_{\text{p,int}}$) (see Equation 8.1), which in turn would have reduced the $P_{\text{QSML,th}}$. This is based on a laser with an output coupler reflectivity of 65 %. The calculation also involved using a laser spot size radius on the crystal (w_L) of 250 μm which resulted in a saturation energy of the crystal of 118 μJ . Also a laser spot size radius of 170 μm on the SESAM was used which resulted in an absorber saturation ($E_{\text{sat,A}}$) of 0.9 nJ for the single quantum SESAM and 12.7 nJ for the double quantum SESAM.

The calculations show that the possibilities of damaging the SESAM are very limited, because the damage internal pulse energy ($E_{\text{p,int}}$) threshold for the SESAM is 3.6 μJ for the single quantum well (SQW) SESAM and 9.0 μJ for the double quantum well (DQW) SESAM, which is much more than the values of 32.7 nJ for the SQW SESAM and 122.4 nJ for the DQW SESAM, the present laser will be operating on. The method of monitoring that there is no damage on the SESAM is by monitoring the threshold output power ($P_{\text{QSML,th}}$) using a power meter. If the threshold output power is above the damage

$P_{QSM,th}$ of 231 W for the SQW SESAM and 566 W for the DQW SESAM then the SESAM's will be damaged.

Table 8.2: Designed and calculated parameters of the modelocked laser. Non bold numerical figures are design parameters and bold numerical figures are calculated parameters.

<u>Laser</u>	<u>Single Quantum</u>	<u>Double Quantum</u>
Cavity Length, L_{tot} [mm]	825	825
Speed of light, C [m/s]	3.00E+08	3.00E+08
PRF [MHz]	181.8	181.8
OC Reflectivity, OCR [%]	65	65
OC Reflectivity Times	1	1
Effective OC Transmission [%]	35	35
<u>Crystal</u>	<u>Single Quantum</u>	<u>Double Quantum</u>
w_L [μm]	250	250
$A_{eff,L}$ [cm^2]	1.96E-03	1.96E-03
Planck's constant, h [J s]	6.63E-34	6.63E-34
Speed of light, C [m/s]	3.00E+08	3.00E+08
Laser wavelength, λ [m]	1.06E-06	1.06E-06
Sigma, σ [cm^2]	1.56E-18	1.56E-18
Standing wave laser, m	2	2
Fluence in Crystal, $F_{sat,L}$ [mJ/cm^2]	60	60
$E_{sat,L}$ [μJ]	118	118

<u>SESAM</u>	<u>Single Quantum</u>	<u>Double Quantum</u>
Modulation depth, ΔR [%]	1.0	1.0
Fluence, $F_{\text{sat,A}} \Delta R$ [nJ/cm ²]	10	140
w_A [μm]	170	170
$A_{\text{eff,A}}$ [cm ²]	9.08E-04	9.08E-4
$E_{\text{sat,A}} \Delta R$ [nJ]	9.08E-03	0.127
$E_{\text{sat,A}}$ [nJ]	0.908	12.7
<u>QSML Transition</u>	<u>Single Quantum</u>	<u>Double Quantum</u>
$E_{\text{p,int}}$ [nJ]	32.7	122.4
$E_{\text{p,ext}}$ [nJ]	11.4	42.8
$P_{\text{QSML,th}}$ [W]	2.08	7.79
<u>SESAM Damage</u>	<u>Single Quantum</u>	<u>Double Quantum</u>
Damage, F [mJ/cm ²]	4	9.8
Damage, $E_{\text{p,int}}$ [μJ]	3.63	9.0
Damage, $E_{\text{p,ext}}$ [μJ]	1.27	3.11
Damage, P [W]	231	566

8.4 Results of the 1:1 relay system on the Nd:YVO₄ laser

The calculations have shown that in order to achieve a laser that would have a low cw-modelocking threshold output power, the short cavity laser that is shown in Figure 6-2 would have to be extended in length. This was achieved by coupling the laser to a 1:1 relay system which contained two curved mirrors each with a radius of curvature of 300 mm, which then allowed the laser cavity to have a total length (L_{tot}) of 825 mm, as shown in the following schematic of the laser setup in Figure 8-7.

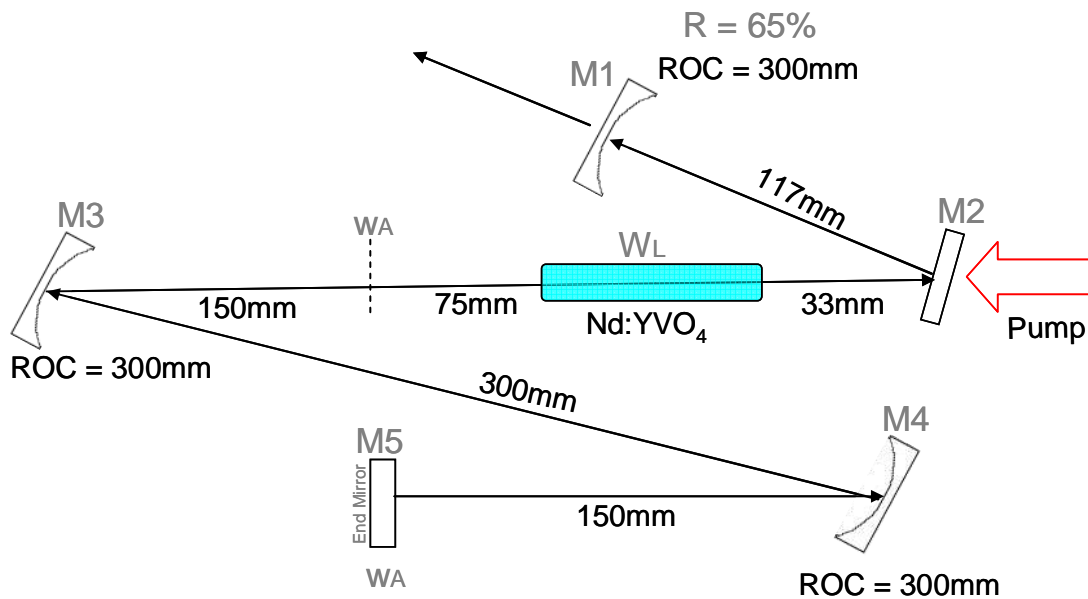


Figure 8-7: Schematic diagram of the 1:1 relay system laser resonator with a cavity length of 825 mm.

The introduction of such a relay system was expected to maintain the same modal properties in the long resonator cavity of 825 mm as that of the short 225 mm cavity without replacing the flat end mirror with the SESAM. The designed spot size in the crystal and on the end mirror were therefore not expected to change when the 1:1 relay system was introduced into the short laser. To check whether indeed the spot sizes on the flat end mirror and in the crystal were not changed, the spot size of the laser beam behind the high reflectivity end mirror was measured using a CCD camera, utilizing the small percentage of laser light that is transmitted through the flat mirror (see Figure 8-8 for the camera setup). The measured spot sizes were recorded at 5 distances away from the end

mirror, from 119.0 mm up to 141.5 mm and are shown by Table 8.3, so as to get the divergence of the laser beam; and this was done at various output powers.

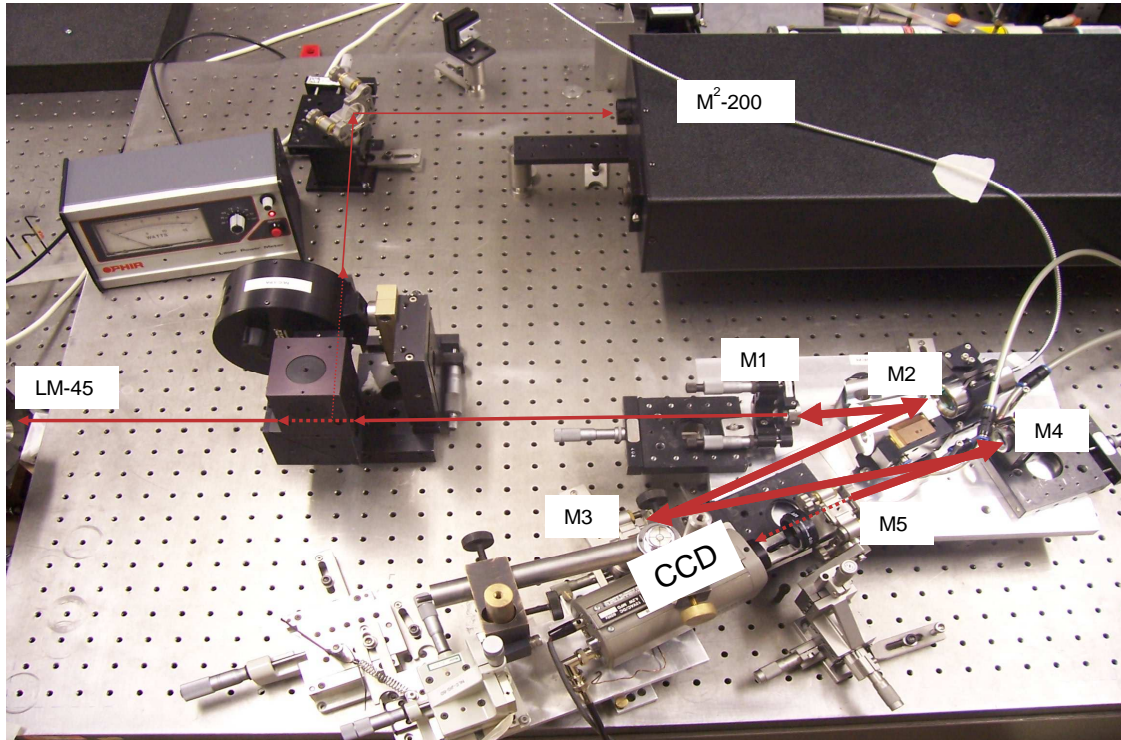


Figure 8-8: Arrangement for measuring the laser spot size using a CCD camera behind the flat high reflectivity end mirror.

The propagation of a Gaussian Beam is given as:

$$w(z) = w_0 \sqrt{1 + \left(\frac{M^2 z \lambda}{\pi w_0^2} \right)^2}, \quad (8.3)$$

and solving it for w_0 leads to a quadratic equation, in which w_0 has two solutions for the positive and negative sign, which can be interpreted as far and near field solutions. The measurements and calculations are shown in Table: 8.2 and Figure 8-9. In Table: 8.2(a) the spot sizes were measured at physical distances given in row 3, while the distances given in row 2 are relative positions to the camera positions. The calculated spot size values of '#NUM!' in Table 8.3 (b) show that there is no solution for w_0 and the far-field solution is represented as +ve and the near-field solution as -ve.

Table 8.3 (a): Measured spot sizes at different distances.

Input Current [A]	Input Power [W]	Output Power [W]	M ²	(a) Measured spot sizes w(z) (mm)				
				2.5	5	10	15	25
				119.0	121.5	126.5	131.5	141.5
				Rad	Rad	Rad	Rad	Rad
11	2.04	0.23	1.04	0.32	0.34	0.33	0.35	0.37
13	3.93	1.00	1.06	0.33	0.34	0.34	0.34	0.37
15	5.82	1.90	1.20	0.34	0.35	0.36	0.36	0.38
17	7.71	2.9	1.33	0.36		0.38	0.39	0.41
19	9.60	3.9	1.39	0.36	0.36	0.38	0.39	0.40
21	11.49	4.9	1.42	0.35	0.35	0.37	0.38	0.39
23	13.38	6.00	1.43	0.36	0.39	0.39	0.40	0.44
25	15.27	7.00	1.42	0.37	0.38	0.40	0.41	0.43
27	17.16	7.90	1.27	0.37	0.38	0.38	0.40	0.42

Table 8.3 (b): Calculated spot sizes at different distances.

(b) Calculated spot size w ₀ (mm)									
2.50		5.00		10.00		15.00		25.00	
+ve	-ve	+ve	-ve	+ve	-ve	+ve	-ve	+ve	-ve
0.29	0.15	0.31	0.14	0.29	0.15	0.32	0.15	0.34	0.15
0.29	0.15	0.30	0.14	0.30	0.15	0.31	0.15	0.34	0.15
0.31	0.16	0.31	0.16	0.32	0.16	0.32	0.17	0.34	0.17
0.33	0.16	#NUM!	#NUM!	0.34	0.17	0.35	0.17	0.37	0.17
0.31	0.18	0.31	0.18	0.33	0.18	0.34	0.18	0.35	0.19
0.29	0.20	0.29	0.20	0.31	0.20	0.33	0.19	0.34	0.20
0.32	0.18	0.35	0.17	0.34	0.18	0.35	0.18	0.41	0.17
0.33	0.17	0.33	0.17	0.36	0.17	0.37	0.17	0.39	0.17
0.33	0.15	0.35	0.15	0.35	0.16	0.36	0.16	0.39	0.16
Average values									
0.31	0.17	0.32	0.16	0.33	0.17	0.34	0.17	0.36	0.17

The graph in Figure 8-9, shows the measured spot sizes $w(z)$ represented as dots and the calculated solutions of spot sizes $w(z)$ represented as lines for the laser versus distance of the CCD camera from the end mirror, measured at a laser output power of 7 W, which corresponds to an input power of 15.3 W or input current of 25 A. The far-field solution (+ve) of Equation 8.3 gives a spot size of between ~0.33 mm and ~0.39 mm on the end mirror; that is at distance $Z = 0$ mm. The near-field solution (-ve) gave a more precise spot size of 0.17 mm on the end mirror; which is similar to the initially designed spot size, shown in Figure 6-1, using the St Andrew's Psst!! software. The same equation was also used to obtain the spot size in centre of the crystal, and it was found to be similar to the designed spot size of 0.25 mm for the near-field solution, which meant that the results for the near-field solution was used to confirm the results.

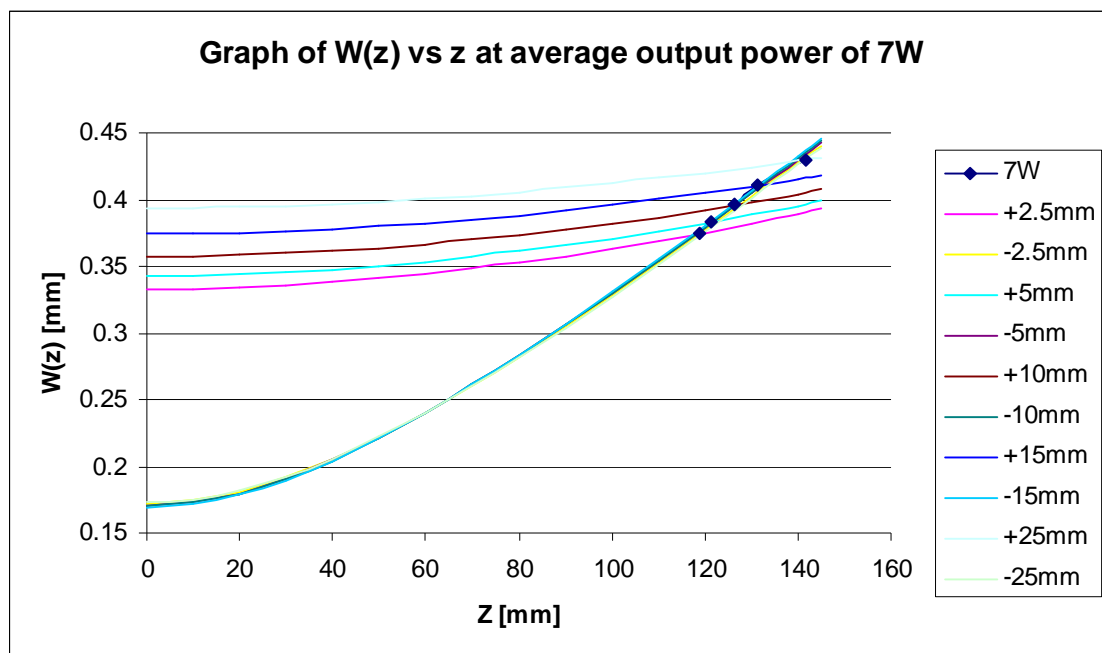


Figure 8-9: Derived spot sizes measured at distances of 2.5 mm up to 25 mm behind the end mirror of the laser with a cavity length of 825 mm at an average output power of 7 W. The + and – sign show the far field and near field solutions for each measured spot size diameter.

The power scaling of the laser with the long cavity length of 825 mm was tested in order to establish whether its performance and behaviour was similar to the original laser with cavity length of 225 mm. The graph in Figure 8-10, shows the output power versus input power of the long lasers. Comparison with the results obtained with the short cavity laser (see Figure 8-2) indicate that both lasers show similar behaviour, having the same threshold, the same maximum output power of 10.5 W and slope efficiency of 55 %.

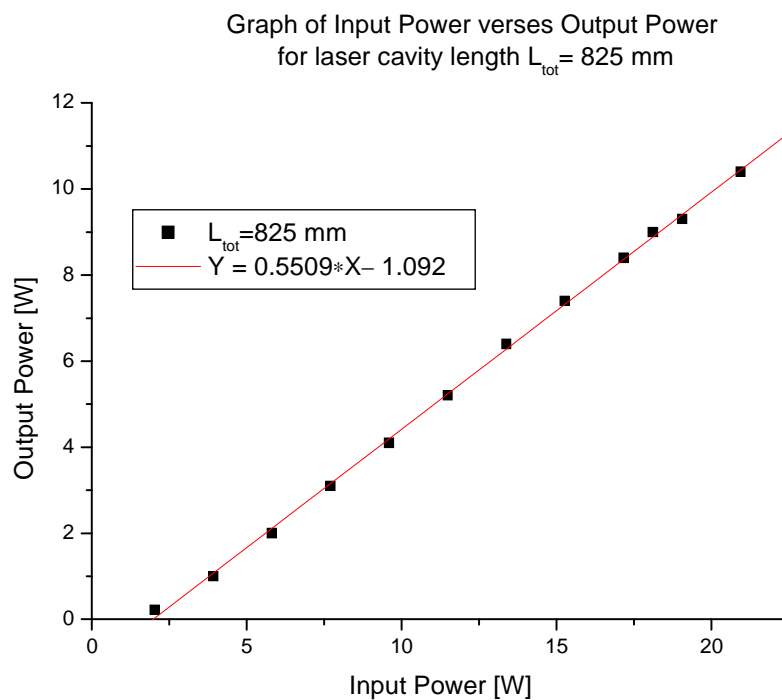


Figure 8-10: Slope efficiency of the laser with cavity length of 825 mm.

The beam quality factor for both lasers was also assessed whether it was changed; Figure 8-11 shows a graph of the beam quality factor M^2 versus input power for both short and long lasers. The graph shows that both lasers had almost identical beam quality factors M^2 at lower input powers, but showed larger differences at high input power levels. Above input powers of 17 W to the maximum power, both lasers showed a deterioration of the beam quality, with the longer resonator of 825 mm length showing slightly better stability.

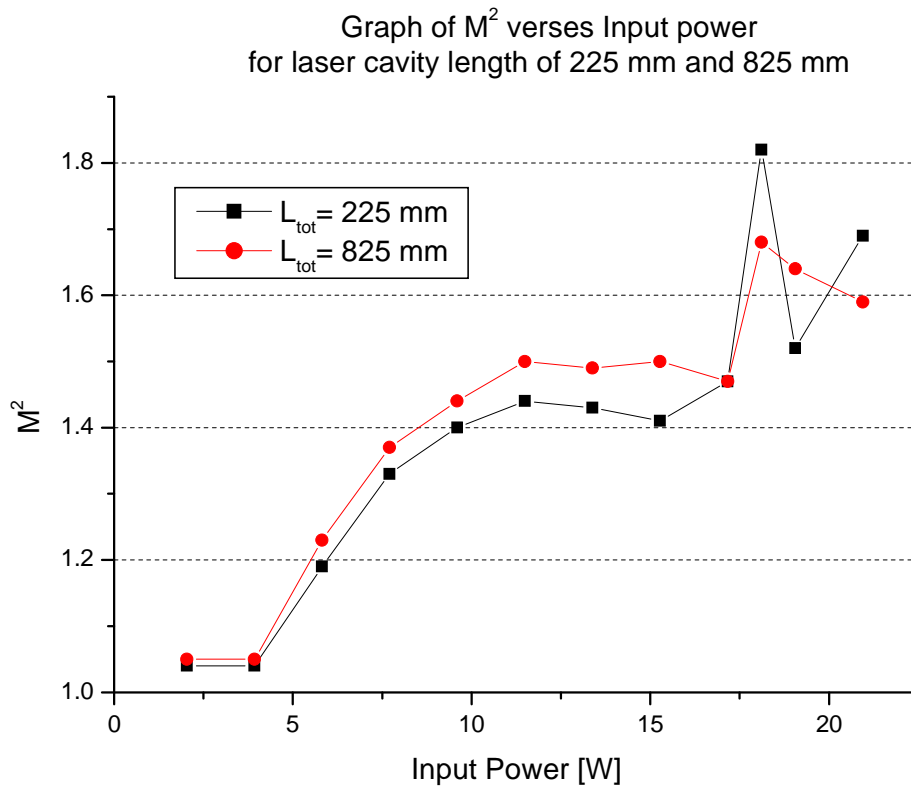


Figure 8-11: Beam quality factor at different input powers of the lasers with cavity lengths of 225 mm and 825 mm.

The sudden increase of M^2 values or deterioration of the beam quality at input powers of 18 W corresponding to an output power of 9.0 W can be explained by the fact that at this specific output power, both lasers had two modes present in the laser cavity, as shown by the images taken by the CCD camera in the following Figure 8-12. Below output powers of 9 W the laser had mostly one mode present in the cavity.

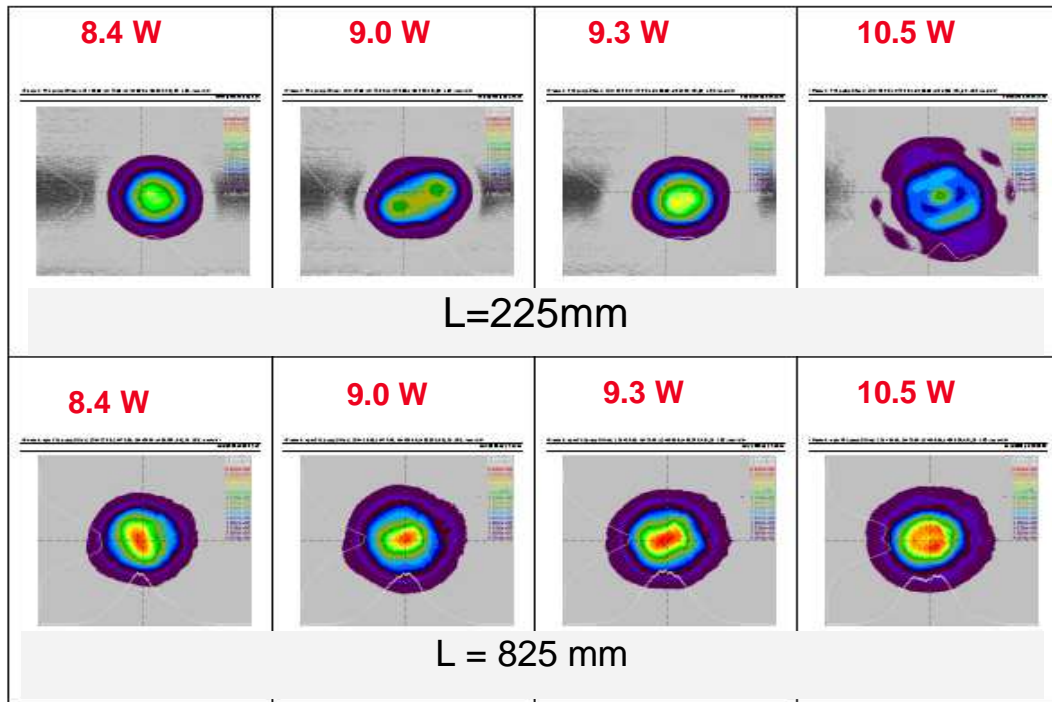


Figure 8-12: Beam profile at different output power for the lasers with cavity lengths of 225 mm and 825 mm.

8.5 Results of modelocking a Nd:YVO₄ laser using a SESAM

The comparison of the shorter and longer resonator cavity has shown that the introduction of a 1:1 relay system does not change the modal properties of the laser and its performance, including beam quality factor M^2 and also its maximum output power. The initial designed spot size on the end mirror of the short laser cavity was maintained even when the laser cavity was increased by the use of 1:1 relay system, which then gave us confidence that by replacing the flat end mirror, with the SESAM, the spot size of $170\ \mu\text{m}$ would still be maintained using the long resonator cavity. The following picture in Figure 8-13 shows how the flat end mirror was replaced with a SESAM mounted onto a thermoelectric device.

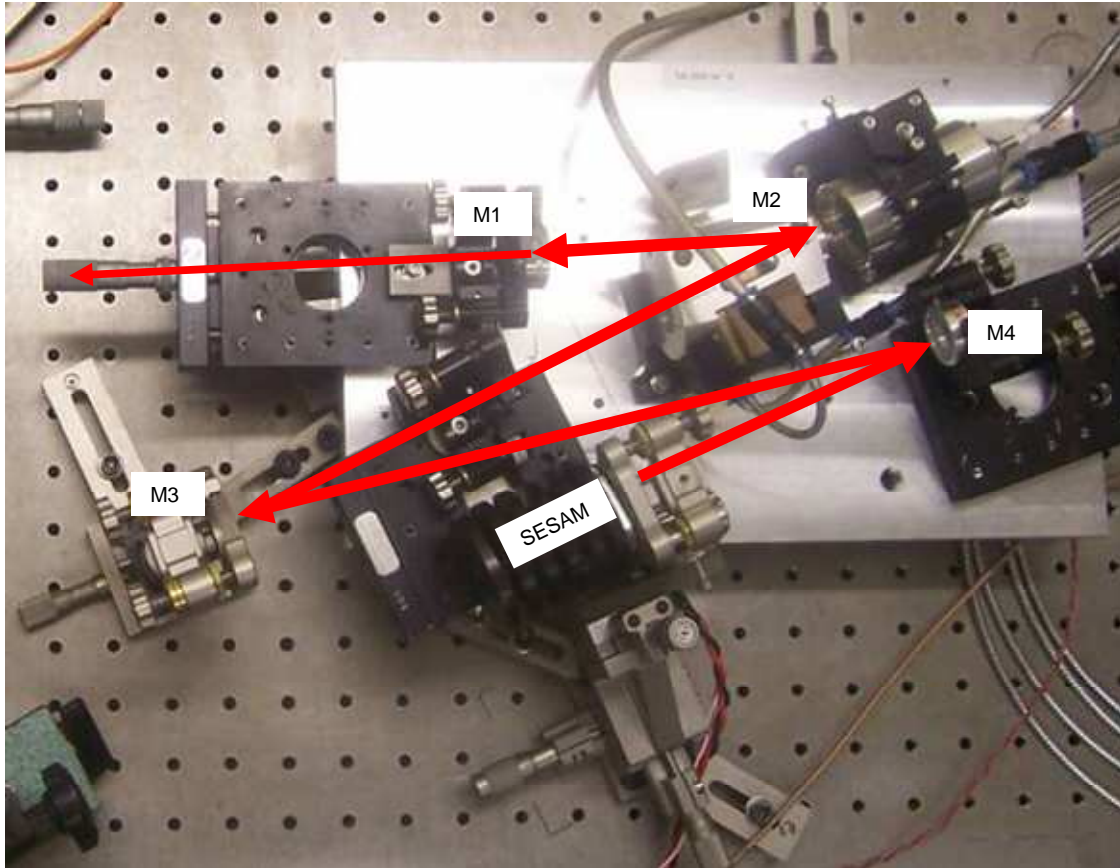


Figure 8-13: Long 825mm laser resonator with a SESAM mounted on to a thermoelectric device.

The use of the long resonator cavity with a total length of $L_{\text{tot}} = 825$ mm shown in Figure 8-13, was designed to greatly reduce Q -switching instabilities which will then lead to a much more stable resonator as describes by Equation 5.18. At room temperature the laser of Figure 8-13, produced stable modelocked pulses, with a pulse repetition frequency of 179 MHz, equivalent to the cavity round trip time of 5.6 ns, as shown by the oscilloscope trace in Figure 8-14. Cw-modelocking was achieved at an input power of 8 W corresponding to an average output power of 2.8 W. This represented a pulse fluence on the SESAM (F_A) of about $49.3 \mu\text{Jcm}^{-2}$. The cause of the oscillations between each pulse on the oscilloscope shown in Figure 8-14 is due to slight mis-alignment of the resonator which creates multiple transverse modes to oscillate [8.4]. However each of the modes in the resonator produces modelocked train pulses which are independent, with no phase relation between them. The output pulse sequence for triple-transverse-mode

shown in Figure 8-14 is reduced to a double-transverse-mode oscillation shown in Figure 8-15 as alignment is improved. The modelocked pulses shown in Figure 8-14 only lasted for about 30 s initially; when the SESAM temperature was not controlled. This could have been due to the changes in the modulation depth of the SESAM, since the saturable absorption greatly depends on the SESAM temperature.

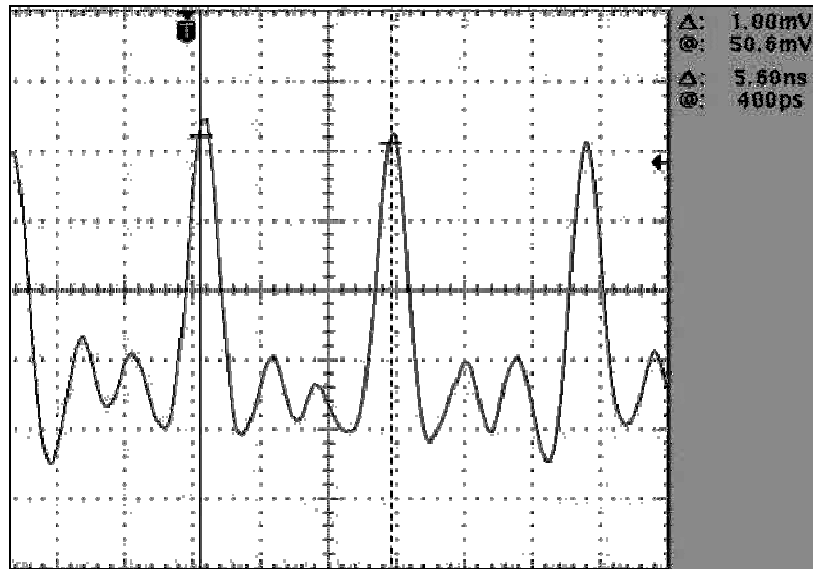


Figure 8-14: Continuous wave modelocking at an average output power of 2.8 W using a SQW SESAM which was not temperature controlled.

When the temperature of the SQW SESAM was controlled and kept at constant temperature, cw-modelocking of the laser was possible at some specific output powers for a long period of time of more than half an hour. The oscilloscope trace in Figure 8-15, shows the cw-modelocked pulse train for the SESAM that was temperature controlled at 30 °C, and at an average output power of 2.8 W. The average output power of 2.8 W is in very good agreement with the calculated modelocked transition $P_{QSM,th}$ of 2.08 W from Table 8.2. The pulse duration of the laser could not be measured since there was no suitable auto-correlator available; however, it was estimated and expected to be about 10-20 ps since an identical SESAM was used by Dr Erwin Bente for modelocking a Nd:YLF laser which emitted pulses with a duration of 21 ps [8.3 & 8.4].

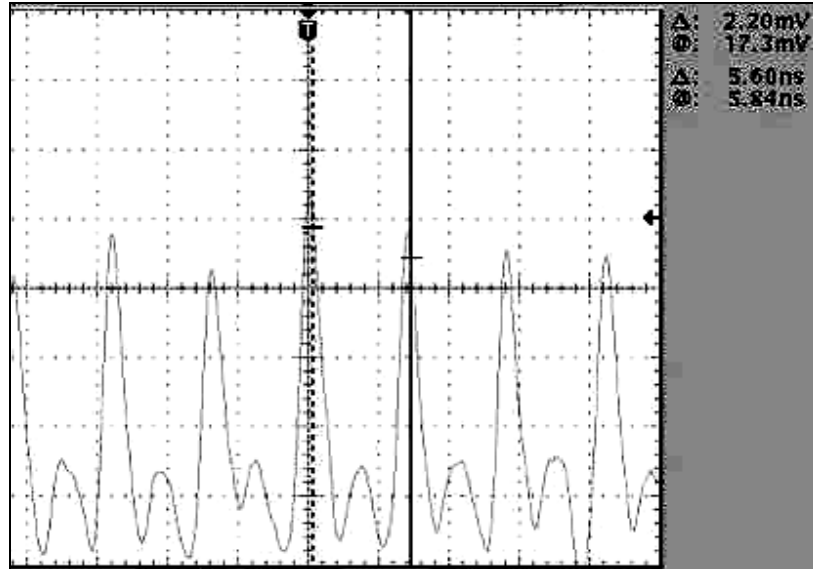


Figure 8-15: Continuous wave modelocking at an average output power of 2.8 W using a SQW SESAM temperature controlled at 30 °C.

A double quantum well SESAM was also used for modelocking of the long $L_{tot} = 825$ mm resonator laser. The oscilloscope trace in Figure 8-16, demonstrates stable *Q*-switch modelocking that was achieved using the DQW SESAM. The repetition frequency of the *Q*-switched modelocked laser was 208 KHz which represented pulse intervals of 4.8 μ s. For *Q*-switched modelocked pulses, a low frequency in the kilohertz region is usually expected; while for cw-modelocked lasers, pulses in the megahertz region are expected since the pulse repetition rate should be equivalent to the cavity round trip time.

Q-switch modelocking was achieved at an average output power of 2.7 W, which corresponded to a fluence on the SESAM (F_A) of about 40.8 mJcm⁻². Cw-modelocking using a DQW SESAM was not achieved, probably due to insufficient energy density of the laser pulse on the SESAM. The laser pulse fluence on the DQW SESAM could have been increased by reducing the spot size by means of replacing the 300 mm radius of the curved mirror M3 with a lower radius of curvature, probably 150 mm, see Figure 8-8. This would have reduced the spot size by half and thereby increasing the pulse fluence by four times, which could probably have overcome the *Q*-switching mode.

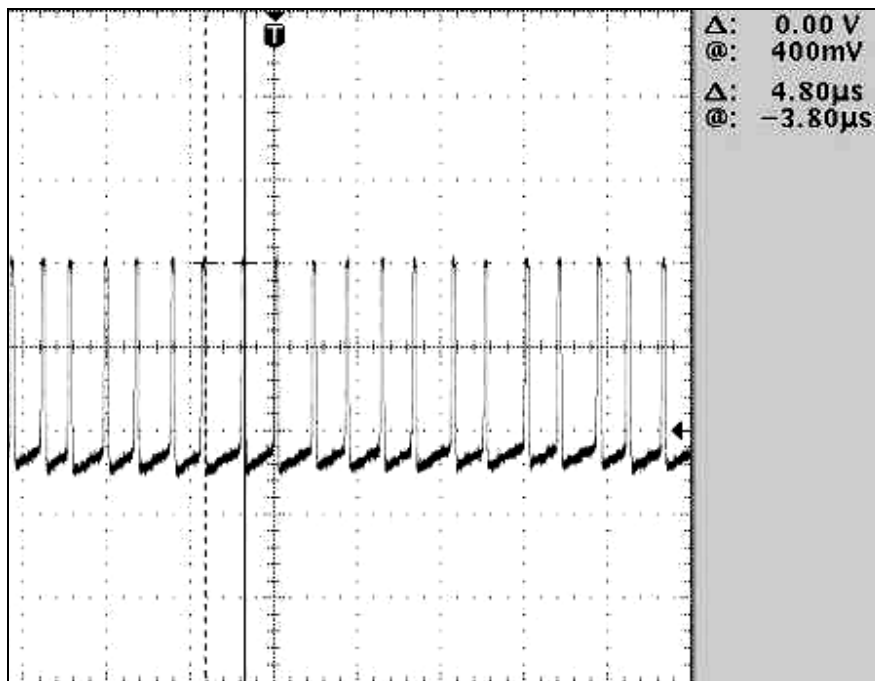


Figure 8-16: Stable Q -switched modelocking at an average output power of 2.7 W using a DQW SESAM temperature controlled at 30 °C.

The modelocked pulses underneath a Q -switched envelope as seen in Figure 5-4 were not visible on the above Figure 8-16. Unfortunately a more detailed investigation was not possible, since there was only one DQW SESAM available and it was damaged while investigating how the laser spot size affects the behaviour of the output pulse. The Q -switched modelocked output pulses of the DQW SESAM were stable as shown by on Figure 8-16, since all the pulses had constant amplitude.

Overall, the good agreement seen between experimental measurements and the calculations confirms the modelling of generating ultrashort pulses using modelocking theory.

9. Conclusion

In the first part of this work; Chapter 1 introduced different types of gain media needed for ultrashort pulse generation. In Chapter 2 the discussion mainly focused on neodymium doped lasers such as Nd:YVO₄ where an analysis of the spectral properties such as energy levels, absorption and emission wavelength was done.

In Chapter 3 different types of optical pump source types were discussed, where the advantages in terms of operating conditions and efficiency of using diode lasers were seen to outweigh those of other sources such as flash lamps. Two different types of diode pumped setups were discussed, end-pumping and side pumping; and it was identified that diode end pumping showed better properties in respect of matching pump volume to laser mode, resulting in high efficiency and also better beam quality, when compared to side pumping.

The gain bandwidth of the laser gain material was discussed in Chapter 4 and it was shown that a laser medium with a very large gain bandwidth and broad emission bandwidth is required for ultrashort pulse generation in the femtosecond range, e.g. Ti:sapphire crystal. Ultrafast lasers based on gain media with a small amplification bandwidth suitable for diode end-pumping and high power cw operation were discussed, such as Nd:YAG and Nd:YVO₄ lasers. These lasers have been shown previously to generate pulses with durations of down to 19 ps and 20 ps respectively with average output powers of 27 W and 20 W respectively.

Modelocking as a technique to generate ultrashort pulses was discussed in Chapter 5 where passive modelocking was shown to be more suitable for creating very short pulse durations down to a few femtoseconds, as compared to active modelocking which can generate pulses with durations in the picosecond region. Saturable absorbers for passive modelocking were also discussed where it was shown that using SESAMs helps in generating reliable self starting modelocked pulses. This was followed by a discussion on the instabilities of the laser introduced by saturable absorbers, where different methods of

reducing these instabilities were discussed, such as using gain media with very small saturation fluence.

Part two Chapter 6 of this work entailed the design and development of a SESAM modelocked diode end pumped Nd:YVO₄ laser. This included a discussion on resonator design criteria for achieving stable modelocking of a diode-end pumped solid-state laser. Where the choice of using Nd:YVO₄ as a gain medium was considered, and it was found to be mainly influenced by its large emission cross sectional area, which is useful in increasing the gain bandwidth for possible ultrashort pulse generation, and also it was shown that a long resonator reduced the resonator energy thereby reducing possibility of developing an unstable laser.

The resonator for high power continuous wave output was designed by using the software “Psst!!” developed by St Andrews University, incorporating the stability criteria such as laser spot size in the crystal and on the end mirror into the software. It was found that the designed laser spot sizes on the crystal and on the SESAM were in good agreement with the experimental values. The resonator pump setup design and the efficient cooling method of the crystal using a copper heat sink were also discussed. The Nd:YVO₄ crystal with a doping level of 0.27% was pumped at its absorption peak of 808 nm for efficient pump absorption.

The methodology of obtaining stable, thermal-lens-invariant, single transverse-mode operation during power scaling of Nd:YVO₄ lasers was also evaluated, where the short resonator produced a maximum average output power of 10.5 W with a beam quality factor M^2 of 1.5. The laser cavity was then extended in length, utilizing a lens relay approach in order to reduce the modelocking repetition rate and to introduce spot size control in the laser crystal and on the end mirror. With this approach also, the long resonator produced equivalent performance as the short resonator as predicted with maximum output power of 10.5 W and an M^2 of 1.5.

The experimental spot sizes in the crystals and on the end-mirror of the short resonator and the long resonator were also in good agreement with the calculated results as modelled using St Andrews software.

In the last Chapter 8 when the SQW SESAM was incorporated into the extended end-pumped Nd:YVO₄ laser, cw-modelocked pulses were observed at an average output power of 2.8 W as predicted for the modelocked transition ($P_{Q\text{SML,th}}$) with a pulse duration estimated to about 20 ps at a repetition frequency of 179 MHz, equivalent to the cavity round trip time of 5.6 ns as predicted using the calculation and theory of modelocking.

The use of a DQW SESAM in the Nd:YVO₄ laser generated stable Q -switched modelocked pulses at an average output power of 2.7 W with a Q -switch repetition frequency of 208 KHz. The fundamental limitations on the power scaling approach were also investigated with a conclusion that high average output powers would be possible with tighter focussing of the laser on the SESAM and improved control of the transverse-mode at high power levels.

Overall, the theory calculations and models reported in this study provided a valuable tool for predicting the laser outputs and the tolerable power that the SESAM could handle, when designing ultrafast high-power solid-state lasers.

References

Section 1

- 1.1 R. Paschotta, "Ultrafast Solid-State Lasers", ETH Honggerberg HPT, 8093 Zurich, (2001).
- 1.2 L. E. Hargrove, R. L. Fork, M. A. Pollack, "Locking of HeNe laser modes induced by synchronous intracavity modulation", *Appl. Phys. Lett.* **5**, 4 (1964).
- 1.3 H. W. Mocker, R. J. Collins, "Mode competition and self-locking effects in a Q-switched ruby laser", *Appl. Phys. Lett.* **7**, 270-273 (1965).
- 1.4 A. J. De Maria, D. A. Stetser, H. Heynau, "Self mode-locking of lasers with saturable absorbers", *Appl. Phys. Lett.* **8**, 174-176 (1966).
- 1.5 U. Keller, D. A. B. Miller, G. D. Boyd, T. H. Chiu, J. F. Ferguson, M. T. Asom, "Solidstate low-loss intracavity saturable absorber for Nd:YLF lasers: an anti resonant semiconductor Fabry-Perot saturable absorber", *Opt. Lett.* **17**, 505-507 (1992).
- 1.6 F. P. Schafer, F. P. W. Schmidh and I. Volze, "Organic dye solution laser", *Appl. Phys. Lett.*, Vol. **9** p.306 (1966).
- 1.7 L. F. Mollenauer & J. C. White. Eds., "Tunable Lasers", (*Topics Appl. Phys.*) Vol. **59** Berlin, Heidelberg Springer (1987) Chapter 6.
- 1.8 C. V. Shank, E. P. Ippen, "Subpicosecond kilowatt pulses from a mode locked cw dye laser", *Appl. Phys. Lett.* **24**, 373-375 (1974).
- 1.9 I. S. Ruddock, D. J. Bradley, "Bandwidth-limited subpicosecond pulse generation in modelocked cw dye lasers", *Appl. Phys. Lett.* **29**, 296-297 (1976).

- 1.10 J. C. Diels, E. W. V. Stryland, G. Benedict, "Generation and measurement of pulses of 0.2 ps duration", *Opt. Commun.* **25**, 93 (1978).
- 1.11 R. L. Fork, B. I. Greene, C. V. Shank, "Generation of optical pulses shorter than 0.1 ps by colliding pulse *modelocking*", *Appl. Phys. Lett.* **38**, 617-619 (1981).
- 1.12 R. L. Fork, O. E. Martinez & I. P. Gordon, "Negative dispersion using a pair of prisms", *Opt. Lett.*, Vol. **9** p.50 (1984).
- 1.13 J. A. Valdmanis, R. L. Fork, J. P. Gordon, "Generation of optical pulses as short as 27 fs directly from a laser balancing self-phase modulation, group-velocity dispersion, saturable absorption, and saturable gain", *Opt. Lett.* **10**, 131-133 (1985).
- 1.14 R. L. Fork, C. H. B. Cruz, P. C. Becker, C. V. Shank, "Compression of optical pulses to six femtoseconds by using cubic phase compensation", *Opt. Lett.* **12**, 483-485 (1987).
- 1.15 D. E. Spence, P. N. Kean, W. Sibbett, "60-fsec pulse generation from a self-mode-locked Ti:sapphire laser", *Opt. Lett.* **16**, 42-44 (1991).
- 1.16 D. H. Sutter, G. Steinmeyer, L. Gallmann, N. Matuschek, F. Morier-Genoud, U. Keller, V. Scheuer, G. Angelow, T. Tschudi, "Semiconductor saturable-absorber mirror-assisted Kerr-lens mode-locked Ti:sapphire laser producing pulses in the two-cycle regime", *Opt. Lett.* **24**, 631-633 (1999).
- 1.17 U. Morgner, F. X. Kartner, S. H. Cho, Y. Chen, H. A. Hall, J. G. Fujimoto, E. P. Ippen, V. Scheuer, G. Angelow, T. Tschudi, "Sub-two-cycle pulses from a Kerr-lens mode-locked Ti:sapphire laser: addenda", *Opt. Lett.* **24**, 920 (1999).

- 1.18 U. Morgner, F. X. Kartner, S. H. Cho, Y. Chen, H. A. Halls, I. G. Fujimoto, E. P. Ippen, V. Scheuer, G. Angelow, T. Tschudi, "Sub-two-cycle pulses from a Kerr-lens mode-locked Ti:sapphire laser", *Opt. Lett.* **24**, 411-413 (1999).
- 1.19 A. Baltuska, Z. Wei, M. S. Pshenichnikov, D. A. Wiersma, R. Szipcs, "All-solid-state cavity dumped *sub*-5-fs laser", *Appl. Phys. B* **65**, 175-188 (1997).
- 1.20 M. Nisoli, S. Stagira, S. D. Silvestri, O. Svelto, S. Sartania, Z. Cheng, M. Lenzner, C. Spielmann, F. Krausz, "A novel high-energy pulse compression system: generation of multigigawatt *sub*-5-fs pulses", *Appl. Phys. B* **65**, 189-196 (1997).
- 1.21 A. Shirakawa, I. Sakane, M. Takasaka, T. Kobayashi, "Sub-5-fs visible pulse generation by pulse-front-matched noncollinear optical parametric amplification", *Appl. Phys. Lett.* **74**, 2268-2270 (1999).
- 1.22 G. Steinmeyer, D. H. Sutter, L. Gallmann, N. Matuschek, U. Keller, "Frontiers in Ultrashort Pulse Generation: Pushing the Limits in Linear and Nonlinear Optics", *Science* **286**, 1507-1512 (1999).
- 1.23 U. Keller, K. J. Weingarten, F. X. Kartner, D. Kopf, B. Braun, I. D. lung, R. Fluck, C. Honninger, N. Matuschek, J. Aus der Au, "Semiconductor saturable absorber mirrors (SESAMs) for femtosecond to nanosecond pulse generation in solid-state lasers," *IEEE J Sel. Top. Quantum Electron.* **2**, 435-453 (1996).
- 1.24 J. Aus der Au, D. Kopf, F. Morier-Genoud, M. Moser, and U. Keller, "60-fs pulses from a diode-pumped Nd:glass laser," *Opt. Lett.* **22**, 307-309 (1997).
- 1.25 F. X. Kartner, U. Keller, "Stabilization of soliton-like pulses with a slow saturable absorber", *Opt. Lett.* **20**, 16-18 (1995).

- 1.26 I. D. Jung, F. X. Kartner, L. R. Brovelli, M. Kamp, U. Keller, "Experimental verification of soliton modelocking using only a slow saturable absorber", *Opt. Lett.* **20**, 1892-1894 (1995).
- 1.27 F. X. Kartner, I. D. Jung, U. Keller, "Soliton Modelocking with Saturable Absorbers", *IEEE J. Sel. Topics in Quantum Electron.* **2**, 540-556 (1996).
- 1.28 G. J. Spuhler, T Sudmeyer, R. Paschotta, M. Moser, K. J. Weingarten, U. Keller, "Passively mode-locked high-power Nd:YAG lasers with multiple laser heads", *Appl. Phys. B* **71**, 19-25 (2000).
- 1.29 A. Giesen, H. Hugel, A. Voss, K. Wittig, U. Brauch, H. Opower, "Scalable Concept for Diode-Pumped High-Power Solid-State Lasers", *Appl. Phys. B* **58**, 363-372 (1994).
- 1.30 J. Aus der Au, G. J. Spuhler, T Sudmeyer, R. Paschotta, R. Hovel, M. Moser, S. Erhard, M. Karszewski, A. Giesen, U. Keller, "16.2 W average power from a diode-pumped femtosecond Yb:YAG thin disk laser", *Opt. Lett.* **25**, 859 (2000).
- 1.31 R. Paschotta, J. Aus der Au, G. J. Spuhler, F. Morier-Genoud, R. Hovel, M. Moser, S. Erhard, M. Karszewski, A. Giesen, U. Keller, "Diode-pumped passively mode-locked lasers with high average power", *Appl. Phys. B* **70**, S25-S31 (2000).
- 1.32 R. Paschotta, J. Aus der Au, G. J. Spuhler, S. Erhard, A. Giesen, U. Keller, "Passive mode locking of thin disk lasers: effects of spatial hole burning", *Appl. Phys. B* **72**, 267-278 (2001).

Section 2

- 2.1 J. R. O'Connor: *Appl. Phys Lett.* **9**, 407 (1966).

- 2.2 W. Koechner “Solid-state laser Engineering” 5th rev and updated ed. *Springer series in Optical Sciences Volume 1*, Springer-Verlag Berlin Heidelberg, Germany (1999).
- 2.3 S. Kuck, L. Fornasiero, E. Mix and G. Huber “Excited state absorption and stimulated emission of Nd³⁺ in crystals. Part 1: Y₃Al₅O₃, YAlO₃, and Y₂O₃”, *Applied Physics. B* **67**, 151-156 (May 1998).
- 2.4 D. K. Sardar and R. M. Yow, “Stark components of ⁴F_{3/2}, ⁴I_{9/2} and ⁴I_{11/2} manifold energy levels and effects of temperature on the laser transition of Nd³⁺ in YVO₄”, *Optical Material*. **14**, 5-11 (2000).
- 2.5 H. Zhan, X. Meng, L. Zhu, C. Wang, Y. T. Chow, M. Lu, “Growth, spectra and influence of annealing effect on laser properties of Nd:YVO₄ crystal”, *Optical Materials* **14**, 25-30 (2000).

Section 3

- 3.1 New Source Technology , <http://www.newsourcetechology.com>
- 3.2 Wikipedia The Free Encyclopedia, http://en.wikipedia.org/wiki/Diode_laser

Section 4

- 4.1 W. Koechner “Solid-state laser Engineering” 5th rev and updated ed. *Springer series in Optical Science Volume 1*, Sprinder-Verlag Berlin Heidelberg, Germany (1999).
- 4.2 L. Krainer, R. Paschotta, M. Moser, U. Keller, "77 GHz soliton modelocked Nd:YVO₄ laser", *Electron. Lett.* **36**, 1846-8 (2000).

- 4.3 J. Goodberlet, J. Jacobson, J. G. Fujimoto, P. A. Schulz, T. Y. Fan, "Self-starting additive pulse modelocked diode-pumped Nd:YAG laser", *Opt. Lett.* **15**, 504-506 (1990).
- 4.4 F. Brunner, G. J. Spuhler, J. Aus der Au, L. Krainer, F. Morier-Genoud, R. Paschotta, N. Lichtenstein, S. Weiss, C. Harder, A. A. Lagatsky, A. Abdolvand, N. V. Kuleshov, U. Keller, "Diode-pumped femtosecond Yb:KGd(WO₄)₂ laser with 1.1- W average power", *Opt. Lett.* **25**, 1119-1121 (2000).
- 4.5 C. Honninger, R. Paschotta, M. Graf, F. Morier-Genoud, G. Zhang, M. Moser, S. Biswal, I. Nees, A. Braun, G. A. Mourou, I. Johannsen, A. Giesen, W. Seeber, U. Keller, "Ultrafast ytterbium-doped bulk lasers and laser amplifiers", *Appl. Phys. B* **69**, 3-17 (1999).
- 4.6 J. Aus der Au, D. Kopf, F. Morier-Genoud, M. Moser, U. Keller, "60-fs pulses from a diode-pumped Nd:glass laser", *Opt. Lett.* **22**, 307-309 (1997).
- 4.7 I. T. Sorokina, E. Sorokin, E. Wintner, A. Cassanho, H. P. Jenssen, R. Szipocs, "14-fs pulse generation in Kerr-lens modelocked prismless Cr:LiSGaF and Cr:LiSAF lasers observation of pulse self-frequency shift", *Opt. Lett.* **22**, 1716-1718 (1997).
- 4.8 D. H. Sutter, G. Steinmeyer, L. Gallmann, N. Matuschek, F. Morier-Genoud, U. Keller, V. Scheuer, G. Angelow, T. Tschudi, "Semiconductor saturable-absorber mirror-assisted Kerr-lens mode-locked Ti:sapphire laser producing pulses in the two-cycle regime", *Opt. Lett.* **24**, 631-633 (1999).
- 4.9 C. Honninger, R. Paschotta, M. Graf, F. Morier-Genoud, G. Zhang, M. Moser, S. Biswal, J. Nees, A. Braun, G. A. Mourou, L. Johannsen, A. Giesen, W. Seeber, U. Keller, "Ultrafast ytterbium-doped bulk lasers and laser amplifiers", *Appl. Phys. B* **69**, 3-17 (1999).

- 4.10 G. J. Spuhler, T Sudmeyer, R. Paschotta, M. Moser, K. J. Weingarten, U. Keller, "Passively mode-locked high-power Nd:YAG lasers with multiple laser heads", *Appl. Phys. B* **71**, 19-25 (2000).
- 4.11 D. Burns, M. Hetterich, A. L Ferguson, E. Bente, M. D. Dawson, J. L Davies, S. W. Bland, "High-average-power (>20 W) Nd:YV04 lasers mode locked by strain-compensated saturable Bragg reflectors", *J. Opt. Soc. Am. B* **17**, 919-926 (2000).
- 4.12 G. P. A. Malcolm, P. F. Curley, A. L Ferguson, "Additive pulse modelocking of a diode pumped Nd:YLF laser", *Opt. Lett.* **15**, 1303-1305 (1990).
- 4.13 P. F. Moulton, "Spectroscopic and laser characteristics of Ti:Al₂O₃", *J. Opt. Soc. Am. B* **3**, 125-132 (1986).
- 4.14 U. Morgner, F. X. Kartner, S. H. Cho, Y. Chen, H. A. Haus, J. G. Fujimoto, E. P. Ippen, V. Scheuer, G. Angelow, T. Tschudi, "Sub-two-cycle pulses from a Kerr-lens mode-locked Ti:sapphire laser", *Opt. Lett.* **24**, 411-413 (1999).
- 4.15 D. H. Sutter, G. Steinmeyer, L. Gallmann, N. Matuschek, F. Morier-Genoud, U. Keller, V. Scheuer, G. Angelow, T. Tschudi, "Semiconductor saturable-absorber mirrorassisted Kerr-lens mode-locked Ti:sapphire laser producing pulses in the two-cycle regime", *Opt. Lett.* **24**, 631-633 (1999).
- 4.16 F. X. Kartner, I. D. Jung, U. Keller, "Soliton Modelocking with Saturable Absorbers", *IEEE J. Sel. Topics in Quantum Electron.* **2**, 540-556 (1996).
- 4.17 T J. Carrig, G. J. Wagner, A. Sennaroglu, J. Y Jeong, C. R. Pollock, "Mode-locked Cr³⁺:ZnSe laser", *Opt. Lett.* **25**, 168-170 (2000).

- 4.18 J. Aus der Au, D. Kopf, F. Morier-Genoud, M. Moser, U. Keller, "60-fs pulses from a diode-pumped Nd:glass laser", *Opt. Lett.* **22**, 307-309 (1997).
- 4.19 F. X. Kartner, I. D. Jung, U. Keller, "Soliton Modelocking with Saturable Absorbers", *IEEE J. Sel. Topics in Quantum Electron.* **2**, 540-556 (1996).
- 4.20 J. Aus der Au, F. H. Loesel, F. Morier-Genoud, M. Moser, U. Keller, "Femtosecond diode-pumped Nd:glass laser with more than 1-W average output power", *Opt. Lett.* **23**, 271 -273 (1998).
- 4.21 R. Paschotta, J. A. d. Au, U. Keller, "Thermal effects in high power end-pumped lasers with elliptical mode geometry", *J. Set. Topics in Quantum Electron.* **6**, 636-642 (2000).
- 4.22 C. Honninger, G. Zhang, U. Keller, A. Giesen, "Femtosecond Yb: YAG laser using semiconductor saturable absorbers", *Opt. Lett.* **20**, 2402-2404 (1995).
- 4.23 J. Aus der Au, S. F. Schaer, R. Paschotta, C. Honninger, U. Keller, M. Moser, "Highpower diode-pumped passively modelocked Yb:YAG lasers", *Opt. Lett.* **24**, 1281-1283 (1999).
- 4.24 A. Giesen, H. Hugel, A. Voss, K. Wittig, U. Brauch, H. Opower, "Scalable Concept for Diode-Pumped High-Power Solid-State Lasers", *Appl. Phys. B* **58**, 363-372 (1994).
- 4.25 J. Aus der Au, G. J. Spuhler, T. Sudmeyer, R. Paschotta, R. Hovel, M. Moser, S. Erhard, M. Karszewski, A. Giesen, U. Keller, "16.2 W average power from a diodepumped femtosecond YbY AG thin disk laser", *Opt. Lett.* **25**, 859 (2000).
- 4.26 R. Paschotta, F. Brummer, E. Innerhofer, T. Sudmeyer, U. Keller, "High average power femtosecond and picosecond lasers", ASSL, Canada, (2002).

- 4.27 V. Petrov, V. Shcheslavskiy, T Mirtchev, F. Noack, T Itatani, T. Sugaya, T Nakagawa, "High-power self-starting femtosecond Cr:forsterite laser", *Electron. Lett.* **34**, 559-561 (1998).
- 4.28 F. Brunner, G. J. Spuhler, J. Aus der Au, L. Krainer, F. Morier-Genoud, R. Paschotta, N. Lichtenstein, S. Weiss, C. Harder, A. A. Lagatsky, A. Abdolvand, N. V. Kuleshov, U. Keller, "Diode-pumped femtosecond Yb:KGd(WO₄)₂ laser with 1.1-W average power", *Opt. Lett.* **25**, 1119-1121 (2000).
- 4.29 G. J. Valentine, A. J. Kemp, D. J. L. Birkin, D. Burns, F. Balembois, P. Georges, H. Bernas, A. Aron, G. Aka, W. Sibbett, A. Brun, M. D. Dawson, E. Bente, "Femtosecond Yb: YCOB laser pumped by narrow-stripe laser diode and passively mode locked using ion implanted saturable-absorber mirror", *Electron. Lett.* **36**, 1621-1623 (2000).
- 4.30 F. Druon, F. Balembois, P. Georges, A. Brun, A. Courjaud, C. Honninger, F. Salin, A. Aron, F. Mougel, G. Aka, D. Vivien, "Generation of 90-fs pulses from a modelocked diode-pumped Yb:Ca₄GdO(Bo₃)₃ laser", *Opt. Lett.* **25**, 423-425 (2000).
- 4.31 M. Larionov, J. Gao, S. Erhard, A. Giesen, K Contag, V. Peters, E. Mix, L. Fornasiero, K. Petermann, G. Huber, J. A. d. Au, G. J. Spuhler, R. Paschotta, U. Keller, A. A. Lagatsky, A. Abdolvand, N. V. Kuleshov, "Thin disk laser operation and spectroscopic characterization of Yb-doped sesquioxides and potassium tungstates", in *Advanced Solid State Lasers*, (OSA), 2001.

Section 5

- 5.1 A.E. Siegman, "LASERS", University of Science Books, Sausalito, California (1986).

- 5.2 U. Keller, "Recent developments in compact ultrafast laser", *Nature*, **424** 831-838 (2003).
- 5.3 W. Koechner, "Solid-state laser Engineering", 5th rev and updated ed. *Springer series in Optical Science Volume 1*, Sprinder-Verlag Berlin Heidelberg, Germany (1999).
- 5.4 <http://www.rp-photonics.com>
- 5.5 D. J. Kuizenga, A E. Siegman, "FM und AM mode locking of the homogeneous laser Part I: Theory, Part II: Experimental results", *IEEE J. Quantum Electron.* **6**, 694-715 (1970).
- 5.6 D. J. Kuizenga, A E. Siegman, "FM and AM Mode Locking of the Homogeneous Laser - Part II: Experimental Results in a Nd:YAG Laser with Internal FM Modulation", *IEEE J. Quantum Electron.* **6**, 709-715 (1970).
- 5.7 S. J. Walker, H. Avramopoulos, T. Sizer, "Compact mode-locked solid-state lasers at 0.5- and 1-GHz repetition rates", *Opt. Lett.* **15**, 1070-1072 (1990).
- 5.8 D. E. Spence, J. M. Evans, W. E. Sleat, W. Sibbet, "Regeneratively initiated self-mode-locked Ti:sapphire laser," *Opt. Lett.* **16**, 1762-(1991).
- 5.9 R. Paschotta, "Ultrafast Solid-State Lasers", ETH Honggerberg HPT, 8093 Zurich, (2001).
- 5.10 H. A. Haus, J. G. Fujimoto, E. P. Ippen, "Structures for additive pulse mode locking", *J. Opt. Soc. Am. B* **8**, 2068-2076 (1991).
- 5.11 I. D. Jung, F. X. Kartner, N. Matuschek, D. H. Sutter, F. Morier-Genoud, Z. Shi, V. Scheuer, M. Tilsch, T Tschudi, U. Keller, "Semiconductor saturable absorber

- mirrors supporting sub-10 fs pulses", *Appl. Phys. B: Special Issue on Ultrashort Pulse Generation* **65**, 137-150 (1997).
- 5.12 U. Keller, D. A. B. Miller, G. D. Boyd, T. H. Chiu, J. F. Ferguson, M. T. Asom, "Solid-state low-loss intracavity saturable absorber for Nd:YLF lasers: an anti resonant semiconductor Fabry-Perot saturable absorber", *Opt. Lett.* **17**, 505-507 (1992).
- 5.13 S. Tsuda, W. H. Knox, E. A. d. Souza, W. Y. Jan, J. E. Cunningham, "Low-loss intracavity AlAs/AlGaAs saturable Bragg reflector for femtosecond mode locking in solid-state lasers", *Opt. Lett.* **20**, 1406-1408 (1995).
- 5.14 D. Burns, M. Hetterich, A. L. Ferguson, E. Bente, M. D. Dawson, J. L. Davies, S. W. Bland, "High-average-power (>20 W) Nd:YVO₄ lasers mode locked by strain compensated saturable Bragg reflectors", *J. Opt. Soc. Am. B* **17**, 919-926 (2000).
- 5.15 M. Haiml, U. Siegner, F. Morier-Genoud, U. Keller, M. Luysberg, P. Specht, E. R. Weber, "Femtosecond response times and high optical nonlinearity in Beryllium doped low-temperature grown GaAs", *Appl. Phys. Lett.* **74**, 1269-1271 (1999).
- 5.16 M. Haiml, U. Siegner, F. Morier-Genoud, U. Keller, M. Luysberg, R. C. Lutz, P. Specht, E. R. Weber, "Optical nonlinearity in low-temperature grown GaAs microscopic limitations and optimization strategies", *Appl. Phys. Lett.* **74**, 3134-3136 (1999).
- 5.17 C. Honninger, R. Paschotta, F. Morier-Genoud, M. Moser, U. Keller, "Q-switching stability limits of continuous-wave passive mode locking", *J. Opt. Soc. Am. B* **16**, 46-56 (1999).

- 5.18 F. X. Kartner, L. R. Brovelli, D. Kopf, M. Kamp, I. Calasso, U. Keller, "Control of solid-state laser dynamics by semiconductor devices", *Optical Engineering* **34**, 20242036 (1995).

Section 6

- 6.1 P.J. Hardman, W.A. Clarkson, G.J. Friel, M. Pollnau and D.C. Hanna "Energy Transfer Upconversion and Thermal Lensing in High-Power End-Pumped Nd:YLF Laser Crystals" *IEEE Journal of Quantum Electronics* **35** (4) 647-655 (April 1999).
- 6.2 <http://www.st-andrews.ac.uk/~psst/>
- 6.3 M. Pollnau, P.J. Hardman, M.A. Kern, W.A. Clarkson and D.C. Hanna "Upconversion-induced heat generation and thermal lensing in Nd:YLF and Nd:YAG" *Physical Review B* **58** (24) 16076-16092 (1998).
- 6.4 W. Koechner "Solid-state laser Engineering" 5th rev and updated ed. *Springer series in Optical Science Volume 1*, Springer-Verlag Berlin Heidelberg, Germany (1999).
- 6.5 <http://www.las-cad.com/>
- 6.6 C. Czeranowsky "Resonatorinterne Frequenzverdopplung von diodengepumpten Neodym-Lasern mit hohen Ausgangsleistungen im blauen Spektralbereich" *PhD Dissertation*, University of Hamburg (2002).

Section 8

- 8.1 D. Burns, M. Hetterich, A. L. Ferguson, E. Bente, M. D. Dawson, J. L. Davies, S. W. Bland, "High-average-power (>20 W) Nd:YV04 lasers mode locked by strain-compensated saturable Bragg reflectors", *J. Opt. Soc. Am. B* **17**, 919-926 (2000).

- 8.2 C. Honninger, R. Paschotta, M. Graf, F. Morier-Genoud, G. Zhang, M. Moser, S. Biswal, J. Nees, A. Braun, G. A. Mourou, L. Johanssen, A. Giesen, W. Seeber, U. Keller, "Ultrafast ytterbium-doped bulk lasers and laser amplifiers", *Appl. Phys. B* **69**, 3-17 (1999).
- 8.3 D. Burns, M. Hetterich, A. L. Ferguson, E. Bente, M. D. Dawson, J. L. Davies, S. W. Bland, "High-average-power (>20 W) Nd:YV04 lasers mode locked by strain-compensated saturable Bragg reflectors", *J. Opt. Soc. Am. B* **17**, 919-926 (2000).
- 8.4 D. Burns, G.J. Valentine, W. Lubeigt, E. Bente, A.I. Ferguson, "Development of High Average Power Picosecond Laser Systems", *Opto-Electronic Devices*, (2002).

Appendix

The condition for stable cw-modelocking is given as [5.18]:

$$E_{p,int}^2 > E_{sat,L} E_{sat,A} \Delta R. \quad A.1$$

Where $E_{p,int}$ is the intracavity pulse energy, $E_{L,sat}$ the gain saturation energy which is given as $E_{L,sat} = F_{sat,L} A_{eff,L}$, where $F_{sat,L}$ is the gain fluence and $A_{eff,L}$ is the laser beam effective area on the gain crystal, while $E_{A,sat}$ is the absorber saturation energy which is given as $E_{A,sat} = F_{sat,A} A_{eff,A}$, where $F_{sat,A}$ is the saturable absorber fluence and $A_{eff,A}$ is the laser beam effective area on the saturable absorber.

At the transition from Q -switched modelocking to cw-modelocking, Equation A1 becomes:

$$E_{p,int}^2 = E_{sat,L} E_{sat,A} \Delta R. \quad A.2$$

The intracavity pulse energy $E_{p,int}$ can then be shown to be:

$$E_{p,int} = \frac{E_{p,ext}}{T_{OC}}, \quad A.3$$

where $E_{p,ext}$ is the external pulse energy and T_{OC} is the output coupler transmission.

The $E_{p,ext}$ can also be transformed and be finally represented as:

$$E_{p,ext} = \frac{P_{QSM,th}}{f}, \quad A.4$$

where $P_{QSM,th}$ is the output power at the QSM,th transition and f the pulse repetition frequency which can further be broken down to:

$$f = \frac{c}{2L} \quad A.5$$

with c being the speed of light and L is the cavity length.

The insertion of Equation A.5 and A.4 into A.3 shows that the intracavity pulse energy $E_{P,int}$ can now be represented as:

$$E_{P,int} = \frac{2}{c} \frac{L}{T_{OC}} P_{QSM,th} . \quad A.6$$

The saturation energy in the crystal $E_{sat,L}$ can be written as:

$$E_{sat,L} = F_{sat,L} A_{eff,L} , \quad A.7$$

where $F_{sat,L}$ is the saturation fluence of the crystal and $A_{eff,L}$ the effective laser mode area inside the crystal.

The saturation fluence of the crystal can be written:

$$E_{sat,L} = \frac{hc}{m \lambda \sigma_L} , \quad A.8$$

where h is Plank's constant, m the number of passes through the crystal, λ the operating wavelength and σ_L - the emission cross sectional area.

The effective laser mode area $A_{eff,L}$ inside the laser crystal is given by:

$$A_{eff,L} = \pi w_L^2 , \quad A.9$$

with w_L the spot size radius inside the crystal.

The combination of Equations A.9 and A.8 therefore represents the saturation fluence $F_{sat,L}$ as:

$$F_{sat,L} = \pi \frac{hc}{\lambda} \frac{w_L^2}{m \sigma_L} . \quad A.10$$

The saturation energy of the absorber $E_{sat,A}$ can be represented as

$$E_{sat,A} = F_{sat,A} A_{eff,A} , \quad A.11$$

where $F_{sat,A}$ is the saturation fluence of the absorber and $A_{eff,A}$ the effective laser mode area on the saturable absorber.

The effective laser mode area $A_{eff,A}$ on the saturable absorber is:

$$A_{eff,A} = \pi w_A^2, \quad A.12$$

with w_A the spot size radius on the saturable absorber.

Equation A.12 with A.11 shows that the saturation fluence on the absorber is given by:

$$E_{sat,A} = \pi F_{sat,A} w_A^2. \quad A.13$$

The insertion of Equations A.13, A.10 and A.6 into A.2 shows that the Q-SML transition can be represented as:

$$\left[\frac{2}{c} \frac{L}{T_{OC}} P_{QSM,th} \right]^2 = \frac{\pi h c}{\lambda} \frac{w_L^2}{m \sigma_L} \pi F_{sat,A} w_A^2 \Delta R \quad A.14$$

Solving Equation A.14 for the threshold Q-switched modelocked transition average output power results in the formula

$$P_{QSM,th} = \sqrt{\frac{\pi^2 h c^3}{4 m \sigma_L \lambda}} T_{OC} \frac{w_L w_A}{L} \sqrt{F_{sat,A} \Delta R} \quad A.15$$

and by letting $K = \sqrt{\frac{\pi^2 h c^3}{4 m \sigma_L \lambda}}$ = constant we finally obtain an equation describing the threshold average output power for the Q-switched modelocked transition:

$$\boxed{P_{QSM,th} = K T_{OC} \frac{w_L w_A}{L} \sqrt{F_{sat,A} \Delta R}} \quad A.16$$